Photochromic Reaction Behavior and Solid State Property Changes of Diarylethene Crystals

March 2014

Daichi Kitagawa

Photochromic Reaction Behavior and Solid State Property Changes of Diarylethene Crystals

（ジアリールエテン結晶のフォトクロミック反応挙動と固体物性変化）

March 2014

Graduate School of Engineering

Osaka City University

Daichi Kitagawa

北川　大地

Contents

General Introduction

1. Photochromism

Photochromic Compounds

Photochromism is referred to as a phenomenon of chromatic change upon photoirradiation. Compounds which show photochromism are called photochromic compounds. A photochromic compound was first reported for tetracene by M. Fritsche in 1867.[1] It becomes colorless upon photoirradiation and it is recolorized by heating. Since then, a lot of artificial photochromic compounds have been synthesized and investigated so far. Photochromic compounds are classified into two types, T-type and P-type, as shown in Figure 1.[2]

(a) T-type photochromic compounds

Azobenzene

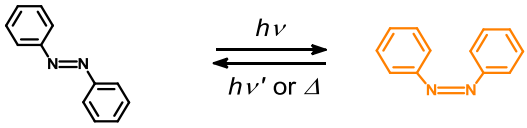

Spiropyran

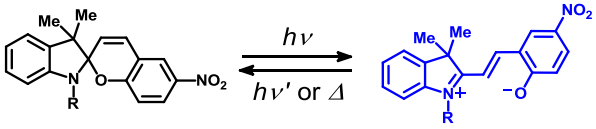

(b) P-type photochromic compounds

Furylfulgide

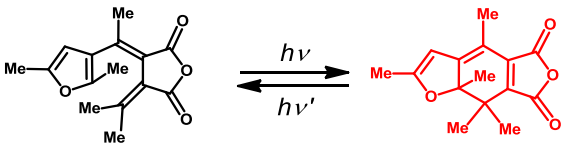

Diarylethene

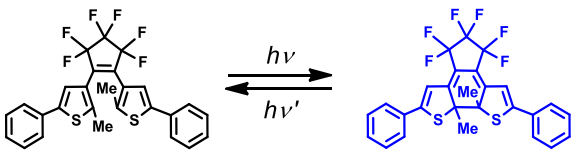

Figure 1. Typical photochromic compounds.

T-type photochromic compounds undergo thermally reversible photochromism. The photogenerated colored isomer returns to the initial colorless isomer by not only photoreaction but also thermal reaction at room temperature. Azobenzene and spiropyran are classified into T-type photochromic compounds. T-type photochromic compounds are suitable for photomodulated materials such as photochromic ophthalmic lenses.[3] On the other hand, furylfulgide and diarylethene are classified into P-type photochromic compounds. P-type photochromic compounds can be reversibly isomerized by only photoirradiation. Both the colorless and colored isomers are thermally stable at room temperature. P-type photochromic compounds have potential for application to various optoelectronic devices such as optical memory,[4] photooptical switching,[5] displays,[6] nonlinear optics,[7] and so on.

Diarylethene

A diarylethene derivative was first reported as a P-type photochromic compound by Irie *et al*. in 1988.[8] Diarylethene can reversibly undergo photoisomerization between the open-ring isomer and the closed-ring isomer upon alternating irradiation with ultraviolet (UV) and visible light. Diarylethene has heterocyclic aryl groups connected to ethene moiety. The photocyclization and photocycloreversion of diarylethene are based on the Woodward-Hoffmann rule for 1,3,5-hexatriene/cyclohexadiene.[9] Among a number of photochromic compounds, diarylethenes with heterocyclic aryl groups are the most promising compounds for applications to optical memories and switches because of their thermal stability, fatigue resistance, high sensitivity, and rapid response.[10-12]

The most commonly used diarylethenes are diarylperfluorocyclopentenes. The absorption maximum of the colored closed-ring isomer can be modulated by changing the molecular structure or introducing various substituents.[10] Figure 2 shows molecular structures of the closed-ring isomers with different absorption maximum. The color of the closed-ring isomer is mainly determined by the π-conjugation length through the two aryl groups. When thiophene rings are connected to the ethene unit at the 2-position of the thiophene, the color of the closed-ring isomer is yellow with the absorption maximum at 425 nm. The diarylethene with thiophene rings connected to the ethene moiety at the 3-position becomes red with the absorption maximum at 534 nm. The closed-ring isomer of the diarylethene introduced phenyl groups at the 5-position of thiophene moieties show blue color with the absorption maximum at 575 nm.

Diarylethene has two stable conformations in the open-ring isomer, parallel (with the aryl rings in mirror symmetry) and antiparallel (with the aryl rings in C_2 symmetry) conformations.[13] The parallel and antiparallel conformations are in the almost equal amounts and they can interconvert with each other in the solution. Only from antiparallel conformation, the conrotatory photocyclization can proceed, as shown in Figure 3.[9,14] Therefore, the

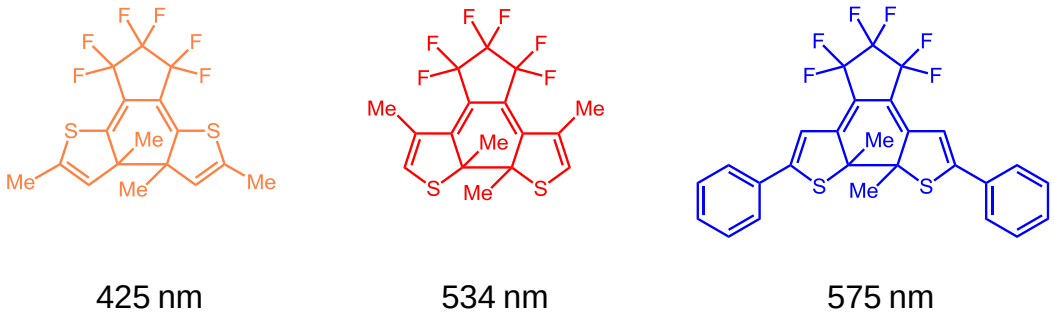

Figure 2. Molecular structures of the closed-ring isomers with different absorption maximum.

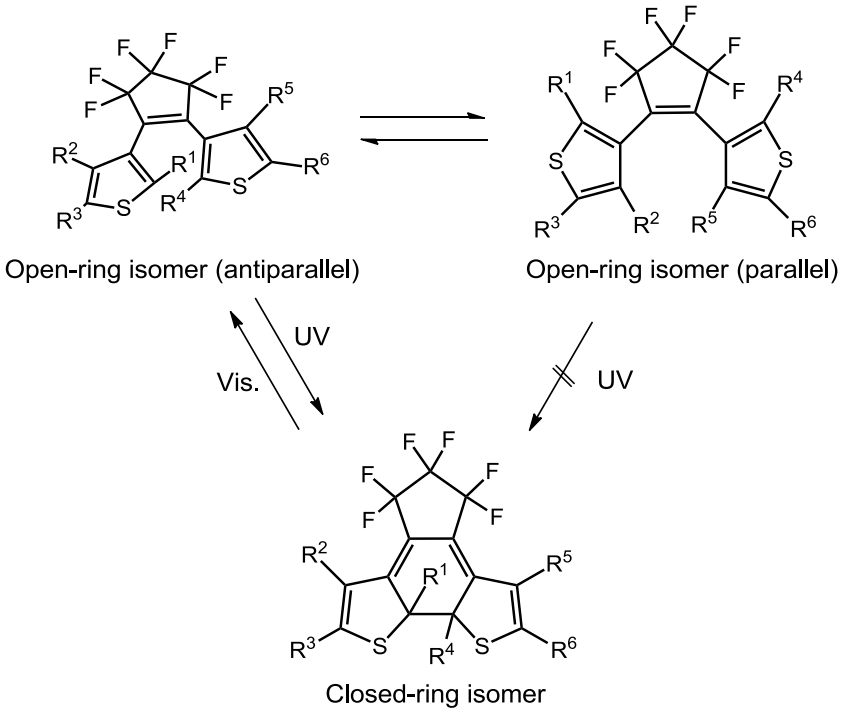

Figure 3. Photochromic reaction of diarylethenes.

quantum yield of the photocyclization cannot excess 50% on the basis of the abundance ratio of the antiparallel conformation. However, the quantum yield can be increased by improving the proportion of the antiparallel conformation.[15-22] For example, Takeshita *et al*. performed the enhancement of the photocyclization quantum yield of a diarylethene by inclusion in a cyclodextrin cavity.[19] Kawai *et al*. have also reported photon-quantitative reaction of a dithiazolylarylene with multiple intramolecular noncovalent interactions, such as weak CH-N hydrogen bonds, S-N and CH-π interactions.[22] In all cases, it is a key to regulate the ground-state geometry of diarylethenes in antiparallel conformation.

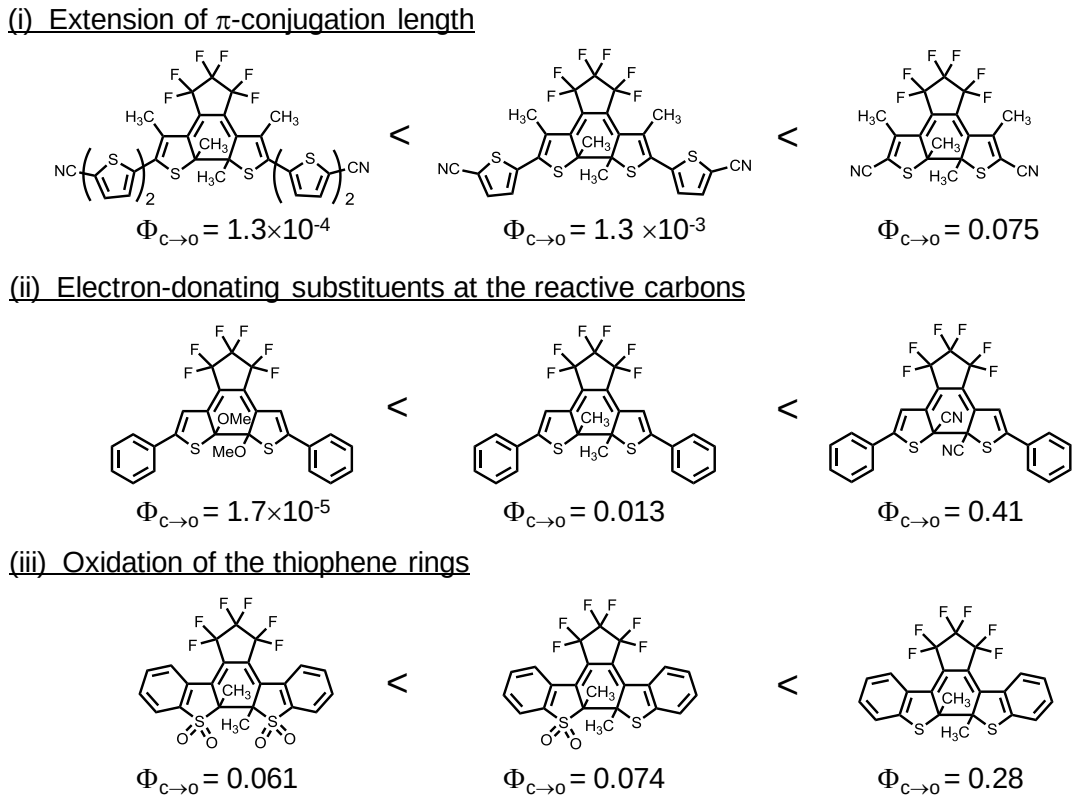

Figure 4. Photocycloreversion reactivity of diarylethene closed-ring isomers.

The quantum yield of the photocycloreversion can also be controlled by three factors, (i) Extension of π-conjugation length,[23,24] (ii) Electron-donating substituents at the reactive carbons,[25-27] and (iii) Oxidation of the thiophene rings,[28-31] as shown in Figure 4. In the case of (i), the electron density of the reactive carbons decreases with the extension of π-conjugation length. Then, the photocycloreversion reactivity is suppressed. In the case of (ii) and (iii), the photocycloreversion is suppressed because the activation energy for photocycloreversion in the excited state of the closed-ring isomer increases with the introduction of the electron-donating substituents at the reactive carbons or the oxidation of the thiophene rings.

Thermal stability of the closed-ring isomer can also be modulated by following three factors. (i) Aromatic stabilization energy of the aryl groups,[9] (ii) Electron-withdrawing substituents at the aryl groups,[32,33] and (iii) Steric hindrance of the substituents at the reactive carbons,[34-36] as shown in Figure 5. In the case of (i), when the aryl groups are thiophene or benzothiophene groups, the closed-ring isomers are thermally stable, while closed-ring isomers having phenyl, pyrrolyl, or indolyl groups are thermally unstable. The decrease in the thermal stability is due to the high aromatic stabilization energies of the aryl substituents. In the case of (ii), when electron-withdrawing substituents are introduced at the aryl group, the

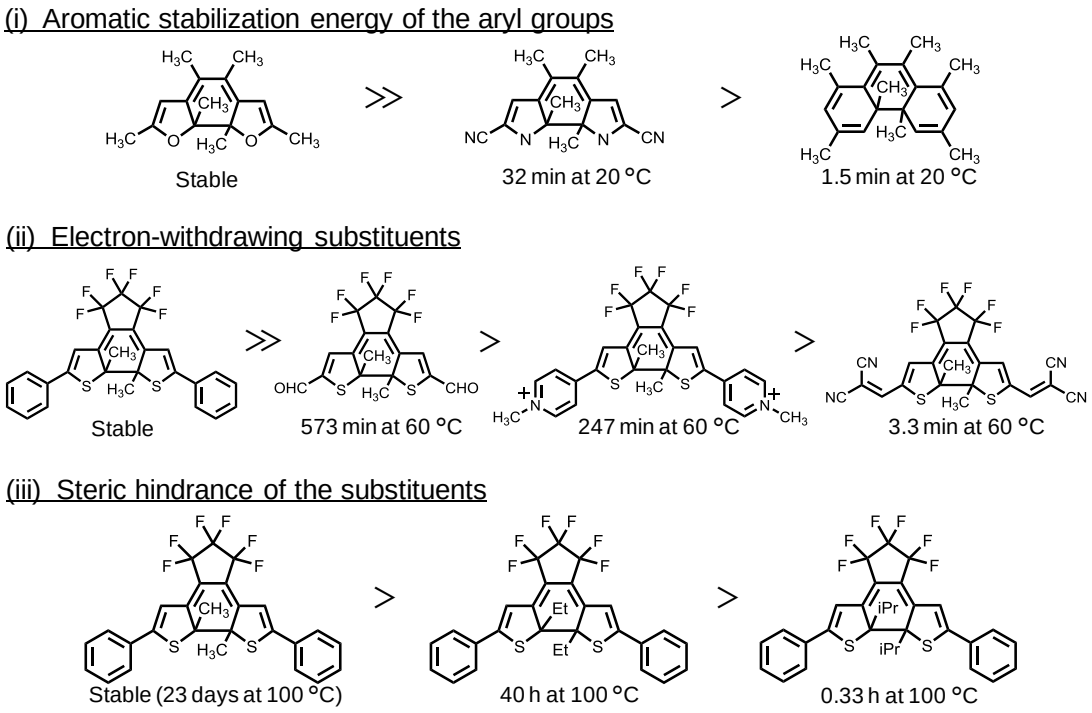

Figure 5. Thermal stability of diarylethene closed-ring isomers. The values below the molecular structures show the half-life of thermal cycloreversion.

closed-ring isomers become thermally unstable because the central carbon-carbon bonds in the photogenerated closed-ring isomers are weakened by the electron-withdrawing substituents. In the case of (iii), the bulky substituents at the reacting positions led to thermal cycloreversion reactions of the closed-ring isomers. The theoretically calculated bond length of the central carbon-carbon bond is related to the thermal stability.[37] The rate constant and activation energy of thermal cycloreversion of compounds with alkyl or alkoxy groups are correlated with the steric substituent.[36]

Photochromic compounds which show photochromism in the crystalline phase are rare. Typical photochromic compounds that show photochromism in the crystalline phase are known for paracyclophanes,[38] triarylimidazole dimer,[39,40] diphenylmaleronitrile,[41] aziridines,[42] 2-(2,4-dinitrobenzyl)pyridine,[43-46] *N*-salicylideneanilines,[47-49] and triazenes,[50] as shown in Figure 6,[51] whereas in many cases, their photogenerated isomers are thermally unstable. On the other hand, diarylethene derivatives show photochromism even in the crystalline phase and their photogenerated isomers are thermally stable.

Figure 7 shows the diarylethene crystals which can undergo photochromic reaction in the crystalline phase. Upon irradiation with UV light, the colorless crystals change to yellow, red, blue, or green, depending on the molecular structure of the diarylethenes. The colors remain

stable so far as being stored in the dark, but the colors disappeared by irradiation with visible light. When the diarylethene molecules are fixed in the antiparallel conformation and the distance between the reactive carbons is less than 4 Å, the photochromism in the crystalline phase can proceed with the photocyclization quantum yield of unity.[52] The photoinduced coloration/decoloration cycles of the crystals can be repeated more than 10^4 times while maintaining the shape of the crystals.

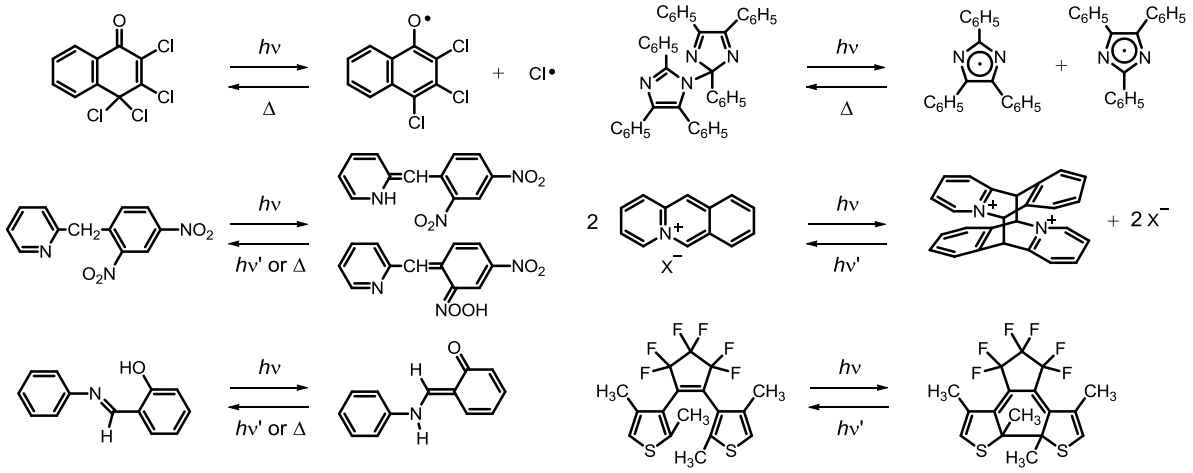

Figure 6. Typical examples of crystalline photochromic compounds.

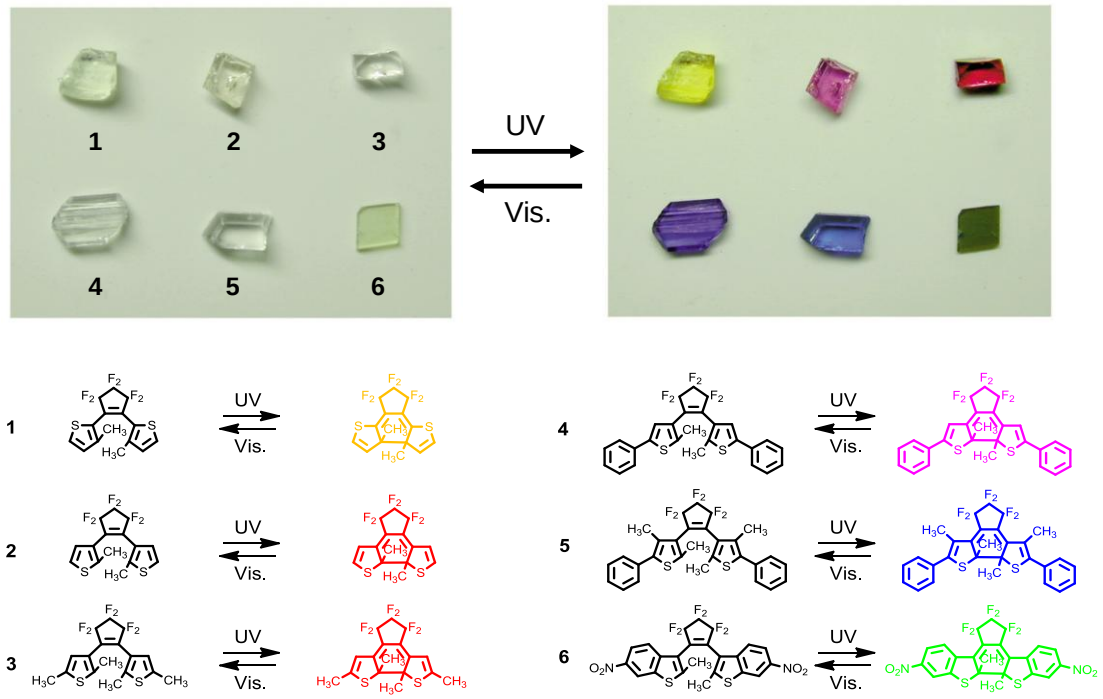

Figure 7. Diarylethene derivatives that show photochromism in the single crystalline phase.

Table 1. Topics of photochromic diarylethene crystals.

Topics	Ref.
Multicolor photochromism	53-56
Dichroism under polarized light	57-59
Fluorescence	60
Three-dimensional optical memory	61
Thermal cycloreversion reaction	11, 34
Measurement of quantum yield	52, 62-64
Diastereoselective cyclization	65-67
Selective photochromism reaction under polarized light	68, 69
Theoretical study	70, 71
Raman spectroscopic study	72
Molecular motion observed by X-ray crystallography	73-75
Reversible surface morphology changes	76-84
Rapid and reversible crystal shape changes	85-89
Nano structures	90-95

In the past decade, a lot of researches on the photochromic diarylethene crystals have been reported, as shown in Table 1. Especially, the following researches have been attracted much attention: (a) multicolored photochromic crystals,[53-56] (b) dichroism observed under polarized light,[56-59] and (c) crystal shape change by photoirradiation.[85-89] The crystal shown in Figure 8a was composed of three different kinds of diarylethenes, and turned yellow, orange, red, purple, blue, green, or black upon irradiation with light of appropriate wavelengths. The colors of the crystals were thermally stable in the dark and completely bleached by irradiation with visible light. The mixed crystal composed of three diarylethenes exhibited multi-color photochromism. Diarylethene single crystals reversibly change the color upon alternating irradiation with UV and visible light. The single crystal, shown in Figure 8b, changes from colorless to green upon UV light irradiation. However, when the color was observed under polarized light, the colored crystal showed dichroism, yellow and blue. When the crystal was rotated under polarized light, the color changed from yellow to blue. The yellow and blue colors were attributed to two perpendicular electronic transitions at 465 and 600 nm of the closed-ring form. The two transition moments coincide with the directions of short and long axes of the closed-ring form isomers, which were regularly packed in the crystal lattice.

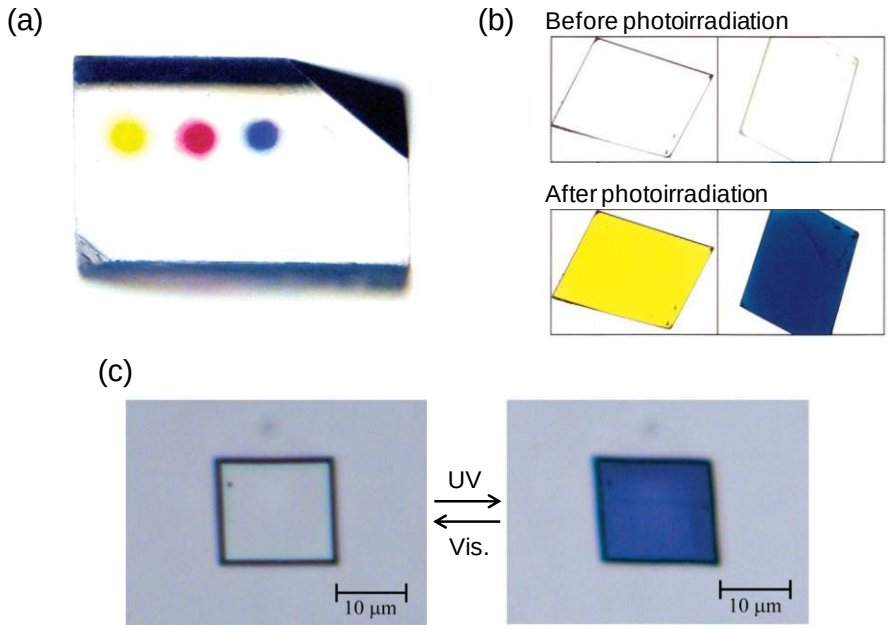

Figure 8. Representative researches of diarylethene crystals; (a) multicolored photochromic crystal, (b) dichroism of single crystal observed under polarized light, and (c) crystal shape change by photoirradiation.

Figure 8c shows a micrometer size single crystal of a diarylethene which changes from a square shape to a lozenge shape upon irradiation with UV light. The deformed crystal is thermally stable, and switches back to their original state on irradiation with visible light. The diarylethene crystals can be potentially used for application to optoelectronic devices such as optical memory media, switching devices, display materials, nonlinear optics, and photo-mechanical actuators.

2. Solid State Properties

Polymorphism

Since Mitscherlich used the word 'polymorphism' for the first time in the context of crystallography in 1822, polymorphism has attracted the attention of many scientists because of the importance in many areas of chemical researches.[96] Polymorphs provide different properties, such as conductivity,[97] magnetic properties,[98,99] fluorescence,[100,101] and photochromism[68,102] on the basis of molecular packing in each crystal. 5-Methyl-2-[(2-nitrophenyl)amino]-3-thiophenecarbonitrile, known as ROY, is the most famous compound which shows polymorphic crystallization. ROY has at least seven polymorphs with solved structures by single-crystal X-ray crystallographic analysis, which is the largest number in the Cambridge Structural Database, as shown in Figure 9.[103,104]

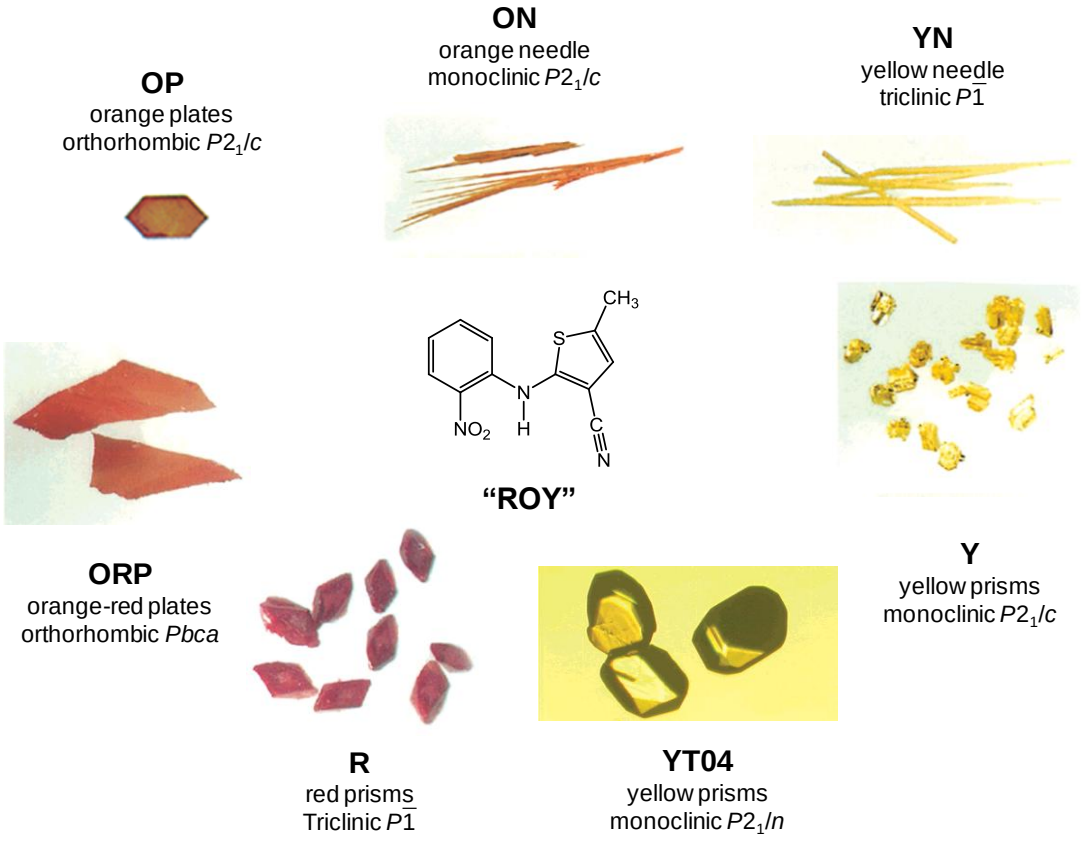

Figure 9. Photomicrographs of seven polymorphs of ROY.

A phase transition between polymorphic crystals has also been studied with developing the research on polymorphism.[96] The phase transition of molecular crystals can be divided into two types of processes: crystal-to-melt-to-crystal process and crystal-to-crystal process. The former phase transition is accompanied with melting the crystal. The crystal shape and the molecular packing before and after the phase transition are quite different. In contrast, the latter phase transition takes place with keeping the shape of the crystal. The movement of molecules in the crystal is very small; thus, the molecular packing before and after the phase transition is very similar. The solid state properties of the crystal also change before and after the phase transition on the basis of the molecular packing in each crystal. Furthermore, in the polymorphic phase transition, it is well-known that there are also two types of the phase transition, monotropic and enantiotropic phase transition.[96] Monotropic phase transition means that the phase transition occurs irreversiblely. In the monotropic system, the polymorphic form with the higher melting point is always thermodynamically stable. Then, a thermodynamically metastable polymorphic form converts another stable polymorphic form irreversibly at the temperature below the melting point of the stable form. In contrast, the reversible phase transition is called as the enantiotropic phase transition. Although the

polymorphic form with the lower melting point is thermodynamically stable below the phase transition temperature, the polymorphic form with the higher melting point becomes thermodynamically stable form when the temperature increases over the phase transition temperature. At the phase transition temperature, Gibbs free energy of the two polymorphic forms is equal. Then, the phase transition takes place reversibly at the phase transition temperature.

There are few reports on the polymorphism of diarylethene derivatives.[68,102] However, there is no research on the phase transition between polymorphic forms. The combination of photochromism and polymorphism is expected to provide a new functional material.

Surface Wettability

Recently, the wettability of solid surfaces has been a topic of much attention in both industrial and academic research fields because of its importance in applications relating to adsorption, adhesion, dewetting, lithography, and biomedical engineering. There are two factors that control wettability on solid surfaces, namely chemical and topological factors.[105] As an example of the chemical factor, the well-known properties of polytetrafluoroethylene may be cited.[106] The hydrophobic surface of the polymer is attributable to the low free-energy surface due to the aggregate effect of carbon-fluorine bonds. On the other hand, superhydrophobic surfaces with water contact angles above 150°, such as the leaves of the lotus plant, are affected by the topological factor.[107] Studies on the topological factor have been centered on the research field of biomimetic architectures, such as those of plant leaves[108] and insect wings[109] and legs[110] that exhibit superhydrophobic character. Superhydrophobic surfaces have a wide range of potential applications, for example as self-cleaning surfaces, print technology, biomedical engineering, and so on.

Recent reports on the wettability of solid surfaces have described the control of surface wettability using external stimuli such as light, temperature, electricity, pH, and solvents, as shown in Figure 10.[111] Among these stimuli, light irradiation offers a non-contact, non-destructive method to induce a response. Then, photoresponsive surfaces with controllable wettability have played a significant role in the research of functional materials such as inorganic oxides (titanium dioxide,[112] zinc oxide,[113] and tungsten oxide[114]) and photochromic compounds (azobenzene,[115,116] spiropyran,[117-121] and diarylethene[77-84]).

Uchida *et al*. reported that the surface topology can be changed by the crystal growth of a photochromic diarylethene, as shown in Figure 11.[77-84] The contact angle with water changed from 120° to 163° upon UV light irradiation because of the generation of the closed-ring isomer crystal of the fibrils on the crystal surface. The reversible changes in the contact angle are attributed to reversible changes in the surface roughness. However, one drawback of this system is that the crystal growth takes a long time to change the contact angle, as long as 24 h.

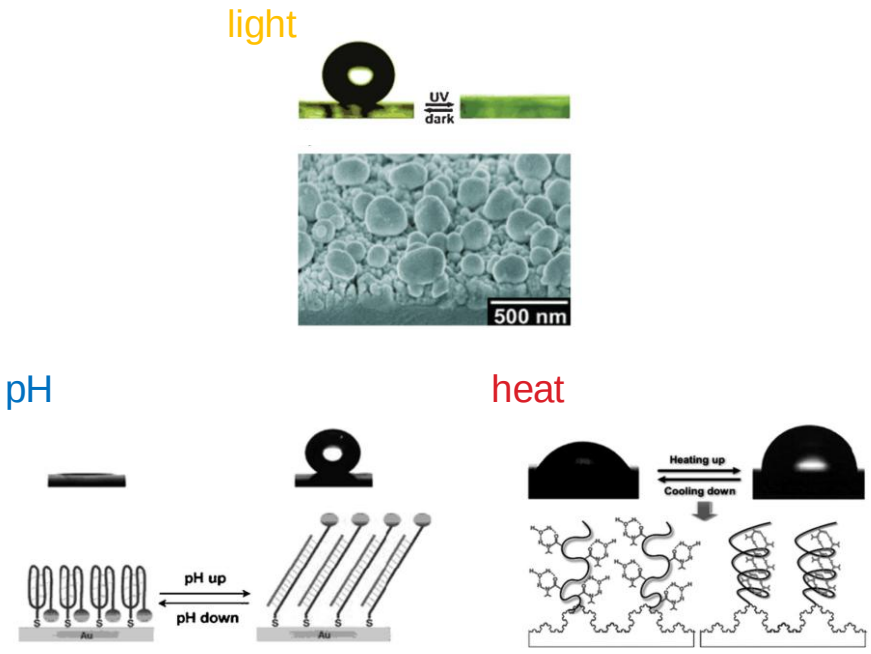

Figure 10. Some examples for control of the surface wettability by external stimuli.

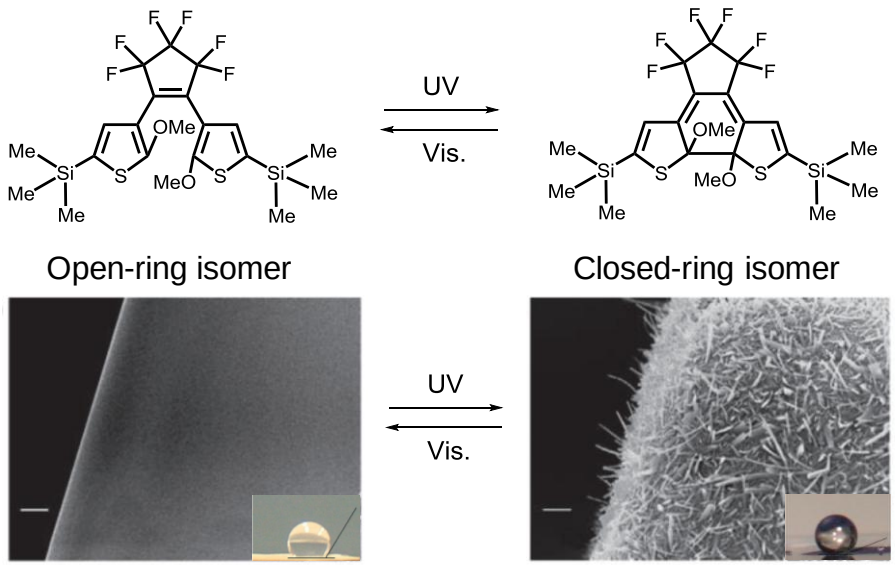

Figure 11. Photoinduced reversible topological change on diarylethene microcrystalline surface.

In many situations, it is difficult to control the crystal growth of organic compounds, especially in the desired space and the desired time.

Photomechanical Crystals

Recently, the study on the photomechanical organic crystals has been much attention because they can work by photoirradiation without any direct contact and electronic wires.

This is an advantage in comparison with piezoelectric crystals. In order to obtain the photomechanical crystals, it is required for the compounds to change their molecular structure or arrangement in crystalline phase upon photoirradiation. The photomechanical crystals of various compounds have been so far reported for diarylethene,[85-89] furylfulgide,[122] azobenzene,[123-126] salicylideneaniline,[127,128] anthracene carboxylates,[129-134] 4-chlorocinnamic acid,[135] 1,2-bis(4-pyridyl)ethylene salt,[136] benzylidenedimethylimidazolinone,[137] and so on, as shown in Figure 12. There are various photomechanical behaviors such as contraction,

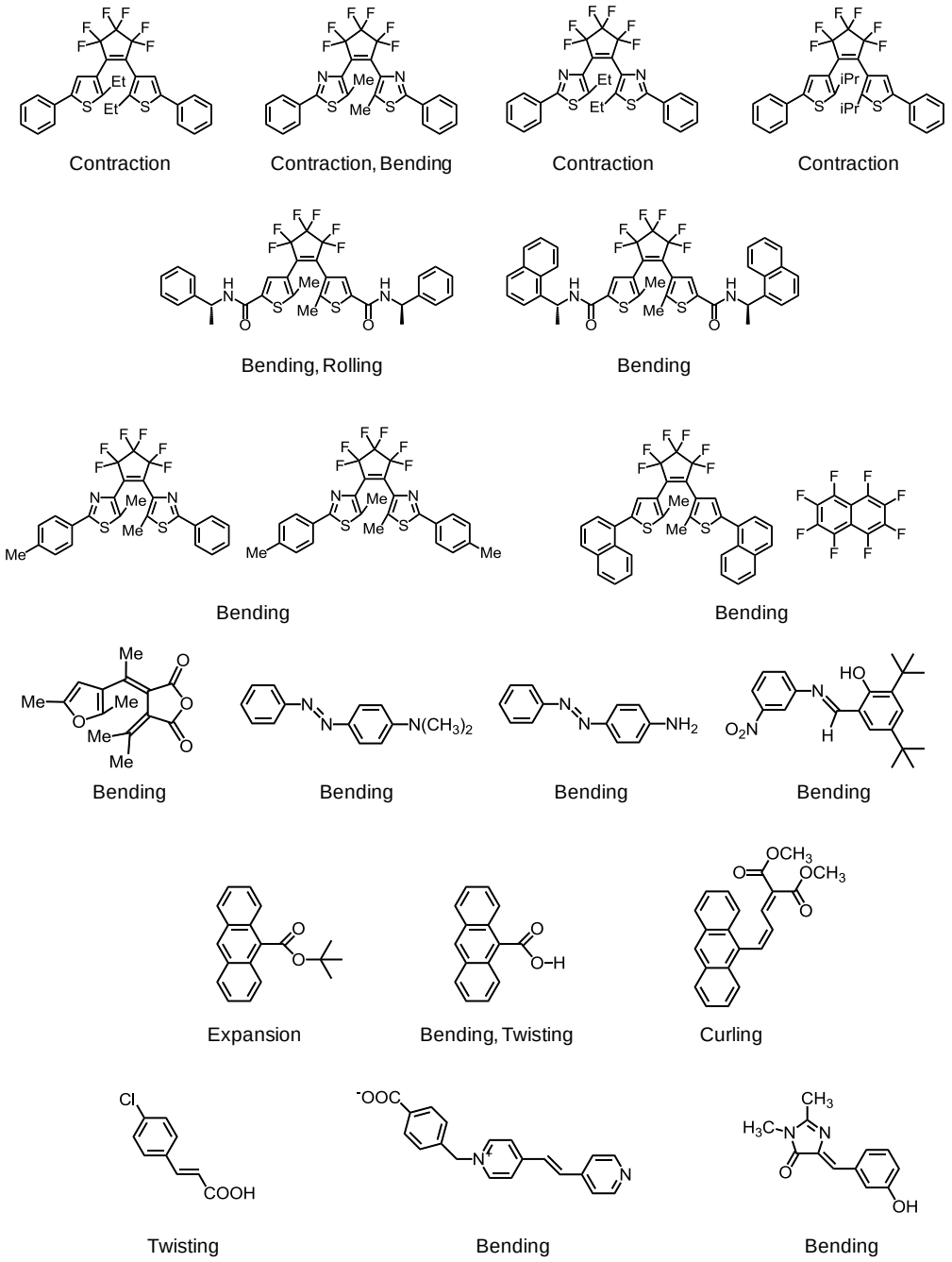

Figure 12. Compounds showing photomechanical behavior.

expansion, bending, separation, twisting, curling, and so on. All of these behaviors are based on the geometry change of molecules in the crystalline phase.

The rapid and reversible crystal shape change of photochromic diarylethene upon alternating irradiation with UV and visible light was first reported by Irie *et al*.[85] When irradiated with UV light, the photoisomerization of the diarylethene molecules from the open-ring isomer to the closed-ring isomer occurs in the crystalline phase. The twisted thiophene rings become coplanar and the thickness of each molecule is reduced. The closed-ring isomers in the photoirradiated crystal can stack each other accompanying the change in the cell dimensions. As a result, the crystal contraction of 1,2-bis(2-ethyl-5-phenyl-3-thienyl)perfluorocyclopentene and 1,2-bis(5-methyl-2-phenyl-3-thiazolyl)-perfluorocyclopentene was observed. When the rod-like crystal of the thiazole derivative was irradiated with UV light from side direction, the crystal bends towards the direction of the incident light because the photoisomerization takes place with a gradient in the extent of photoisomerization caused by high absorption in the vicinity of the crystal surface. The difference between the crystal contraction and bending is ascribed to the thickness of the crystal. There is also the example of the crystal bending away from the incident light.[88] In this case, the short axis of diarylethene molecules expands by the photoisomerization upon UV irradiation. The repulsion between each molecule results in the expansion of the cell dimension. As a result, the crystal bends away from the incident light. The photomechanical behavior can be explained by the contraction or expansion.

The research on the photoinduced bending for practical applications has been reported. The two-component co-crystals composed of 1,2-bis(2-methyl-5-(1-naphthyl)-3-thienyl)per-fluorocyclopentene and perfluoronaphthalene with 1-5 mm size in length are reversibly bended upon alternating irradiation with UV and visible light.[88] The photoinduced bending of such a large crystal is attractive for practical use. The mixed crystals composed of two diarylethene derivatives, 1-(5-methyl-2-phenyl-4-thiazolyl)-2-(5-methyl-2-*p*-tolyl-4-thiazol-yl)perfluorocyclopentene and 1,2-bis(5-methyl-2-*p*-tolyl-4-thiazolyl)perfluorocyclopentene, also exhibit reversibly bending upon alternating irradiation with UV and visible light.[89] The mixed crystals can be reversibly bent over 1000 cycles and exhibit bending in wide temperature range from 4.6 to 370 K. To develop photomechanical crystals, following researches should be performed; (i) investigation of photomechanical works in various compounds, (ii) quantitative evaluation of photomechanical behaviors, and (iii) new photomechanical motions.

3. Scope of This Thesis

The author has been interested in photochromism of diarylethenes in the crystalline phase because of their unique reactivity in the crystal and solid state properties. The combination of

photochromism in the crystalline phase and various solid state properties seems to contribute to the further study of diarylethene crystals. The purpose of this thesis is to provide a novel functional photoresponsive material with diarylethene crystals. In order to accomplish the purpose, polymorphism, surface wettability, and photoinduced crystal shape change with diarylethene crystals are particularly investigated in this thesis. Although a lot of studies on diarylethene crystals have been reported, there are few studies on polymorphism, surface wettability, and photoinduced crystal shape change using diarylethene crystals. By investigations and considerations of their solid state properties, new useful strategy for making functional photoresponsive materials with diarylethene crystal is developed.

This doctoral thesis consists of General Introduction and 6 chapters which are divided in three parts. In General Introduction, the backgrounds of the photochromism of diarylethene, polymorphism, surface wettability, and photomechanical crystal and the scope of this thesis are described.

Part I deals with polymorphism and phase transition between polymorphic forms of diarylethene derivatives. Phase transition between polymorphic forms of diarylethene crystals has never been reported. Two types of polymorphic phase transition of diarylethene crystals, in crystal-to-crystal and crystal-to-melt-to-crystal process, have newly been found. It is necessary to investigate the phase transition in detail for applications. The phase transition through crystal-to-crystal process of 1,2-bis(5-phenyl-2-propyl-3-thienyl)perfluorocyclopentene is described in Chapter 1. In order to investigate the mechanism of the phase transition, the motion of molecules in the phase transition is discussed from the result of single-crystal X-ray crystallography. In Chapter 2, the phase transition through crystal-to-melt-to-crystal process of 1,2-bis(2-methyl-6-nitro-1-benzothiophen-3-yl)-perfluorocyclopentene is described. The phase transition behavior is investigated in detail and the control of the phase transition with the photochromic reaction of diarylethene crystals is discussed.

In Part II, control of surface wettability and photomicropatterning using diarylethene crystals are investigated. The control of the crystallization from amorphous state in a polymer is described in Chapter 3. The surface wettability can be changed by crystallization from amorphous state due to the change of surface roughness. In order to establish the photoresponsive surface with controllable wettability, the control of the crystallization from amorphous state by the photoisomerization of a diarylethene upon UV irradiation is discussed. Chapter 4 provides the superhydrophobic surface with high adhesive force. The superhydrophobic surface (water contact angle >150°) has a wide range of potential applications. In order to fabricate the superhydrophobic surface, the further crystal growth of diarylethene crystals is discussed. The water droplet on the superhydrophobic surface was pinned even when the surface was turned upside down.

Part III deals with photoinduced shape changes of diarylethene crystals. Chapter 5 describes the crystal thickness dependence on the photoinduced bending. In order to clarify the crystal thickness dependence on the bending speed of the crystal, the initial bending speed of crystals with the different crystal thickness is investigated. The relationship between the bending speed and the crystal thickness is discussed with Timoshenko's bimetal model. In Chapter 6, the photoinduced twisting of a diarylethene crystal is described. As a new photomechanical motion, the photoinduced crystal twisting has been found. The mechanism of the photoinduced twisting is discussed.

4. References

1. M. Fritsche, *Comp. Rend.* **1867**, *69*, 1035.
2. H. Dürr, H. B.-Laurent, *Photochromism: Molecules and Systems*, Elsevier, Amsterdam, 2003.
3. J. C. Crano, T. Flood, D. Knowles, A. Kumar, B. V. Gemert, *Pure Appl. Chem.* **1996**, *68*, 1395.
4. M. Irie, K. Matsuda, *Memories*, in *Electron Transfer in Chemistry*, ed. V. Balzani, Wiley-VCH, Weinheim, 2001, vol. 5, pp. 215‑242.
5. M. Irie, *Photoswitchable Molecular Systems Based on Diarylethenes*, in *Molecular Switchings*, ed. B. L. Feringa, Wiley-VCH, Weinheim, 2001, pp. 37‑62.
6. J. A. Delaire, K. Nakatani, *Chem. Rev.* **2000**, *100*, 1817.
7. C. Bechinger, S. Ferrer, A. Zaban, J. Sprague, B. A. Gregg, *Nature* **1996**, *383*, 608.
8. M. Irie, M. Mohri, *J. Org. Chem.* **1988**, *53*, 803.
9. S. Nakamura, M. Irie, *J. Org. Chem.* **1988**, *53*, 6136.
10. M. Irie, *Chem. Rev.* **2000**, *100*, 1685.
11. M. Irie, T. Lifka, S. Kobatake, N. Kato, *J. Am. Chem. Soc.* **2000**, *122*, 4871.
12. H. Miyasaka, T. Nobuto, A. Itaya, N. Tamai, M. Irie, *Chem. Phys. Lett.* **1997**, *269*, 281.
13. K. Uchida, Y. Nakayama, M. Irie, *Bull. Chem. Soc. Jpn.* **1990**, *63*, 1311.
14. A. Staykov, K. Yoshizawa, *J. Phys. Chem. C* **2009**, *113*, 3826.
15. M. Irie, O. Miyatake, K. Uchida, *J. Am. Chem. Soc.* **1992**, *114*, 8715.
16. Y. Yokoyama, H. Shiraishi, Y. Tani, Y. Yokoyama, Y. Yamaguchi, *J. Am. Chem. Soc.* **2003**, *125*, 7194.
17. T. Shiozawa, M. K. Hossain, T. Ubukata, Y. Yokoyama, *Chem. Commun.* **2010**, *46*, 4785.
18. K. Matsuda, Y. Shinkai, T. Yamaguchi, K. Nomiyama, M. Isayama, M. Irie, *Chem. Lett.* **2003**, *32*, 1178.
19. M. Takeshita, C. N. Choi, M. Irie, *Chem. Commun.* **1997**, 2265.
20. M. Takeshita, M. Nagai, T. Yamato, *Chem. Commun.* **2003**, 1496.

21. S. Aloïse, M. Sliwa, Z. Pawlowska, J. Réhault, J. Dubois, O. Poizat, G. Buntinx, A. Perrier, F. Maurel, S. Yamaguchi, M. Takeshita, *J. Am. Chem. Soc.* **2010**, *132*, 7379.
22. S. Fukumoto, T. Nakashima, T. Kawai, *Angew. Chem. Int. Ed.* **2011**, *50*, 1565.
23. M. Irie, T. Eriguchi, T. Takada, K. Uchida, *Tetrahedron* **1997**, *53*, 12263.
24. A. T. Bens, D. Frewert, K. Kodatis, C. Kryschi, H.-D. Martin, H. P. Trommsdorff, *Eur. J. Org. Chem.* **1998**, 2333.
25. K. Shibata, S. Kobatake, M. Irie, *Chem. Lett.* **2001**, *30*, 618.
26. K. Morimitsu, S. Kobatake, S. Nakamura, M. Irie, *Chem. Lett.* **2003**, *32*, 858.
27. D. Guillaumont, T. Kobayashi, K. Kanda, H. Miyasaka, K. Uchida, S. Kobatake, K. Shibata, S. Nakamura, M. Irie, *J. Phys. Chem. A* **2002**, *106*, 7222.
28. Y.-C. Jeong, J. P. Han, Y. Kim, E. Kim, S. I. Yang, K.-H. Ahn, *Tetrahedron* **2007**, *63*, 3173.
29. K. Uno, H. Niikura, M. Morimoto, Y. Ishibashi, H. Miyasaka, M. Irie, *J. Am. Chem. Soc.* **2011**, *133*, 13558.
30. M. Taguchi, T. Nakagawa, T. Nakashima, T. Kawai, *J. Mater. Chem.* **2011**, *21*, 17425.
31. H. Shoji, S. Kobatake, *Chem. Commun.* **2013**, *49*, 2362.
32. S. L. Gilat, S. H. Kawai, J.-M. Lehn, *Chem. −Eur. J.* **1995**, *1*, 275.
33. S. Nakamura, S, Yokojima, K. Uchida, T. Tsujioka, A. Goldberg, A. Murakami, K. Shinoda, M. Mikami, T. Kobayashi, S. Kobatake, K. Matsuda, M. Irie, *J. Photochem. Photobio. A.* **2008**, *200*, 10.
34. S. Kobatake, K. Shibata, K. Uchida, M. Irie, *J. Am. Chem. Soc.* **2000**, *122*, 12135.
35. S. Kobatake, K. Uchida, E. Tsuchida, M. Irie, *Chem. Lett.* **2000**, *29*, 1340.
36. D. Kitagawa, K. Sasaki, S. Kobatake, *Bull. Chem. Soc. Jpn.* **2011**, *84*, 141.
37. D. Chen, Z. Wang, H. Zhang, *J. Mol. Struct.* **2008**, *859*, 11.
38. J. H. Golden, *J. Chem. Soc.* **1961**, 3741.
39. K. Maeda, T. Hayashi, *Bull. Chem. Soc. Jpn.* **1970**, *43*, 429.
40. M. Kawano, T. Sano, J. Abe, Y. Ohashi, *J. Am. Chem. Soc.* **1999**, *121*, 8106.
41. K. Ichimura, S. Watanabe, *Bull. Chem. Soc. Jpn.* **1976**, *49*, 2220.
42. A. M. Trozzolo, T. M. Leslie, A. S. Sarpotdar, R. D. Small, G. J. Ferraudi, T. DoMinh, R. L. Hartless, *Pure Appl. Chem.* **1979**, *51*, 261.
43. H. Sixl, R. Warta, *Chem. Phys.* **1985**, *94*, 147.
44. Y. Eichen, J.-M. Lehn, M. Scherl, D. Haarer, J. Fischer, A. DeCian, A. Corval, H. P. Trommsdorff, *Angew. Chem. Int. Ed. Engl.* **1995**, *34*, 2530.
45. A. Schmidt, S. Kababya, M. Appel, S. Khatib, M. Botoshansky, Y. Eichen, *J. Am. Chem. Soc*. 1**999**, *121*, 11291.
46. P. Naumov, A. Sekine, H. Uekusa, Y. Ohashi, *J. Am. Chem. Soc.* **2002**, *124*, 8540.
47. E. Hadjoudis, M. Vittorakis, I. Moustakali-Mavridis, *Tetrahedron* **1987**, *43*, 1345.

48. J. Harada, H. Uekusa, Y. Ohashi, *J. Am. Chem. Soc.* **1999**, *121*, 5809.
49. K. Akimoto, H. Kanatomi, A. Nagakari, H. Fukuda, H. Koyama, T. Kawato, *Chem. Commun.* **2003**, 870.
50. Y. Mori, Y. Ohashi, K. Maeda, *Bull. Chem. Soc. Jpn.* **1989**, *62*, 3171.
51. S. Kobatake, M. Irie, *Bull. Chem. Soc. Jpn.* **2004**, *77*, 195.
52. S. Kobatake, K. Uchida, E. Tsuchida, M. Irie, *Chem. Commun.* **2002**, 2804.
53. T. Yamada, S. Kobatake, M. Irie, *Bull. Chem. Soc. Jpn*. **2002**, *75*, 167.
54. M. Morimoto, S. Kobatake, M. Irie, *Adv. Mater.* **2002**, *14*. 1027.
55. M. Morimoto, S. Kobatake, M. Irie, *J. Am. Chem. Soc.* **2003**, *125*, 11080.
56. S. Takami, L. Kuroki, M. Irie, *J. Am. Chem. Soc.* **2007**, *129*, 7319.
57. S. Kobatake, T. Yamada, K. Uchida, N. Kato, M. Irie, *J. Am. Chem. Soc.* **1999**, *121*, 2380.
58. S. Kobatake, M. Yamada, T. Yamada, M. Irie, *J. Am. Chem. Soc.* **1999**, *121*, 8450.
59. S. Kobatake, T. Yamada, M. Irie, *Mol. Cryst. Liq. Cryst.* **2000**, *344*, 185.
60. T. Fukaminato, T. Kawai, S. Kobatake, M. Irie, *J. Phys. Chem. B.* **2003**, *107*, 8372.
61. T. Fukaminato, S. Kobatake, T. Kawai, M. Irie, *Proc. Japan Acad., Ser. B* **2001**, *77*, 30.
62. T. Yamada, K. Muto, S. Kobatake, M. Irie, *J. Org. Chem.* **2001**, *66*, 6164.
63. K. Shibata, K. Muto, S. Kobatake, M. Irie, *J. Phys. Chem. A.* **2002**, *106*, 209.
64. S. Kobatake, H. Muto, M. Irie, *Chem. Lett.* **2006**, *35*, 102.
65. T. Kodani, K. Matsuda, T. Yamada, S. Kobatake, M. Irie, *J. Am. Chem. Soc.* **2000**, *122*, 9631.
66. K. Uchida, M. Walko, J. J. D. de Jong, S. Sukata, S. Kobatake, A. Meetsma, J. van Esch, B. L. Feringa, *Org. Biomol. Chem.* **2006**, *4*, 1002.
67. S. Kobatake, S. Kuma, M. Irie, *J. Phys. Org. Chem.* **2007**, *20*, 960.
68. M. Morimoto, S. Kobatake, M. Irie, *Chem. −Eur. J.* **2003**, *9*, 621.
69. S. Kobatake, S. Kuma, M. Irie, *Bull. Chem. Soc. Jpn.* **2004**, *77*, 945.
70. Y. Asano, A. Murakami, T. Kobayashi, S. Kobatake, M. Irie, S. Yabushita, S. Nakamura, *J. Mol. Struct.(Theochem)* **2003**, *625*, 227.
71. S. Kobatake, M. Morimoto, Y. Asano, A. Murakami, S. Nakamura, M. Irie, *Chem. Lett.* **2002**, 1224.
72. K. Saita, S. Kobatake, T. Fukaminato, S. Nanbu, M. Irie, H. Sekiya, *Chem. Phys. Lett.* **2008**, *454*, 42.
73. T. Yamada, S. Kobatake, K. Muto, M. Irie, *J. Am. Chem. Soc.* **2000**, *122*, 1589.
74. T. Yamada, S. Kobatake, M. Irie, *Bull. Chem. Soc. Jpn*. **2000**, *73*, 2179.
75. T. Hamazaki, K. Matsuda, S. Kobatake, M. Irie, *Bull. Chem. Soc. Jpn*. **2000**, *80*, 365.
76. M. Irie, S. Kobatake, M. Horichi, *Science* **2001**, *291*, 1769.

77. K. Uchida, N. Izumi, S. Sukata, Y. Kojima, S. Nakamura, M. Irie, *Angew. Chem. Int. Ed.* **2006**, *45*, 6470.
78. N. Izumi, T. Minami, H. Mayama, A. Takata, S. Nakamura, S. Yokojima, K. Tsujii, K. Uchida, *Jpn. J. Appl. Phys*. **2008**, *47*, 7298.
79. N. Izumi, N. Nishikawa, S. Yokojima, Y. Kojima, S. Nakamura, S. Kobatake, M. Irie, K. Uchida, *New J. Chem.* **2009**, *33*, 1324.
80. K. Uchida, N. Nishikawa, N. Izumi, S. Yamazoe, H. Mayama, Y. Kojima, S. Yokojima, S. Nakamura, K. Tsujii, M. Irie, *Angew. Chem. Int. Ed.* **2010**, *49*, 5942.
81. A. Uyama, S. Yamazoe, S. Shigematsu, M. Morimoto, S. Yokojima, H. Mayama, Y. Kojima, S. Nakamura, K. Uchida, *Langmuir* **2011**, *27*, 6395.
82. N. Nishikawa, A. Uyama, T. Kamitanaka, H. Mayama, Y. Kojima, S. Yokojima, S. Nakamura, K. Tsujii, K. Uchida, *Chem. −Asian J.* **2011**, *6*, 2400.
83. N. Nishikawa, H. Kiyohara, S. Sakiyama, S. Yamazoe, H. Mayama, T. Tsujioka, Y. Kojima, S. Yokojima, S. Nakamura, K. Uchida, *Langmuir* **2012**, *28*, 17817.
84. N. Nishikawa, S. Sakiyama, S. Yamazoe, Y. Kojima, E. Nishihara, T. Tsujioka, H. Mayama, S. Yokojima, S. Nakamura, K. Uchida, *Langmuir* **2013**, *29*, 8164.
85. S. Kobatake, S. Takami, H. Muto, T. Ishikawa, M. Irie, *Nature* **2007**, *446*, 778.
86. K. Uchida, S. Sukata, Y. Matsuzawa, M. Akazawa, J. J. D. de Jong, N. Katsonis, Y. Kojima, S. Nakamura, J. Areephong, A. Meetsma, B. L. Feringa, *Chem. Commun.* **2008**, 326.
87. L. Kuroki, S. Takami, K. Yoza, M. Morimoto, M. Irie, *Photochem. Photobiol. Sci.* **2010**, *9*, 221.
88. M. Morimoto, M. Irie, *J. Am. Chem. Soc.* **2010**, *132*, 14172.
89. F. Terao, M. Morimoto, M. Irie, *Angew. Chem. Int. Ed.* **2012**, *51*, 901.
90. M. Morimoto, S. Kobatake, M. Irie, *Cryst. Growth Des.* **2003**, *3*, 847.
91. M. Morimoto, S. Kobatake, M. Irie, *Chem. Rec.* **2004**, *4*, 23.
92. M. Morimoto, S. Kobatake, M. Irie, *Photochem. Photobiol. Sci.* **2003**, *2*, 1088.
93. S. Kobatake, Y. Matsumoto, M. Irie, *Angew. Chem. Int. Ed.* **2005**, *44*, 2148.
94. S. Kobatake, M. Morimoto, M. Irie, *Mol. Cryst. Liq. Cryst.* **2005**, *431*, 223.
95. M. Morimoto, S. Kobatake, M. Irie, *Mol. Cryst. Liq. Cryst.* **2005**, *431*, 229.
96. J. Bernstein, *Polymorphism in Molecular Crystals*, Oxford University Press, New York, **2002**.
97. T. Mori, *Chem. Rev.* **2004**, *104*, 4947.
98. H. Kobayashi, H, Cui, A, Kobayashi, *Chem. Rev.* **2004**, *104*, 5265.
99. M. Sorai, M. Nakano, Y. Miyazaki, *Chem. Rev.* **2006**, *106*, 976.
100. T. Mutai, H. Tomoda, T. Ohkawa, Y. Yabe, K. Araki, *Angew. Chem. Int. Ed.* **2008**, *47*, 9522.

101. G. Zhang, J. Lu, M. Sabat, C. L. Fraser, *J. Am. Chem. Soc.* **2010**, *132*, 2160.
102. S. Yamamoto, K. Matsuda, M. Irie, *Org. Lett.* **2003**, *5*, 1769.
103. L. Yu, G. A. Stephenson, C. A. Mitchell, C. A. Bunnell, S. V. Snorek, J. J. Bowyer, T. B. Borchardt, J. G. Stowell, S. R. Byrn, *J. Am. Chem. Soc.* **2000**, *122*, 585.
104. S. Chen, I. A. Guzei, L. Yu, *J. Am. Chem. Soc.* **2005**, *127*, 9881.
105. K. Tsujii, *Surface Activity*: *Principles, Phenomena, and Applications*, Academic Press, New York, 1998, pp. 52‑54.
106. T. Nishino, M. Meguro, K. Nakamae, M. Matsushita, Y. Ueda, *Langmuir* **1999**, *15*, 4321.
107. Y. Liu, L. Tang, R. Wang, H. Lu, L. Li, Y. Kong, K. Qi, J. H. Xin, *J. Mater. Chem.* **2007**, *17*, 1071.
108. L. Feng, S. Li, Y. Li, H. Li, L. Zhang, J. Zhai, Y. Song, B. Liu, L. Jiang, D. Zhu, *Adv. Mater.* **2002**, *14*, 1857.
109. T. Wagner, C. Neinhuis, W. Barthlott, *Acta Zool.* **1996**, *77*, 213.
110. Z. Gu, H. Uetsuka, K. Takahashi, R. Nakajima, H. Onishi, A. Fujishima, O. Sato, *Angew. Chem. Int. Ed.* **2003**, *42*, 894.
111. S. Wang, Y. Song, L. Jiang, *J. Photochem. Photobiol. C* **2007**, *8*, 18.
112. X. Feng, J. Zhai, J. Jiang, *Angew. Chem. Int. Ed.* **2005**, *44*, 5115.
113. W. Zhu, X. Feng, L. Feng, L. Jiang, *Chem. Commun.* **2006**, 2753.
114. S. Wang, X. Feng, J. Yao, L. Jiang, *Angew. Chem. Int. Ed.* **2006**, 45, 1264.
115. W. Jiang, G. Wang, Y. He, X. Wang, Y. An, Y. Song, L. Jiang, *Chem. Commun.* **2005**, 3550.
116. H. Ge, G. Wang, Y. He, X. Wang, Y. Song, L. Jiang, D. Zhua, *ChemPhysChem* **2006**, *7*, 575.
117. R. Rosario, D. Gust, A. A. Garcia, M. Hayes, J. L. Taraci, T. Clement, J. W. Dailey, S. T. Picraux, *J. Phys. Chem. B* **2004**, *108*, 12640.
118. A. Athanassiou, M. I. Lygeraki, D. Pisignano, K. Lakiotaki, M. Varda, E. Mele, C. Fotakis, R. Cingolani, S. H. Anastasiadis, *Langmuir* **2006**, *22*, 2329.
119. E. Mele, D. Pisignano, M. Varda, M. Farsari, G. Filippidis, C. Fotakis, A. Athanassiou, R. Cingolani, *Appl. Phys. Lett.* **2006**, *88*, 203124.
120. A. Nayak, H. Liu, G. Belfort, *Angew. Chem. Int. Ed.* **2006**, *45*, 4094.
121. I. Vlassiouk, C.-D. Park, S. A. Vail, D. Gust, S. Smirnov, *Nano Lett.* **2006**, *6*, 1013.
122. H. Koshima, H. Nakaya, H. Uchimoto, N. Ojima, *Chem. Lett.* **2012**, *41*, 107.
123. H. Koshima, N. Ojima, H. Uchimoto, *J. Am. Chem. Soc.* **2009**, *131*, 6890.
124. H. Koshima, N. Ojima, *Dyes Pigm.* **2012**, *92*, 798.
125. O. S. Bushuyev, T. A. Singleton, C. J. Barrett, *Adv. Mater.* **2013**, *25*, 1796.
126. O. S. Bushuyev, A. Tomberg, T. Friščić, C. J. Barrett, *J. Am. Chem. Soc.* **2013**, *135*,

12556.
127. H. Koshima, K. Takechi, H. Uchimoto, M. Shiro, D. Hashizume, *Chem. Commun.* **2011**, *47*, 11423.
128. H. Koshima, R. Matsuo, M. Matsudomi, Y. Uemura, M. Shiro, *Cryst. Growth Des.* **2013**, *13*, 4330.
129. R. O. Al-Kaysi, A. M. Müller, C. J. Bardeen, *J. Am. Chem. Soc.* **2006**, *128*, 15938.
130. R. O. Al-Kaysi, C. J. Bardeen, *Adv. Mater.* **2007**, *19*, 1276.
131. L. Zhu, R. O. Al-Kaysi, R. J. Dillon, F. S. Tham, C. J. Bardeen, *Cryst. Growth Des.* **2011**, *11*, 4975.
132. L. Zhu, R. O. Al-Kaysi, C. J. Bardeen, *J. Am. Chem. Soc.* **2011**, *133*, 12569.
133. L. Zhu, A. Agarwal, J. Lai, R. O. Al-Kaysi, F. S. Tham, T. Ghaddar, L. Muellera, C. J. Bardeen, *J. Mater. Chem.* **2011**, *21*, 6258.
134. T. Kim, M. K. Al-Muhanna, S. D. Al-Suwaidan, R. O. Al-Kaysi, C. J. Bardeen, *Angew. Chem. Int. Ed*. **2013**, *52*, 6889.
135. T. Kim, L. Zhu, L. J. Mueller, C. J. Bardeen, *CrystEngComm* **2012**, *14*, 7792.
136. J.-K. Sun, W. Li, C. Chen, C.-X. Ren, D.-M. Pan, J. Zhang, *Angew. Chem. Int. Ed.* **2013**, *52*, 6653.
137. P. Naumov, J. Kowalik, K. M. Solntsev, A. Baldridge, J.-S. Moon, C. Kranz, L. M. Tolbert, *J. Am. Chem. Soc.* **2010**, *132*, 5845.

Part I
Polymorphism and Phase Transition between Polymorphic Forms of Diarylethene Crystals

Chapter 1

Thermodynamic Phase Transition through Crystal-to-Crystal Process of a Photochromic Diarylethene Crystal

1.1 Introduction

As mentioned in General Introduction, polymorphism has attracted the attention of many scientists because of the importance in many areas of chemical researches.[1] Phase transition between polymorphic forms has also been much attention because the solid state properties can change on the basis of molecular packing in each crystal forms.[2-6] It can be expected that the combination of photochromism and phase transition provides new functional photo- and thermal-responsive materials.

There are some reports on the polymorphism of diarylethene derivatives.[7,8] 1,2-Bis(2-methyl-5-*p*-methoxyphenyl-3-thienyl)perfluorocyclopentene can form four polymorphic crystals by recrystallization from *n*-hexane, and the photocycloreversion quantum yields of the photogenerated closed-ring isomer in such four crystals are different from each other because of a difference in the conformation of the closed-ring isomers in the crystals.[7] However, there is no research on the phase transition between polymorphic forms of diarylethene crystals.

In this chapter, it has been found that the diarylethene (**1a**) has two polymorphs and one undergoes thermodynamic phase transition to the other without any melting. Polymorphs, photochromism, and thermodynamic phase transition via a crystal-to-crystal process of diarylethene **1a** are investigated in detail. Furthermore, the motion of molecules in the phase transition is proposed based on single-crystal X-ray crystallography of two polymorphs in this chapter.

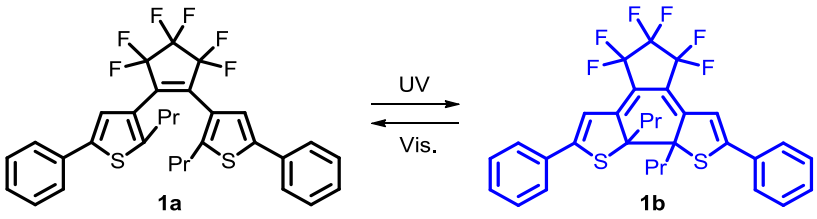

1.2 Experimental Section

1.2.1 General

A phase transition of crystals was observed using a Nikon ECLIPSE E600POL polarizing optical microscope or a Keyence VHX-500 digital microscope, equipped with a Mettler-Toledo FP82HT hot stage and FP90 central processor. Differential scanning

calorimetry (DSC) was run using a Seiko DSC-6200. Polarized absorption spectra were measured using the polarizing optical microscope connected with a Hamamatsu PMA-11 photodetector. Powder X-ray diffraction profiles were recorded on a Rigaku RINT-2100 diffractometer employing $Cu_{K\alpha}$ radiation (λ = 1.54184 Å). Single crystal X-ray crystallographic analysis was carried out using a Rigaku RAXIS RAPID imaging plate diffractometer with $Mo_{K\alpha}$ radiation (λ = 0.71073 Å) monochromated by graphite. The crystal structures were solved by a direct method using SIR92 and refined by the full-matrix least-squares method on F^2 with anisotropic displacement parameters for non-hydrogen atoms using SHELXL-97.[9] UV irradiation was carried out using a Keyence UV-LED UV-400 (365-nm light), and a super high pressure mercury lamp (100 W; UV-1A filter (365 nm light excitation)) attached with the polarizing optical microscope. Visible light irradiation was carried out using a halogen lamp (100 W).

1.2.2 Materials

Diarylethene **1a** was synthesized according to the literature.[10] The single crystals of **1a-α** and **1a-β** were first obtained by recrystallization from acetone and *n*-hexane, respectively.

1.3 Results and Discussion

1.3.1 Polymorphism

When diarylethene **1a** was recrystallized from acetone or *n*-hexane, two types of crystals with different shapes, denoted as **1a-α** and **1a-β**, were obtained from each solution. Figure 1-1 shows the shapes of α- and β-crystals. The α-crystal has a block shape, which was obtained from acetone. By contrast, the β-crystal has a plate shape with a parallelogram, which was obtained from *n*-hexane. X-ray crystallographic analysis of these crystals was performed to examine which of those are polymorphic forms. The crystallographic data are summarized in

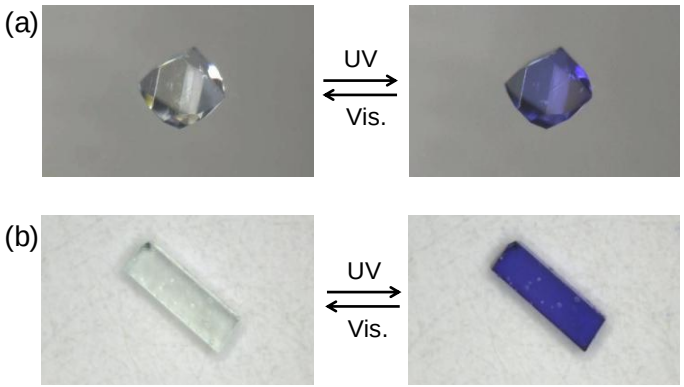

Figure 1-1. Photochromism of **1a-α** (a) and **1a-β** (b) in the single-crystalline phase. Both **1a-α** and **1a-β** turned blue upon irradiation with UV light.

Table 1-1.[11] The crystal system of both crystals is monoclinic, but the space groups of **1a-α** and **1a-β** are $P2_1/c$ and $C2/c$, respectively. The crystal of **1a-α** has one molecule in the asymmetric unit, while the crystal of **1a-β** has half of a molecule in the asymmetric unit. In both crystal forms, there are four molecules in the unit cell. The distances between the reactive carbons in the α- and β-crystals were 3.73 and 3.77 Å, respectively, which are sufficiently short for photocyclization to take place in the crystalline phase.[12] Indeed, both crystals underwent a photochromic reaction in the crystalline phase upon alternating irradiation with UV and visible light. Upon UV irradiation, the initially colorless single crystals of α- and β-crystals turned blue. Both colored crystals had absorption maxima at 600 nm. The blue-colored crystals turned colorless again upon irradiation with visible light, as shown in Figure 1-1. The molecular packing diagrams of **1a** in the α- and β-crystals are shown in Figure 1-2. The molecular packings in both crystals are quite similar to each other. The difference between the molecular packings is ascribed to the orientation of two of four molecules in the unit cell. In the α-crystal, CH-π intermolecular interactions exist between propyl and phenyl groups. By contrast, no such interaction is observed in the β-crystal.

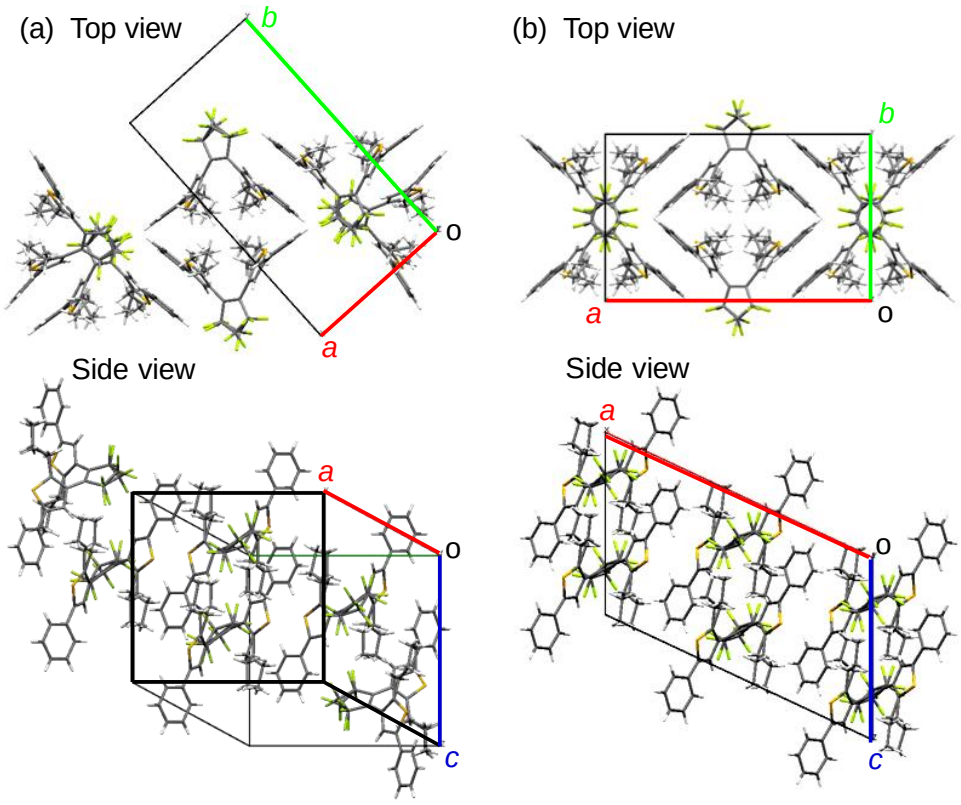

Figure 1-2. Molecular packing diagrams of **1a-α** (a) and **1a-β** (b). The propyl groups and perfluorocyclopentene rings in **1a-α** and **1a-β** are disordered.

Table 1-1. X-ray crystallographic data for **1a-α**, **1a-β**, and **1a-α** after heating for 0.5 h at 100 °C.

	1a-α	**1a-β**	after heating of **1a-α**[a]
Formula	$C_{31}H_{26}F_6S_2$	$C_{31}H_{26}F_6S_2$	$C_{31}H_{26}F_6S_2$
Formula weight	576.66	576.66	576.66
Temperature	303(2) K	303(2) K	303(2) K
Crystal system	Monoclinic	Monoclinic	–
Space group	$P2_1/c$	$C2/c$	–
Unit cell dimensions	a = 11.765(5) Å	a = 21.000(4) Å	a = 20.720 Å
	b = 19.985(7) Å	b = 11.980(2) Å	b = 11.810 Å
	c = 13.298(6) Å	c = 12.943(3) Å	c = 12.720 Å
	α = 90°	α = 90°	α = 89.940°
	β = 111.99(3)°	β = 115.058(4)°	β = 115.080°
	γ = 90°	γ = 90°	γ = 89.860°
Volume	2899(2) Å^3	2949.7(10) Å^3	2819.1 Å^3
Z	4	4	–
Density	1.321 g cm^{-3}	1.298 g cm^{-3}	–
Goodness-of-fit on F^2	1.063	0.942	–
$R(I > 2\sigma(I))$	$R1$ = 0.0402	$R1$ = 0.0560	–
R(all data)	$wR2$ = 0.1122	$wR2$ = 0.1599	–

[a] Although X-ray crystallographic analysis could not be established, the cell dimensions could be determined. The cell dimensions were used for determining face indices.

1.3.2 Thermodynamic Phase Transition

The thermodynamic stability of the polymorphic crystals was examined by differential scanning calorimetry (DSC). Figure 1-3 shows the DSC traces of the α- and β-crystals. When

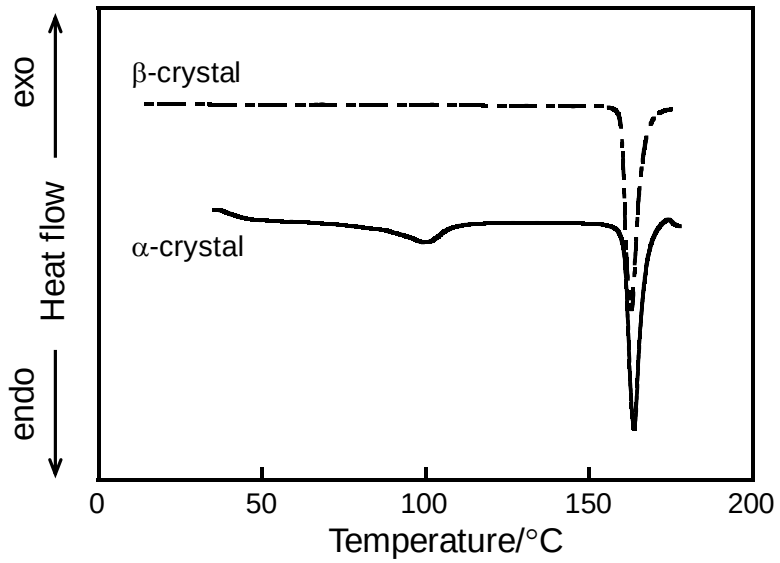

Figure 1-3. DSC traces of **1a-α** and **1a-β** at a heating rate of 10 °C min^{-1}.

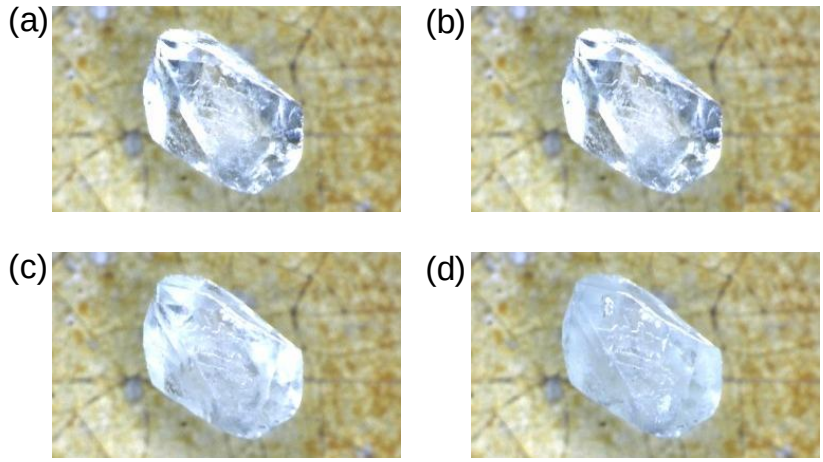

Figure 1-4. Optical microscopic photographs of an α-crystal observed in the reflection mode at increasing temperature: (a) 100, (b) 110, (c) 120, and (d) 130 °C.

the powder crystal of **1a-α** was heated at a rate of 10 °C min^{-1}, the crystal exhibited a small endothermic behavior due to a phase transition at 100 °C and a large endothermic behavior due to the crystal melting at 160 °C. The β-crystal showed only a large endothermic behavior corresponding to the crystal melting at 160 °C. The melting point after the phase transition for the α-crystal is the same as that for the β-crystal, which suggests that the phase transition occurred from the α-form to the β-form.

To examine the phase-transition behavior of the single crystal of **1a-α**, the crystal was observed by optical microscopy in the reflection mode. The initial α-crystal is colorless transparent. When the α-crystal was heated at a rate of 10 °C min^{-1}, the colorless crystal

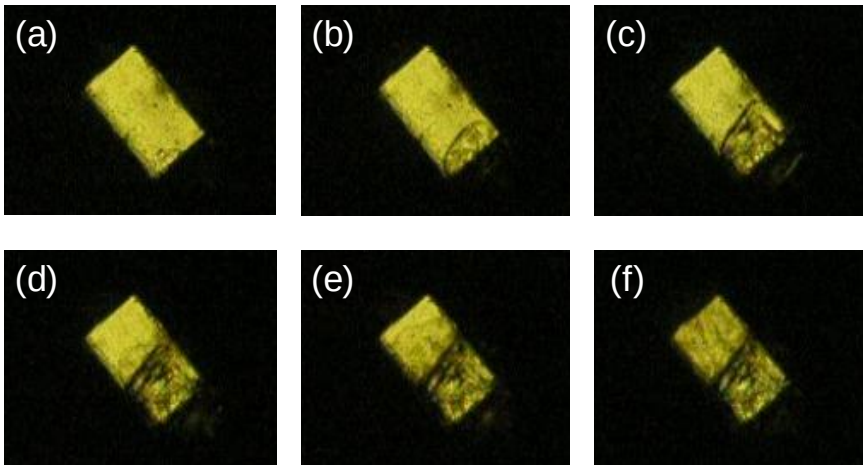

Figure 1-5. Optical microscopic photographs of an α-crystal observed crossed Nicols at increasing temperature: (a) 110.0, (a) 112.5, (c) 113.3, (d) 114.2, (e) 115.0, and (f) 120.0 °C.

turned gradually opaque without melting of the crystal, as shown in Figure 1-4. This opaque appearance is ascribed to a slight decrease in the crystallinity due to a crystal-to-crystal phase transition. Figure 1-5 also shows the phase-transition behavior observed under crossed Nicols at a rate of 10 °C min^{-1}. When the temperature reached 110 °C, a thermodynamic phase transition was initiated from the right bottom, and the phase-transition behavior continued until 120 °C. The crystal was bright from the beginning to the end of the transitions, which means that the crystallinity was maintained during the phase transition.

To examine the motion of the molecules during the phase transition, a photoirradiated colored crystal was observed under polarized light. At a certain angle (θ = 0°), the color became more intense. When the crystal was rotated as much as 90°, the color became weak. The polarized absorption spectra of the colored crystals were compared before and after the phase transition. Figure 1-6a shows the polarized absorption spectra of the photogenerated closed-ring isomer on the (0 2 $\bar{1}$) face of the α-crystal. The angle of 0° was set to a direction of the maximum absorbance. The absorption spectra had a maximum at 600 nm. The polar plots of the absorbance at 600 nm are shown in Figure 1-6a. After bleaching the crystal by irradiation with visible light, the crystal underwent a phase transition upon heating for 0.5 h at 100 °C. Figure 1-6b shows the polarized absorption spectra of the photogenerated closed-ring isomer and the polar plots after the phase transition. The shapes of the polar plots are similar to each other before and after the phase transition. This indicates that the molecules do not move largely, when the molecular packing is viewed on the face. The order parameter [$(A_{0°} - A_{90°})/(A_{0°} + 2A_{90°})$] was determined to be 0.65 and 0.61 before and after the phase transition, respectively. The small order parameter is due to two electronic transition moments of short and long axes of the molecule **1b**. The similar order parameter before and after the phase transition indicates that the crystallinity is maintained during the phase transition.

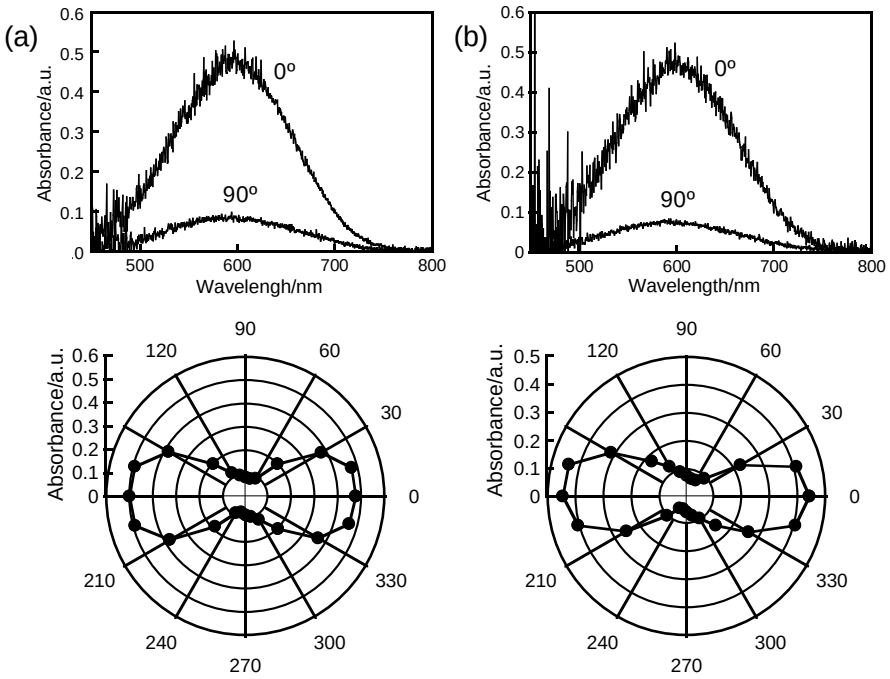

Figure 1-6. Polarized absorption spectra of the photoirradiated colored crystals and the polar plots of absorbance at 600 nm before (a) and after (b) the phase transition. The measurement was carried out on the (0 2 $\bar{1}$) face of α-crystal. The angle of 0° was set to a direction of the maximum absorbance before the phase transition. The same face and angle was used for the measurement after the phase transition.

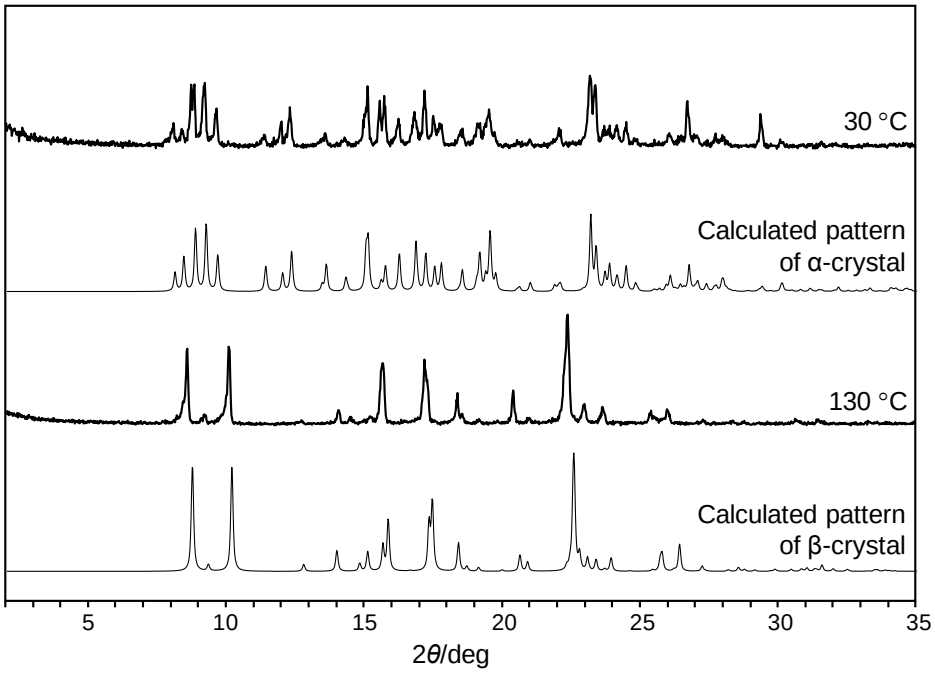

Figure 1-7. Powder X-ray diffraction patterns measured at 30 and 130 °C. The calculated patterns were obtained using parameters determined from single-crystal X-ray crystallographic analysis of α- and β-forms at 30 °C.

The thermodynamic phase transition from α- to β-forms was analyzed by powder X-ray diffraction. Figure 1-7 shows the profiles at 30 and 130 °C and the calculated patterns of α- and β-forms obtained from single-crystal X-ray crystallographic analysis. The diffraction profile after heating above 130 °C was identical to that of the β-form. Thus, a polymorphic phase transition was found to occur from α- to β-forms upon heating. The phase transition was thermally irreversible, and the β-form cannot return to the α-form even at −150 °C.

1.3.3 Movement of Molecules in the Crystal

To investigate the movement of the molecules during the phase transition, in situ X-ray crystallographic analysis of a single crystal before and after the phase transition was performed. However, X-ray crystallographic analysis of the single crystal after the phase transition could not be performed because the crystal often became opaque after the phase transition due to a slight decrease in the crystallinity. Nevertheless, we could determine cell parameters and face indices from the analysis of the crystal after the phase transition. Therefore, we investigated the change of the face indices before and after the phase transition. Figure 1-8 shows the crystal shape and face indices before and after the phase transition viewed from the cross-section. Before the phase transition, the face indices of well-developed surfaces are (0 2 $\bar{1}$), (0 $\bar{2}$ $\bar{1}$), (0 $\bar{2}$ 1), and (0 2 1). When the α-crystal was heated for 0.5 h at 100 °C to undergo the phase transition, the cell dimensions changed to those of the β-form, as shown in Table 1-1. The face indices also changed in two types, patterns A and B, as shown in Figure 1-8: patterns A and B were present 5 times each in the measurement of the face indices of 10 crystals analyzed. This result means that the phase transition takes place like a domino reaction taking advantage of the molecule that moved first. In pattern A, the face indices of (0 2 $\bar{1}$), (0 $\bar{2}$ $\bar{1}$), (0 $\bar{2}$ 1), and (0 2 1) changed to ($\bar{1}$ 1 1), (1 $\bar{1}$ 1), (1 $\bar{1}$ $\bar{1}$), and ($\bar{1}$ 1 $\bar{1}$), respectively. By contrast, in pattern B, they changed to (1 1 1), ($\bar{1}$ $\bar{1}$ 1), ($\bar{1}$ $\bar{1}$ $\bar{1}$), and (1 1 $\bar{1}$), respectively. From these face indices, the molecular packing before and after the phase

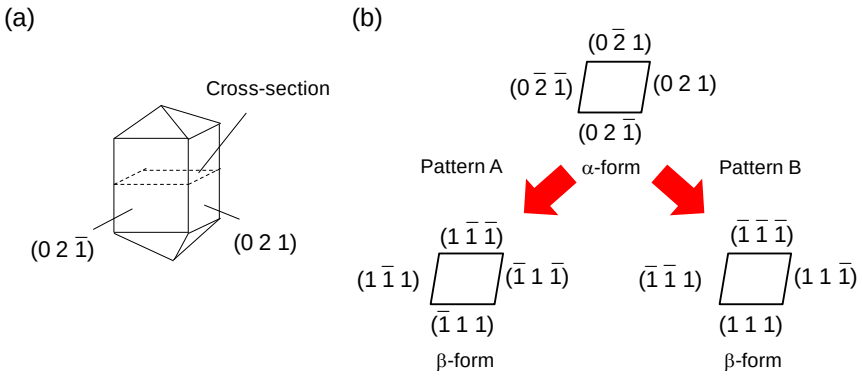

Figure 1-8. The shape of the crystal (a) and the face indices before and after the phase transition viewed from the cross-section (b).

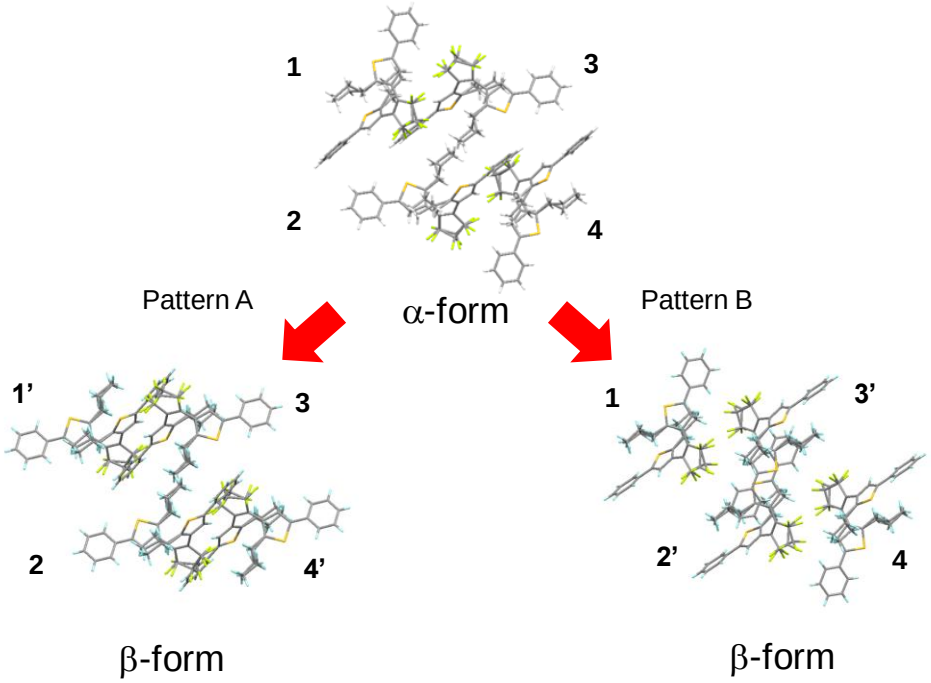

Figure 1-9. The molecular packing before and after the phase transition viewed from the cross-section. The molecules are numbered from 1 to 4, respectively. In pattern A, the molecules of 1 and 4 move to 1' and 4', respectively. In pattern B, the molecules of 2 and 3 move to 2' and 3' respectively.

transition in both patterns has been clarified, as shown in Figure 1-9. The molecules are numbered from 1 to 4 to distinguish the molecules. The result clearly shows that when the phase transition occurs in pattern A, the molecules of 1 and 4 move and those of 2 and 3 do not move. By contrast, in pattern B, the molecules of 2 and 3 moved and those of 1 and 4 do not move. The motion of each molecule is relatively small so that the crystal can maintain its shape after the phase transition.

1.4 Summary

The polymorphism of 1,2-bis(5-phenyl-2-propyl-3-thienyl)perfluorocyclopentene (**1a**) was discovered. Both the block α-crystal and the platelet β-crystal exhibited photochromism in the crystalline phase. The thermodynamic phase transition from α- to β-crystals was investigated using optical microscopy, polarized optical microscopy, and powder X-ray diffraction measurements. The results showed that the phase transition from α- to β-crystals occurs via a crystal-to-crystal process. Moreover, the movement of the molecules in the crystal occurs like a domino reaction, as confirmed by measuring the face indices before and after the phase transition. This is the first example of a thermodynamic phase transition via a crystal-to-crystal process of diarylethene crystals.

1.5 References

1. J. Bernstein, *Polymorphism in Molecular Crystals*, Oxford University Press, New York, **2002**.
2. T. Mori, *Chem. Rev.* **2004**, *104*, 4947.
3. H. Kobayashi, H, Cui, A, Kobayashi, *Chem. Rev.* **2004**, *104*, 5265.
4. M. Sorai, M. Nakano, Y. Miyazaki, *Chem. Rev.* **2006**, *106*, 976.
5. T. Mutai, H. Tomoda, T. Ohkawa, Y. Yabe, K. Araki, *Angew. Chem. Int. Ed.* **2008**, *47*, 9522.
6. G. Zhang, J. Lu, M. Sabat, C. L. Fraser, *J. Am. Chem. Soc.* **2010**, *132*, 2160.
7. M. Morimoto, S. Kobatake, M. Irie, *Chem. −Eur. J.* **2003**, *9*, 621.
8. S. Yamamoto, K. Matsuda, M. Irie, *Org. Lett.* **2003**, *5*, 1769.
9. G. M. Sheldrick, *SHELXL-97*, *Program for Crystal Structure Refinement*, University of Göttingen, Germany, **1997**.
10. D. Kitagawa, K. Sasaki, S. Kobatake, *Bull. Chem. Soc. Jpn.* **2011**, *84*, 141.
11. CCDC 950555 (**1a-α**), and CCDC 950556 (**1a-β**) contain the supplementary crystallographic data. These data can be obtained free of charge from The Cambridge Crystallographic Data Centre via www.ccdc.cam.ac.uk/data_request/cif.
12. S. Kobatake, K. Uchida, E. Tsuchida, M. Irie, *Chem. Commun.* **2002**, 2804.

Chapter 2

Photoinduced Phase Transition between Polymorphic Crystals of a Photochromic Diarylethene

2.1 Introduction

Polymorphism and phase transition between polymorphic forms have been much attention because solid state properties are different in their crystal forms on the basis of molecular packings as described in General Introduction.[1-6] There are two types in phase transition processes: crystal-to-crystal and crystal-to-melt-to-crystal processes. In Chapter 1, the phase transition between the polymorphic forms via the crystal-to-crystal process of diarylethene **1a** has been described. In the crystal-to-crystal process, the motion of molecules in the crystal is small. Therefore, no large change of solid properties is expected. On the other hand, it can be expected that the solid state properties change largely in crystal-to-melt-to-crystal process because the molecules move largely before and after the phase transition.

Diarylethene **2a** adopts three polymorphic forms. The α-form of **2a** is obtained by recrystallization from *n*-hexane, toluene, or ethyl acetate.[7] The β-form of **2a** is obtained by recrystallization from acetone or chloroform,[7] and the solvent is incorporated into the crystal in this form. Here, it has newly been found that the α-form undergoes a thermodynamic phase transition upon heating at 180−190 °C to form the needle-like γ-form in a few minutes. The phase transition from the α-form to the γ-form requires the melting of crystal. Then, the molecular packings between the α-from and γ-from are quite different. Furthermore, it has been clarified that the phase transition temperature can be controlled by irradiation with UV light. Photoinduced micropatterning of phase transition has also been performed. The patterning is established with the resolution of ca. 20 μm

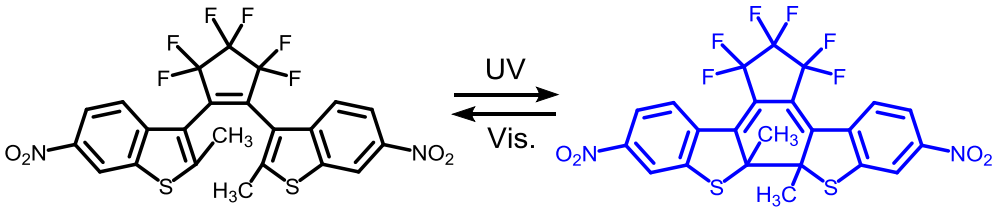

2a **2b**

2.2 Experimental Section

2.2.1 General

Differential scanning calorimetry (DSC) was run using a Seiko DSC-6200. Film surfaces were observed using a Keyence VK-8700 laser scanning microscope, and a Keyence VHX-500 digital microscope. Powder X-ray diffraction profiles were recorded on a Rigaku

RINT-2100 diffractometer employing $Cu_{K\alpha}$ radiation. UV irradiation was carried out using a Keyence UV-LED UV-400 (365-nm light). The photopatterning was performed using DNP FINE LINE TEST PATTERN-I. The sample was kept away a distance of 4.5 cm from a UV-50A head. Visible light irradiation was carried out using a halogen lamp.

2.2.2 Materials

Diarylethene **2a** was synthesized according to the method described in the literature.[7] The α-crystalline form of **2a** was obtained by recrystallization from *n*-hexane.

2.2.3 Preparation of Film

A thin microcrystalline film of **2a** was prepared by dropping 3-5 drops of a solution of **2a** (30 mg) in ethyl acetate (3 mL) onto a thin cover glass to be followed by drying in air for 1h at 70 °C. The film thickness was estimated to be about 2.5 μm.

2.3 Results and Discussion

2.3.1 Phase Transition of Polymorphic Forms by Heating

When the platelet-shaped α-crystals of **2a** were heated at 180−190 °C, the crystal morphology changed from platelet to the needle-shaped due to the thermodynamic phase transition. First, the phase transition behavior of the powder microcrystals was observed by optical microscopy. Figure 2-1 shows the change in the crystal morphology observed under crossed Nicols before and after the phase transition. Before the phase transition, powder crystals of the α-form were present on the glass plate. When the crystals were heated at a rate of 1 °C min^{-1}, the crystal morphology changed significantly as a result of the phase transition at 180−190 °C. Small needle-like crystals were observed over the entire glass surface, and none of the initial α-form remained.

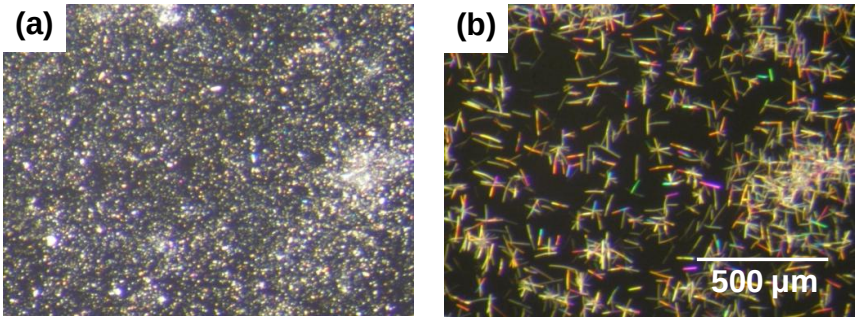

Figure 2-1. Photographs of microcrystals of **2a** observed under crossed Nicols (a) before and (b) after the thermodynamic phase transition. At a rate of temperature increase of 1 °C min^{-1}, (b) was observed at 180−190 °C.

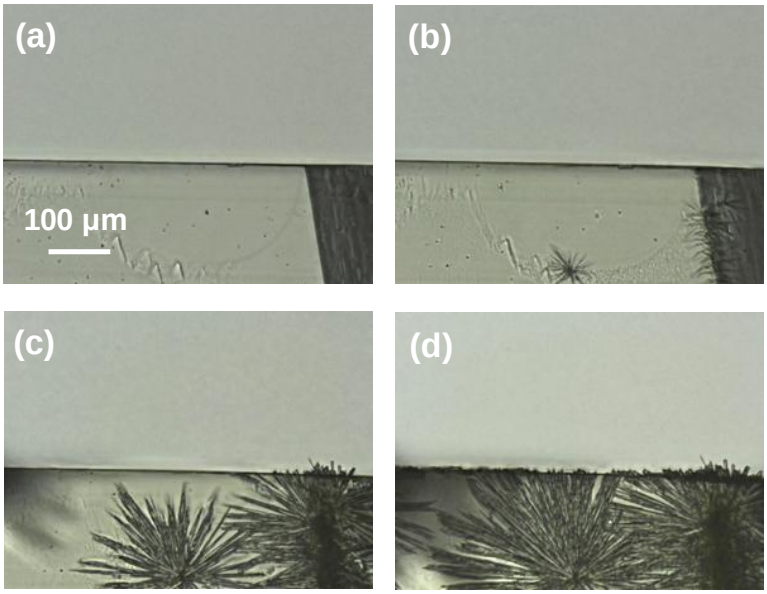

Figure 2-2. Photographs taken during the thermodynamic phase transition between the α-crystal and the γ-crystal: (a) at room temperature, (b) after heating for 1, (c) 3, and (d) 5 min at 190 °C.

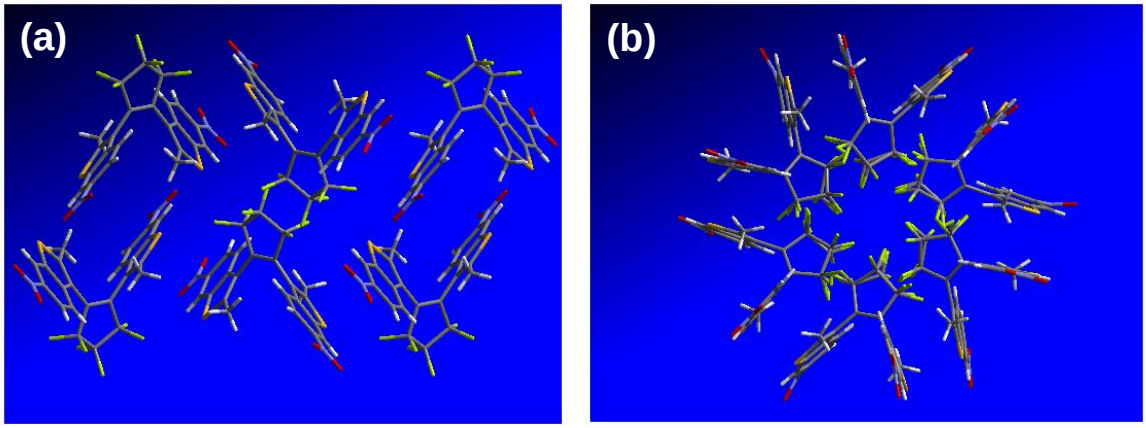

Figure 2-3. Molecular packing of **2a**: (a) α- and (b) γ-forms.

Figure 2-2 displays optical microscopic photographs of a single crystal observed during the thermodynamic phase transition. When the single crystal of the α-form was heated for a few minutes at 190 °C, needle-like crystals of **2a-γ** appeared on the crystal surface. These needle-like crystals of **2a-γ** were developed with the crystal growth on the crystal surface to become stable at temperature. X-ray crystallographic data revealed that the molecular packing of **2a** in the γ-crystal was quite different from that in the α-crystal, as shown in Figure 2-3 and Table 2-1, which indicates that the thermodynamic phase transition from the α-form to γ-form is not accompanied by the crystal-to-crystal phase transition. The initiation of the phase transition is due to the melting of the α-crystal.

Table 2-1. X-ray crystallographic data of **2a-α** and **2a-γ**.

	2a-α	**2a-γ**
Formula	$C_{23}H_{12}F_6N_2O_4S_2$	$C_{23}H_{12}F_6N_2O_4S_2$
Formula weight	558.47	558.47
Temperature	296(2) K	190(2) K
Crystal system	Monoclinic	Trigonal
Space group	$P2_1/c$	$R\bar{3}$
Unit cell dimensions	a = 9.9409(17) Å	a = 32.1473(15) Å
	b = 15.748(3) Å	b = 32.1473(15) Å
	c = 14.492(3) Å	c = 11.6175(8) Å
	α = 90°	α = 90°
	β = 100.297(4)°	β = 90°
	γ = 90°	γ = 120°
Volume	2232.1(7) Å^3	10397.6(10) Å^3
Z	4	18
Density	1.662 g cm^{-3}	1.605 g cm^{-3}
Goodness-of-fit on F^2	1.068	1.104
$R(I > 2\sigma(I))$	$R1$ = 0.0413	$R1$ = 0.0692
R(all data)	$wR2$ = 0.1320	$wR2$ = 0.1208
χ	−	0.12(7)

Next, the change was observed by differential scanning calorimetry (DSC). Figure 2-4 shows DSC traces of the crystal. When the powder crystal of **2a-α** was heated up at a rate of 5 °C min^{-1} (1st scan), the crystal underwent the phase transition according to the endothermic and the exothermic behavior at 190 °C and then melted at 220 °C. The isotropic melt was cooled to −20 °C at a rate of 10 °C min^{-1} and then re-heated to 230 °C at a rate of 5 °C min^{-1} (2nd scan). The exothermic behavior in the 2nd scan was observed at 130 °C, which was due to crystallization of the γ-crystal from the isotropic liquid. This indicates that the γ-crystal was thermodynamically stable at this high temperature. The endothermic behavior at 220 °C in the 2nd scan was due to melting of the γ-form.

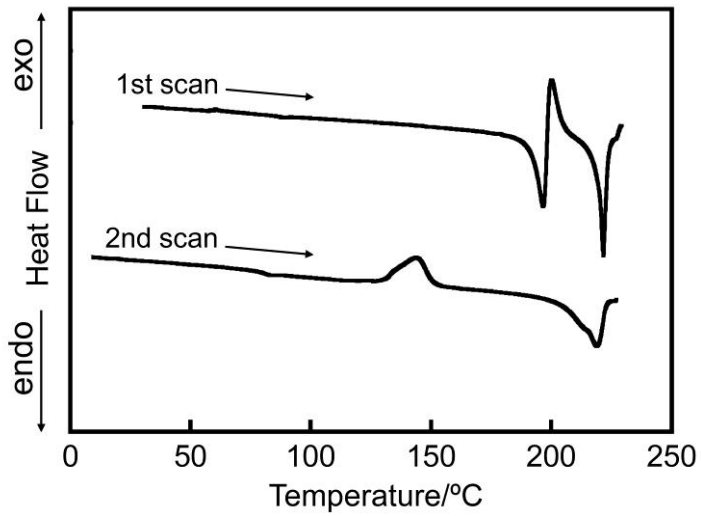

Figure 2-4. Differential scanning calorimetry (DSC) traces of **2a** obtained at a heating rate of 5 °C min^{-1}. The α-crystal of **2a** was used as the initial sample.

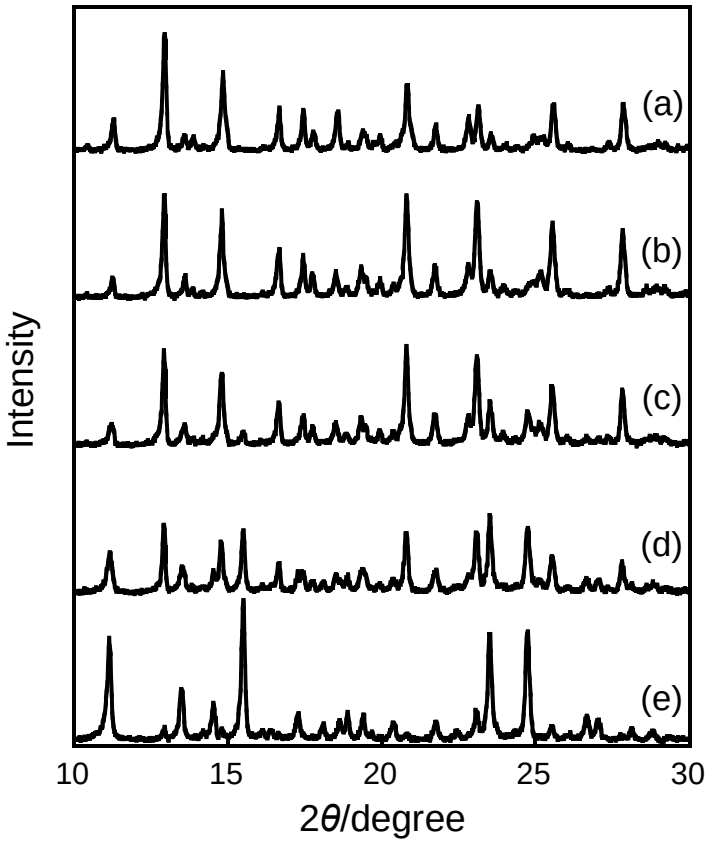

Figure 2-5. Powder diffraction pattern profiles obtained during heating of the α-crystal of **2a** at (a) 170, (b) 190, (c) 195, (d) 200, and (e) 205 °C.

Powder X-ray diffraction spectra were measured to reveal the mechanism of the phase transition from the α-crystal to the γ-crystal upon heating. Figure 2-5 shows the powder

diffraction profiles at various temperatures. With increasing temperature, the peaks of the α-crystal gradually decreased, while those of the γ-crystal became clearly discernible above 195 °C, and no peak shift was observed. This result further indicated that the phase transition from the α-crystal to the γ-crystal occurred via the isotropic state by melting of the α-crystal. The isotropic state was unstable at such high temperature, and rapidly crystallized to form the γ-crystal.

2.3.2 Photomicropatterning by Photoinduced Phase Transition

The phase transition temperature from the α-crystal to the γ-crystal involves melting of the α-crystal and growth of the γ-crystal. If the melting temperature of the α-crystal is controlled by the photochromic conversion from **2a** to **2b**, reaction, the phase transition may be selectively induced in a defined space upon photoirradiation. To clarify the melting temperature (phase transition temperature) of the crystal after photoirradiation, a mixture of the open- and closed-ring isomers was employed to determine this temperature. The initial phase transition temperature was measured by observation with a microscope at various mixing ratios of **2a** and **2b** at a heating rate of 1 °C min^{-1} as shown in Figure 2-7. The initial phase transition of the neat α-crystal was observed at 180 °C. When the content of **2b** in the mixture of **2a** and **2b** was increased, the initial phase transition temperature decreased. This can be ascribed to the impurity effect of the presence of **2b**. However, when the content of **2b** exceeded 20 mol%, the phase transition temperature increased with increasing content of **2b**. When 20 mol% of **2b** was present in the mixture, the phase transition temperature attained its

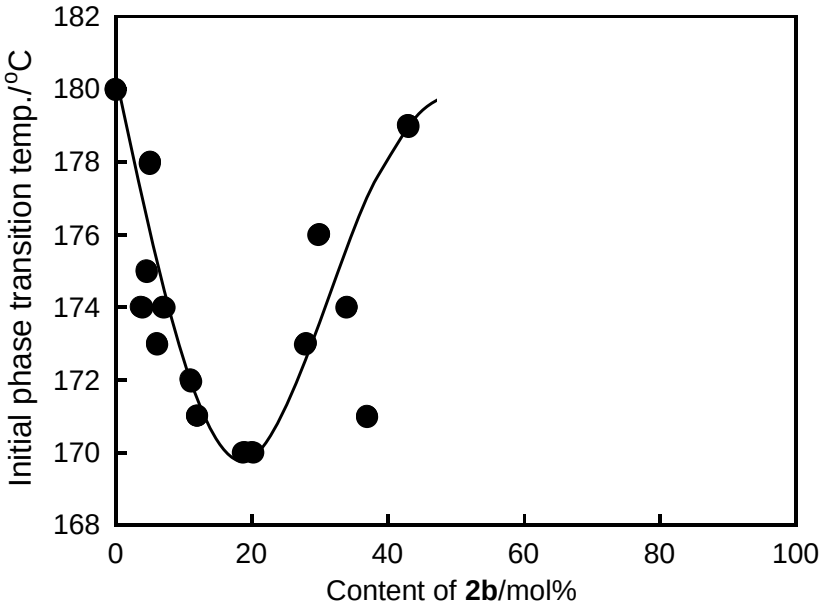

Figure 2-7. Relationship between the initial phase transition temperature and the content of **2b**. The rate of increasing temperature is 1 °C min^{-1}.

lowest value, 170 °C. These results revealed that a photoirradiated area including as much as 20 mol% of **2b** could undergo the phase transition even at 170 °C, as shown in Figure 2-8. In other words, the phase transition can occur in the photoirradiated area and not in the non-irradiated area at 170 °C.

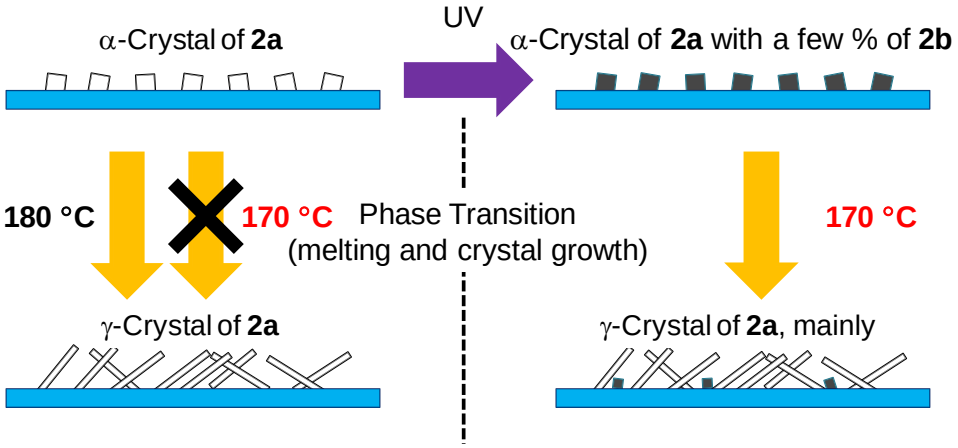

Figure 2-8. Schematic illustration of the difference in the phase transition by heating at 180 °C (left side) and heating at 170 °C after UV irradiation (right side).

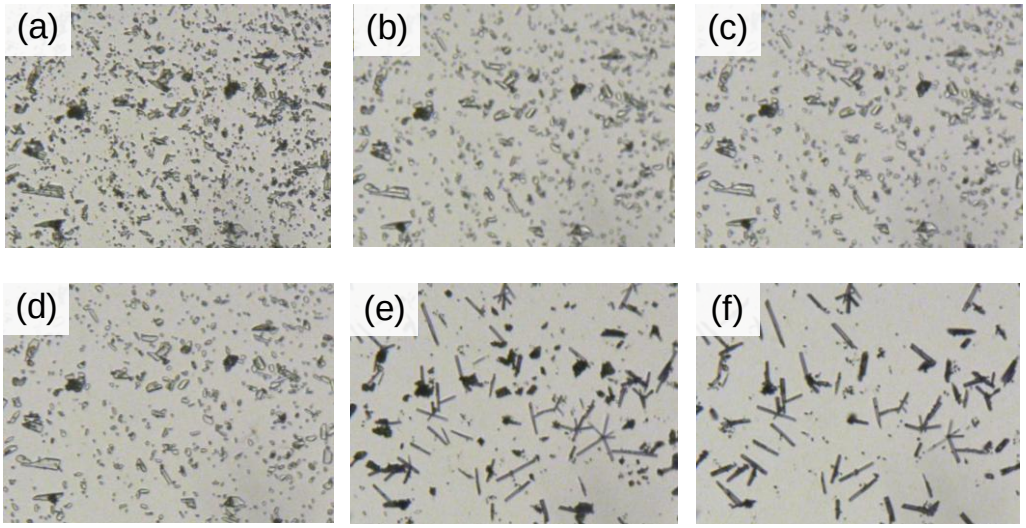

Figure 2-9. Photographs of the powder crystals of **2a** on (a–c) the non-irradiated area and (d–f) the UV-irradiated area after heating for (a, d) 0, (b, e) 10, and (c, f) 20 min at 170 °C. All of the photographs were obtained at room temperature.

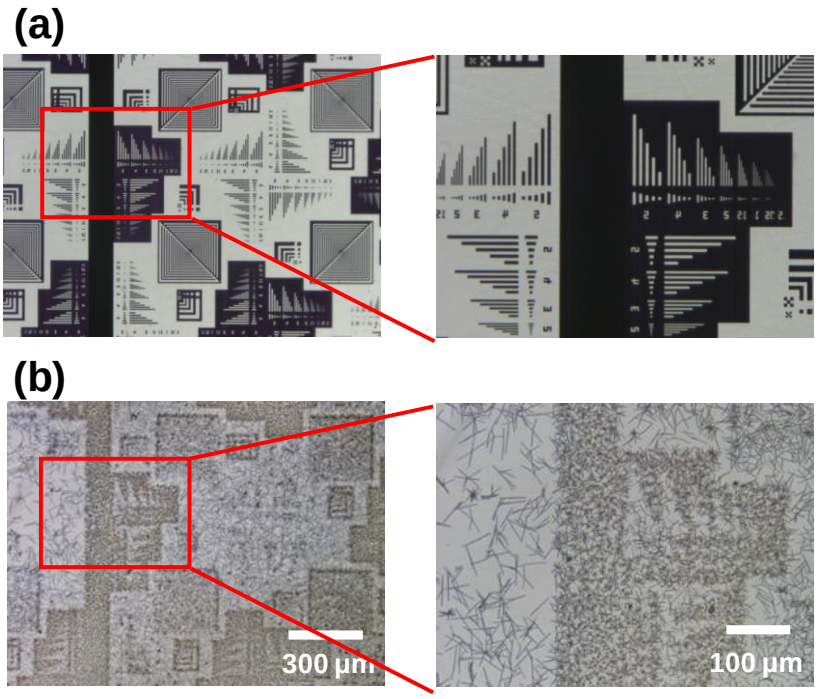

Figure 2-10. Optical microphotographs of (a) the mask pattern and (b) the patterning by the phase transition upon heating for 1 h at 170 °C after irradiation with 365 nm light using the photomask.

Figure 2-9 displays photographs of the microcrystalline surfaces in the non-irradiated and photoirradiated areas before and after heating at 170 °C. In the UV-irradiated area the crystal shape changed to the needle-like γ-crystals due to the phase transition at 170 °C, whereas in the non-irradiated area the crystal morphology was scarcely changed by heating at 170 °C. This indicates that the photopatterning based on the phase transition can be accomplished by this method.

Photoinduced surface morphology patterning based on the phase transition was attempted using a photomask. After irradiating an α-microcrystalline film with UV light through a photomask, the film was heated for 1 h at 170 °C and then irradiated with visible light. Figure 2-10 shows the photographs of the mask pattern and the patterning by the phase transition. In the UV-irradiated area, the crystal morphology showed the needle-like crystals. However, in the non-irradiated area, the initial small α-crystals still existed. The patterning resolution by the phase transition was about 20 μm.

2.4 Summary

The thermodynamic phase transition from the platelet α-crystal of **2a** to the needle-like γ-crystal of **2a** via crystal melting was newly found and investigated by optical microscopy, single-crystal X-ray crystallography, powder X-ray diffraction profiles. The molecular packing of **2a** in the γ-crystal was quite different from that in the α-crystal because the

initiation of the phase transition is due to melting of the α-crystal. Moreover, the photoinduced phase transition and the photomicropatterning were performed. The presence of **2b** produced by UV light irradiation lowered the phase transition temperature, thereby enabling photopatterning based on the phase transition. The photomicropatterning was established with the resolution of ca. 20 μm.

2.5 References

1. J. Bernstein, *Polymorphism in Molecular Crystals*, Oxford University Press, New York, **2002**.
2. T. Mori, *Chem. Rev.* **2004**, *104*, 4947.
3. H. Kobayashi, H, Cui, A, Kobayashi, *Chem. Rev.* **2004**, *104*, 5265.
4. M. Sorai, M. Nakano, Y. Miyazaki, *Chem. Rev.* **2006**, *106*, 976.
5. T. Mutai, H. Tomoda, T. Ohkawa, Y. Yabe, K. Araki, *Angew. Chem. Int. Ed.* **2008**, *47*, 9522.
6. G. Zhang, J. Lu, M. Sabat, C. L. Fraser, *J. Am. Chem. Soc.* **2010**, *132*, 2160.
7. S. Kobatake, M. Yamada, T. Yamada, M. Irie, *J. Am. Chem. Soc.* **1999**, *121*, 8450.

Part II
Control of Surface Wettability and Photomicropatterning Using Diarylethene Crystals

Chapter 3

Photoinduced Micropatterning by Polymorphic Crystallization of a Photochromic Diarylethene in a Polymer Film

3.1 Introduction

In Part I, two types of polymorphism and phase transition of diarylethene crystals have been described. In order to utilize polymorphism and phase transition of diarylethene crystals for applications, the surface wettability is focused on in Part II. As mentioned in General Introduction, the surface wettability has been a topic of much attention in both industrial and academic research fields. It is generally known that there are two factors that control wettability on solid surfaces: chemical and topological factors.[1] A lot of studies on the control these two factors by external stimuli such as light, temperature, electricity, pH, and solvents have been reported.[2] Among these stimuli, light irradiation is the most useful stimuli because it can induce a response without any contact and destruction. A number of researches on the surface with controllable wettability by using light have been reported. [3-12]

The needle-like γ-crystal of **2a** can also be crystallized from amorphous state, as shown in Figure 2-4 in Chapter 2. If the crystallization from amorphous state can be controlled by photochromic reaction, the surface wettability can be controlled by photoirradiation. This chapter deals with rapid crystallization of **2a** from the amorphous state in poly(methyl methacrylate) by heating at 130 °C. Moreover, the crystallization can be controlled by photochromic reaction from the open-ring isomer **2a** to the closed-ring isomer **2b**. The diarylethene amorphous film has successfully been patterned to form microcrystals upon ultraviolet (UV) light irradiation through a photomask, showing a high resolution as good as ca. 4 μm under optimal conditions.

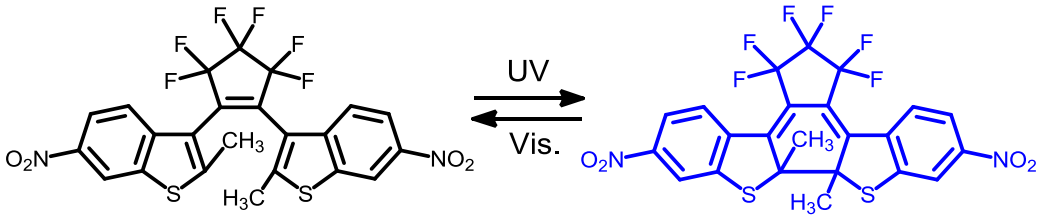

2a **2b**

3.2 Experimental Section

3.2.1 General

Differential scanning calorimetry (DSC) was run using a Seiko DSC-6200. Film surfaces were observed using a Keyence VK-8700 laser scanning microscope and a Keyence VHX-500 digital microscope. Powder X-ray diffraction profiles were recorded on a Rigaku

RINT-2100 diffractometer employing $Cu_{K\alpha}$ radiation. UV irradiation was carried out using a Keyence UV-LED UV-400 (365-nm light). The photopatterning was performed using DNP FINE LINE TEST PATTERN-I. The sample was kept away a distance of 4.5 cm from a UV-50A head in the UV-LED equipment. The light intensity was ~250 mW cm^{-2} on the sample surface. Visible light irradiation was carried out using a halogen lamp. Contact angles were measured by the drop method using a 2.0 μL drops of water.

3.2.2 Materials

Diarylethene **2a** was synthesized according to the method described in the literature.[13] The α-crystalline form of **2a** was obtained by recrystallization from *n*-hexane. Polystyrene (PSt), poly(methyl methacrylate) (PMMA), poly(vinyl chloride) (PVC), and polycarbonate (PC) were obtained from commercial sources and were used without further purification. Number-average molecular weights (M_n) and polydispersities (M_w/M_n) were as follows: PSt (M_n = 72400, M_w/M_n = 2.35), PMMA (M_n = 43700, M_w/M_n = 2.35), PVC (M_n = 18400, M_w/M_n = 2.64), and PC (M_n = 54700, M_w/M_n = 1.88).

3.2.3 Preparation of film

Transparent films of **2a**/polymer mixtures were prepared by dropping 3-5 drops of a solution of **2a** (50 mg) and the respective polymer (10 mg) in toluene or THF (5 mL) onto a thin cover glass. The substrate was dried in air for at least 12 h to afford a solvent-free film. The thicknesses of the films were 2-3 μm.

3.3 Results and Discussion

3.3.1 Polymorphic Crystallization from Amorphous State in a Polymer

As mentioned in Chapter 2, diarylethene **2a** has at least three polymorphic forms. The α-form is obtained by recrystallization from *n*-hexane, toluene, or ethyl acetate.[13] The β-form is obtained by recrystallization from acetone or chloroform,[13] and in this form, the solvent is incorporated into the crystal. Additionally, the α-crystal was found to undergo a thermodynamic phase transition at 180−190 °C to form a γ-crystal. That is, when a single crystal of the α-form was heated for a few minutes at 190 °C, needle-like crystals of the γ-form came out on the crystal surface of the α-form, as shown in Figure 2-2 and Figure 2-4 (1st scan). The γ-crystal can also be crystallized out from amorphous state. The γ-crystal melts at 220 °C, and the isotropic state is stable at room temperature. The isotropic amorphous state did not crystallize at room temperature over the entire observation period. Crystallization starts from the isotropic state of **2a** at 130 °C to produce the γ-crystal. Diarylethene **2a** can produce the γ-crystals at high temperature, as shown in Figure 2-4 (2nd scan).

A stable amorphous state can also be produced by mixing with a polymer. Diarylethene

2a was incorporated into polymers to make stable amorphous films. Polystyrene (PSt), poly(methyl methacrylate) (PMMA), poly(vinyl chloride) (PVC), and polycarbonate (PC) were used as the polymer matrices. Each transparent film had a different initial contact angle with water because this parameter depends on the surface polarity and surface tension of the polymer used.[1] When the polymer films were heated beyond 180 °C, the contact angle with water changed according to the crystallization of **2a**. The crystalline form was confirmed to be the γ-crystal based on the X-ray diffraction pattern, as shown in Figure 3-1 and Figure 3-2. The changes in the contact angles on the films are shown in Table 3-1 and Figure 3-3. The contact angle on each film increased with the heating time. The change in the contact angle due to the crystallization of **2a** was largest in the case of PMMA. It is ascribed to a large change in roughness as a result of growth of the γ-crystal. Therefore, the film of **2a**/PMMA was used in subsequent experiments.

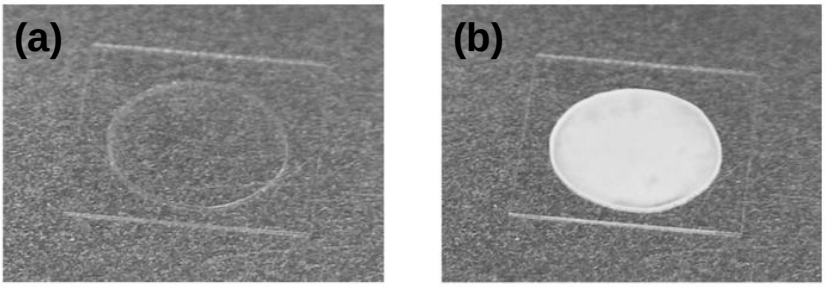

Figure 3-1. Polymorphic crystallization of **2a-γ** from the transparent film of the mixture containing **2a** /PMMA (5:1 wt ratio); (a) before heating, and (b) after heating for 2 min at 130 °C, respectively.

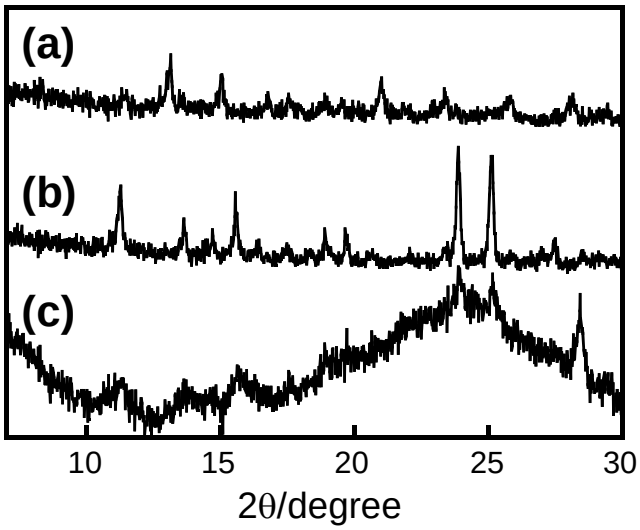

Figure 3-2. Powder X-ray diffraction patterns of microcrystal **2a-α** (a), microcrystal **2a-γ** (b), and **2a**/PMMA film heated for 2 min at 130 °C (c).

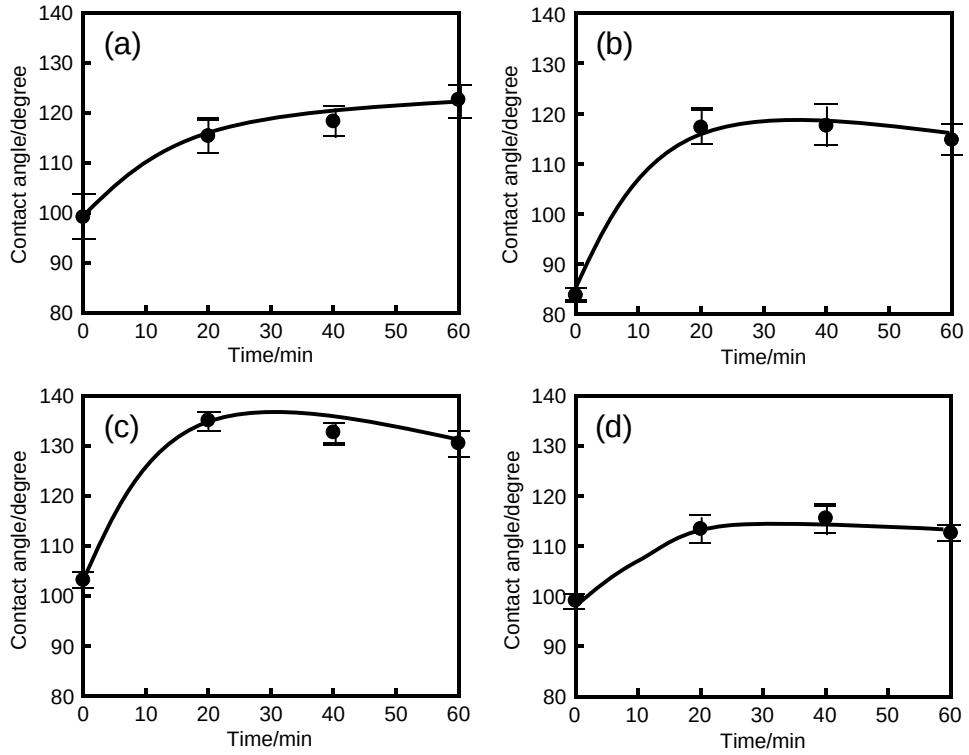

Figure 3-3. Relationships between the contact angle changes with water droplet on **2a**/polymer (5:1 wt ratio) films and heating time at 180 °C: (a) **2a**/PSt, (b) **2a**/PMMA, (c) **2a**/PVC, and (d) **2a**/PC.

Table 3-1. Contact angle changes with water on the mixture films of **2a**/polymer (5:1 wt ratio)

Film	Contact angle with water after heating at 180 °C[a]			
	0 min	20 min	40 min	60 min
2a/PSt	94.6°(±4.6°)	115.4°(±3.2°)	118.3°(±2.7°)	122.6°(±3.4°)
2a /PMMA	83.6°(±1.2°)	117.2°(±3.2°)	117.6°(±3.9°)	114.8°(±2.8°)
2a/PVC	103.8°(±1.6°)	135.1°(±1.8°)	132.8°(±2.1°)	130.6°(±2.1°)
2a/PC	99.2°(±1.4°)	113.5°(±2.7°)	115.7°(±2.8°)	112.7°(±1.6°)

[a] The contact angle with water on the polymer film without **2a** were determined to be 87° (lit. 83°)[14] for PSt, 60° (lit. 70°)[14] for PMMA, 86° for PVC,[14] and 55° (lit. 83°)[14] for PC.

[b] The angles in the parentheses show the standard deviation with 8 time measurement.

3.3.2 Effect of Photochromic Reaction on the Polymorphic Crystallization

A transparent film of **2a**/PMMA prepared under the same conditions was used for the following experiment. In this case, only the left side of the film was irradiated at 365 nm for 30 s, and then the film was heated for 2 min at 130 °C. No crystallization was observed in the UV-irradiated area, in contrast to the non-irradiated area, where the needle-like crystals were observed. In the UV-irradiated area, it was found that diarylethene **2a** in the PMMA film had reacted to the closed-ring isomer **2b** in ~15% conversion, whereas no conversion to this form had occurred in the non-irradiated area. The amorphous state in the UV-irradiated area is more stable than that in the non-irradiated area because of the impurity effect of the closed-ring isomer in the film. Thus, a few percent of the closed-ring isomers prevented the molecules from crystallizing. The initial open-ring isomer **2a** could be reproduced by irradiation of the entire surface of the film with visible light, and a difference in the surface was observed by optical microscopy.

Figure 3-4 shows an optical microphotograph of the surface under crossed Nicols along with the measured contact angle with water in the UV-irradiated and non-irradiated areas. In contrast to the UV-irradiated area, the non-irradiated area was bright when observed under crossed Nicols, indicating the presence of microcrystals on the surface. The contact angles with water on the UV-irradiated and non-irradiated areas were determined to be 81.6 and

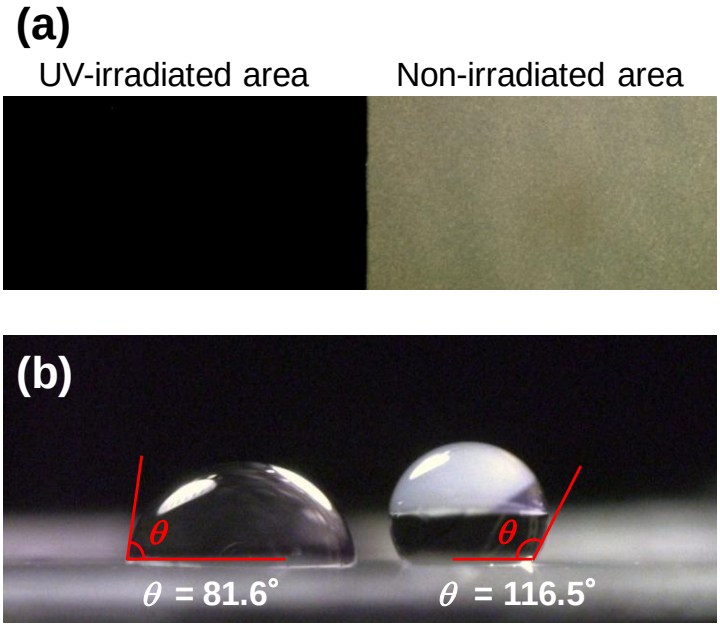

Figure 3-4. Optical microphotographs of (a) the film observed under crossed Nicols and (b) the contact angle with a water droplet on the surface. The left side of the film only was irradiated at 365 nm for 30 s, and the entire film was heated for 2 min at 130 °C before visible light irradiation. The UV-irradiated area and non-irradiated area were found to be in amorphous and crystalline states, respectively. The contact angle was measured by the drop method using a 2.0 μL drop of water.

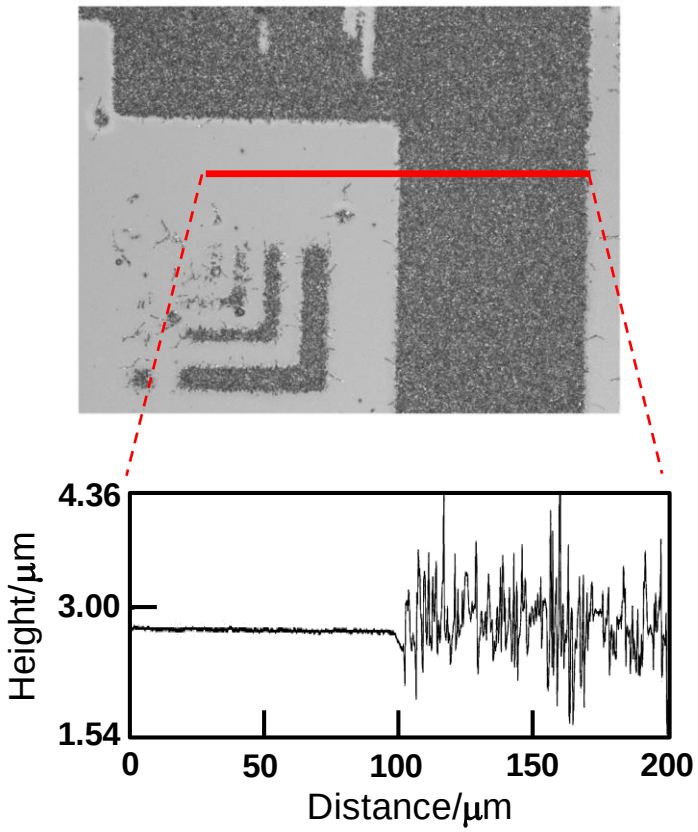

Figure 3-5. Cross-sectional view of a part on photomicropatterning. The left and right sides in the sectional view are the amorphous and microcrystalline states, respectively.

116.5°, respectively. This difference is due to a difference in the surface roughness brought about by crystallization. The surface roughness was evaluated by laser scanning microscopy. The transparent amorphous film has a particularly flat surface, as can be seen from Figure 3-5, with a difference between the maximum and minimum heights on the surface of less than 50 nm. On the other hand, the surface in the crystal growth area was very rough, with the difference in heights estimated to be ~1.5 mm. The cross-sectional traveling along the surface for the microcrystalline state was 1.44 times larger than the actual horizontal distance of the surface. This indicates that the surface roughness increased significantly following crystal growth of the γ-crystal in PMMA. Consequently, the contact angle with water increased with the surface roughness. No more changes in the roughness were observed when heating for more than 2 min.

3.3.3 Photomicropatterning by the Polymorphic Crystallization

High-resolution micro-photopatterning is an important technique for a variety of industrial applications. The micro-photopatterning of the diarylethene by crystallization using a photomask was investigated. The photopatterning resolution was then checked by optical

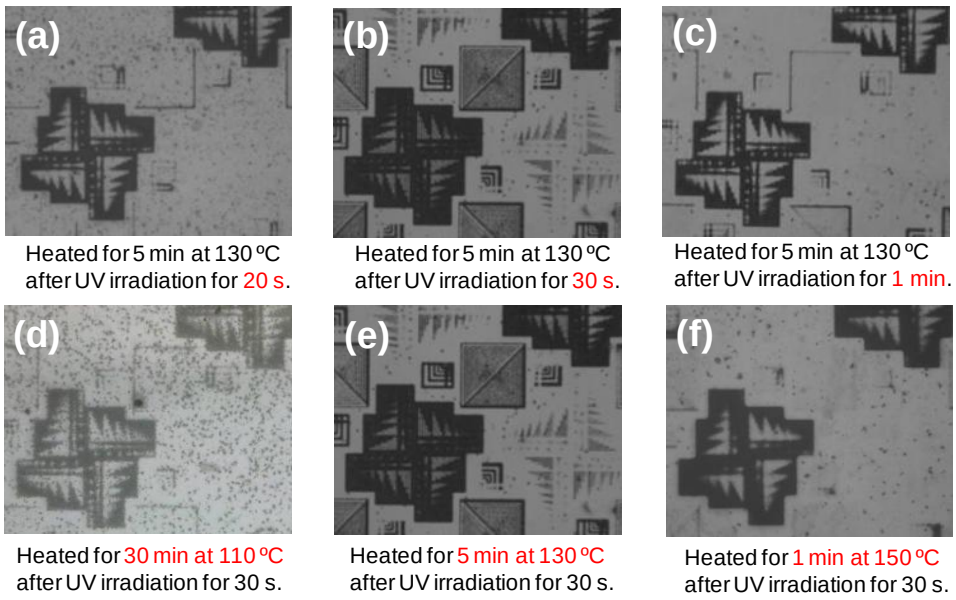

Figure 3-6. Optical microphotographs of photopatterning prepared under the various conditions. The white and black parts are the amorphous and micro-crystalline states, respectively. (b) and (e) are under the same condition.

microscopy under normal view and crossed Nicols. Two parameters, the UV irradiation time and the heating temperature, were optimized to improve the response speed and photopatterning resolution. At higher temperatures, the crystal growth became more rapid, confirming that the response speed of photopatterning depended on the heating temperature. However, when the film was heated above 130 °C, the γ-crystal gradually began to appear on the UV-irradiated area as well. The photopatterning resolution depended on the UV irradiation time, decreasing at longer UV irradiation times because of scattered light propagating through the photomask, as can be seen in Figure 3-6.

Figure 3-7 shows photographs of the photopatterning observed under normal view and under crossed Nicols. The best photopatterning was observed by heating for 2 min at 130 °C after irradiation at 365 nm for 30 s, which gave a resolution of 4‑5 mm. The resolution did not change even after heating for 5 min at this temperature. This photopatterning could be erased by heating at the melting point of the γ-crystal, ~225−230 °C, while the amorphous film could be reproduced by cooling down to room temperature, at which temperature the film is stable. Further, the photopatterning process could be repeated several times. Significantly, the converse of the entire process was also possible. That is, a process of UV irradiation over the entire transparent amorphous film, following visible-light irradiation through a photomask to produce the open-ring isomer, and subsequent heating at 130 °C enabled photopatterning with the reverse pattern. This indicates that the suppression of crystal growth in the UV-irradiated area is ascribed to the impurity effect by the closed-ring isomer.

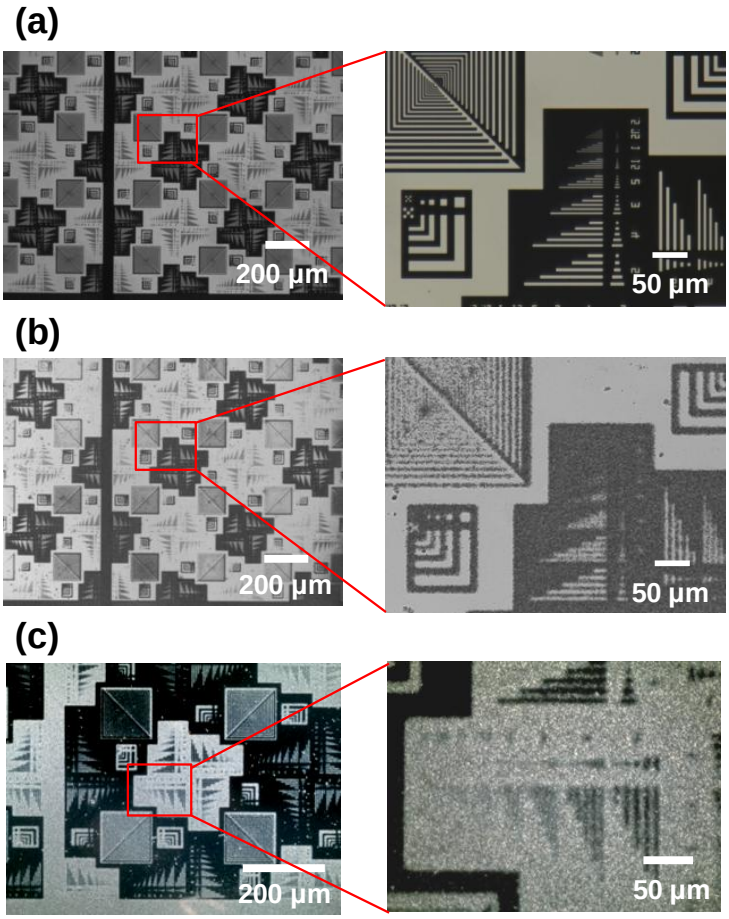

Figure 3-7. Optical microscopic photographs of (a) photomask, (b) photopatterning observed under normal view, and (c) under crossed Nicols. The white part in (a) is transparent, and UV light can penetrate these parts. The white and black parts in (b) are the amorphous and microcrystalline states, respectively. The bright part in (c) is the microcrystalline state.

3.4 Summary

Photoinduced micropatterning via the rapid polymorphic crystal growth of a photochromic diarylethene in a PMMA film has been demonstrated. The crystalgrowth, from a transparent amorphous state, could be controlled by the presence of a few percent of the photoisomer of diarylethene. The surface of the microcrystals had a larger contact angle with water than the amorphous film. Such a photopatterning process offers a useful tool for controlling surface wettability in applications.

3.5 References

1. K. Tsujii, *Surface Activity*: *Principles, Phenomena, and Applications*, Academic Press, New York, 1998, pp. 52‑54.
2. S. Wang, Y. Song and L. Jiang, *J. Photochem. Photobiol. C* **2007**, *8*, 18.
3. X. Feng, J. Zhai and J. Jiang, *Angew. Chem. Int. Ed.* **2005**, *44*, 5115.

4. W. Zhu, X. Feng, L. Feng and L. Jiang, *Chem. Commun.* **2006**, 2753.
5. S. Wang, X. Feng, J. Yao and L. Jiang, *Angew. Chem. Int. Ed.* **2006**, 45, 1264.
6. W. Jiang, G. Wang, Y. He, X. Wang, Y. An, Y. Song and L. Jiang, *Chem. Commun.* **2005**, 3550.
7. H. Ge, G. Wang, Y. He, X. Wang, Y. Song, L. Jiang, D. Zhua, *ChemPhysChem* **2006**, *7*, 575.
8. R. Rosario, D. Gust, A. A. Garcia, M. Hayes, J. L. Taraci, T. Clement, J. W. Dailey, S. T. Picraux, *J. Phys. Chem. B* **2004**, *108*, 12640.
9. A. Athanassiou, M. I. Lygeraki, D. Pisignano, K. Lakiotaki, M. Varda, E. Mele, C. Fotakis, R. Cingolani, S. H. Anastasiadis, *Langmuir* **2006**, *22*, 2329.
10. E. Mele, D. Pisignano, M. Varda, M. Farsari, G. Filippidis, C. Fotakis, A. Athanassiou, R. Cingolani, *Appl. Phys. Lett.* **2006**, *88*, 203124.
11. A. Nayak, H. Liu, G. Belfort, *Angew. Chem. Int. Ed.* **2006**, *45*, 4094.
12. I. Vlassiouk, C.-D. Park, S. A. Vail, D. Gust, S. Smirnov, *Nano Lett.* **2006**, *6*, 1013.
13. S. Kobatake, M. Yamada, T. Yamada, M. Irie, *J. Am. Chem. Soc.* **1999**, *121*, 8450.
14. B. W. Cherry, P. B. Evely, *J. Adhesion* **1987**, *22*, 171.

Chapter 4

Superhydrophobic Surface with High Adhesive Force by Crystal Growth of a Polymorphic Diarylethene

4.1 Introduction

As mentioned in General Introduction, the superhydrophobic surface with water contact angles above 150° has been attracted in both of academic and industrial research fields because of their potential applications, such as self-cleaning surface, print technology, and biomedical engineering. A number of studies for preparing the surfaces with high contact angles and low sliding angles have been performed by mimicking the plant leaves,[1] insect wings,[2,3] and legs.[4] However, there are few strategies to prepare the superhydrophobic surface with high adhesive force.[5-7] Such surfaces are important for print technology, microreactor technology, and various electronic devices because of the water capturing property.

The control of surface wettability and photopatterning using a polymorphic photochromic diarylethene was discussed in Chapter 3. The polymorphic diarylethene, 1,2-bis(2-methyl-6-nitro-1-benzothiophen-3-yl)perfluorocyclopentene (**2a**), takes place crystallization of the needle-like γ-crystal from the amorphous film in poly(methyl methacrylate) (PMMA) at 130 °C. The control of the crystallization was performed by the presence of the closed-ring isomer produced by the photochromic reaction. When the film was heated up for 2 min at 130 °C, the needle-like crystal appeared in the non-irradiated area, whereas the crystal did not appear in the UV-irradiated area. This suppression of the crystallization is due to the impurity effect by the presence of the closed-ring isomer. The contact angles are 82° and 117° in the amorphous area and the crystallization area, respectively. This is ascribed to a difference in roughness of the surface. The resolution of the photopatterning using a photomask reached to about 4 μm under optimal conditions. During a study of crystal growth under various conditions, a formation of a superhydrophobic surface by crystallization of **2a** under a condition was found. In this chapter, a photoinduced control in the formation of the superhydrophobic surface with high adhesive force and the photopatterning by crystal growth of diarylethene **2a**, as shown in Figure 4-1, are discussed.

4.2 Experimental Section

4.2.1 General

The surface of the film was observed using a Keyence VK-8700 Laser Scanning Microscope and a Keyence VHX-500 Degital Microscope. The cross-sectional traveling distance and actual horizontal distance were also measured by a Keyence VK-8700 Laser Scanning Microscope with the resolution of 0.1 μm in all directions. UV irradiation was carried out using a Keyence UV-LED UV- 400 (365-nm light). The photopatterning was performed using

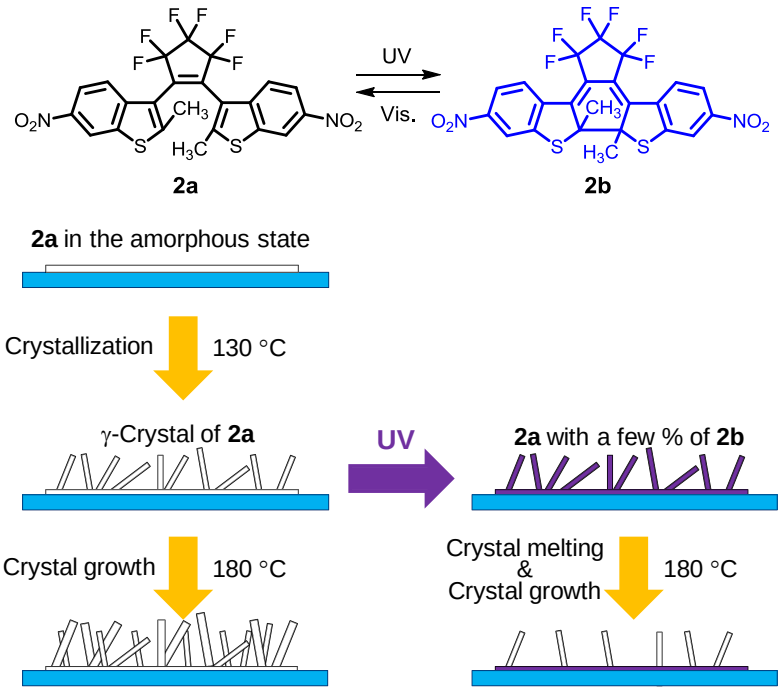

Figure 4-1. Schematic illustration of crystallization and crystal growth from the amorphous state of **2a** to crystal of **2a**-γ.

DNP FINE LINE TEST PATTERN-I. The sample was kept away a distance of 4.5 cm from a UV-50A head. Visible light irradiation was carried out using a halogen lamp. The contact angle was measured by the drop method using a 2.0 μL drop of water.

4.2.2 Materials

Diarylethene **2a** was synthesized according to the method described in the literature.[8] The α-crystal of **2a** was obtained by recrystallization from hexane. PMMA were commercially available and used without further purification. Number-average molecular weight (M_n) and polydispersity (M_w/M_n) were determined to be M_n = 43700 and M_w/M_n = 2.35, respectively. Preparation of the film. The film of the mixture of **2a**/PMMA was prepared by dropping 3−5 drops of a solution of **2a** (50 mg) and PMMA (10 mg) dissolved in toluene (5 mL) on a thin cover glass. The substrate was dried under air for at least 12 h to afford a solvent-free transparent film. The thickness of the film was 2−3 μm.

4.3 Results and Discussion

4.3.1 Change in Contact Angle by Crystallization and Crystal Growth

The flat surface of the mixture of diarylethene **2a** and PMMA was prepared on a thin glass plate. When the film was heated for 2 min at 130 °C, the γ-crystal of **2a** came up the surface. The contact angle with water droplet changed from 82° to 117° along with the surface

roughness change because of the crystallization of the needlelike crystal from the amorphous state by heating. It was attempted here to make the superhydrophobic surface with the crystal growth of the γ-crystal by changing heating temperature and time.

Figure 4-2 shows morphology changes in the surface by crystallization on heating for 60 min at 130 °C, followed by heating at each temperature. When the film was heated at 160 or 170 °C, no change in the surface morphology was observed even after 60 min. When the film was heated at 180 °C, the surface morphology changed according to the crystal growth. This indicates that the heating below 170 °C does not follow the crystal growth of the γ-crystal.

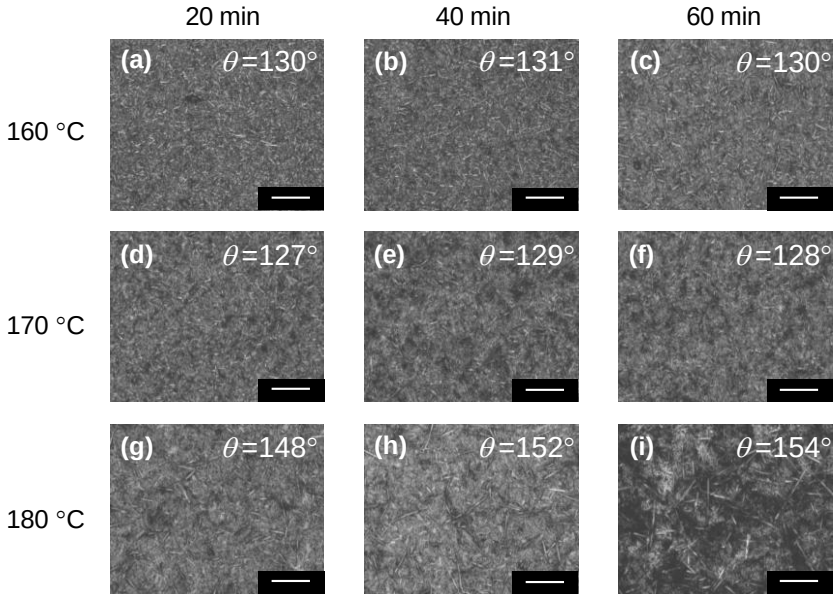

Figure 4-2. Changes in the surface morphology observed by laser scanning microscope after heating the amorphous film of **2a**/PMMA for 60 min at 130 °C, followed by stored at 160 (a–c), 170 (d–f), and 180 °C (g–i). The contact angles are expressed as θ in each panel. Scale bars: 20 μm.

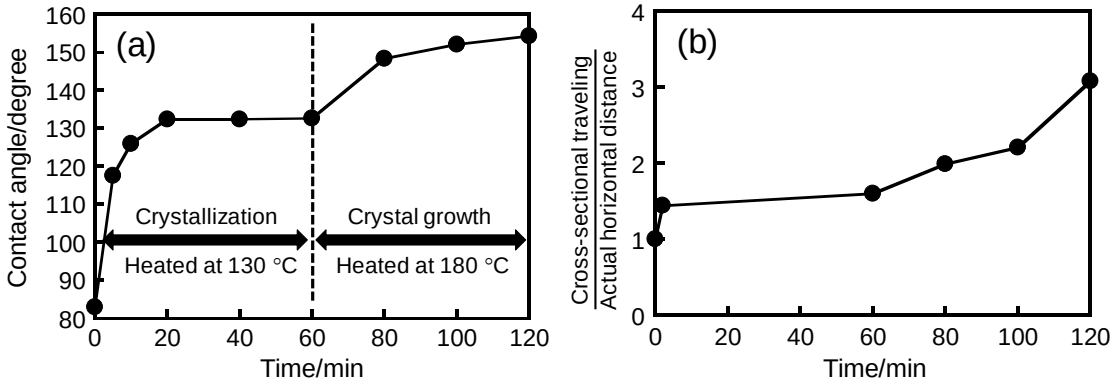

Figure 4-3. Changes in contact angle (a) and surface roughness (b) on the surface produced by the crystallization and the crystal growth processes of **2a** in PMMA.

Figure 4-3 shows the change in the contact angle on the film after heating for 60 min at 130 °C, followed by heating for 60 min at 180 °C. The contact angle with water changed from 82° to 154° in a stepwise via 132°. The high contact angle indicates a superhydrophobic surface with the contact angles of more than 150°. This result suggests that the increase in the contact angle is affected by two factors. One is ascribed to the crystallization process of the γ-crystal from amorphous state by heating for 60 min at 130 °C. The other is ascribed to the drastic crystal growth of the γ-crystal by heating for 60 min at 180 °C corresponding to Ostwald ripening. Some of the large sized crystals show crystal growth to become much larger sized crystals, whereas the small sized crystals melt while providing the molecules to the large crystals. Ostwald ripening tends to take place at higher temperature because the melting point of the γ-crystal is about 200−210 °C. Figure 4-3b shows the change in the surface roughness along with the crystallization and crystal growth. Before heating, the distance of cross-sectional traveling along the surface was as much as the actual horizontal distance of the surface. As making progress of the crystallization of the γ-crystal, the cross-sectional traveling became 1.60 times larger than the initial value. Following the crystal growth, the cross-sectional traveling became 3.08 times larger than the initial value. It is concluded that the change in the contact angle with water was affected by the surface roughness.

4.3.2 Superhydrophobic Surface with High Adhesive Force

Figure 4-4 shows the shape of water droplet on the surface produced by the crystal growth of the γ-crystal. The contact angle is about 154°, showing a supehydrophobicity. However, the water droplet is pinned to the surface, even when the surface is turned upside down. This means that the surface has high-water adhesive property. This phenomenon is often called as the petal effect or the pinned effect. Rose petal is well known as the representative example.[7] Such surfaces have been expected for application to print technology and microreactor technology. In order to examine the details of the wetting property, dynamic advancing (θ_A) and receding (θ_R) contact angles were examined as shown in Figure 4-5. For comparison, the values of θ_A and θ_R on the crystallization surface prepared by heating for 60 min at 130 °C were also determined to be 85° and 42°, respectively. After heating for 60 min at 180 °C, the values of θ_A and θ_R were 154° and 145°, respectively. Generally, the larger the hysteresis of a dynamic contact angle ($\theta_A - \theta_R$) is, the larger the adhesive force to the surface is. Therefore, the common superhydrophobic surfaces have a hysteresis of a dynamic contact angles smaller than 5°.[9,10] However, the superhydrophobic surface prepared by crystal growth of the γ-crystal has the hysteresis of about 10°. This result also means that the superhydrophobic surface prepared by the crystal growth has high-water adhesive property. It should be considered that the surface topology plays an important role in the large hysteresis.

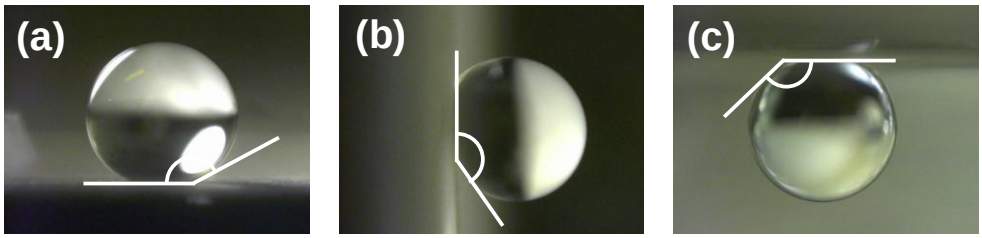

Figure 4-4. The shape of water droplet on the surface produced by heating for 60 min at 130 ℃, followed by heating for 60 min at 180 ℃ when the surface was tilted at 0° (a), 90° (b), and 180° (c).

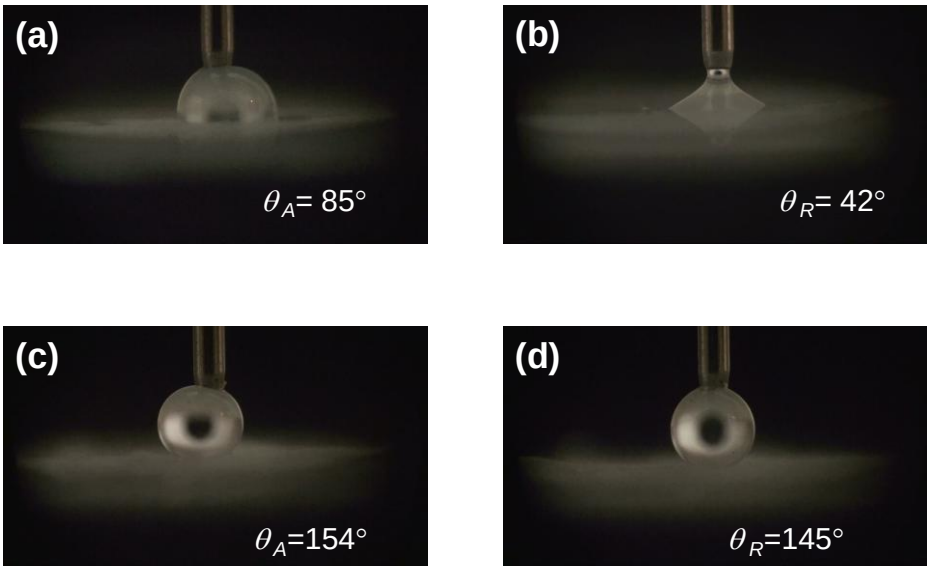

Figure 4-5. The dynamic advancing (θ_A) and receding (θ_R) contact angles on the surface after heating for 60 min at 130 ℃ (a, b), followed by heating for 60 min at 180 ℃ (c, d).

There are famous two models to explain the effect of the surface topology, Wenzel model and Cassie and Baxter model. In addition, L. Jiang *et al.* recently reported on definition of superhydrophobic states.[11] The surface of lotus leaves shows superhydrophobicity with low sliding angles and has the micro- and nanoscale hierarchical structure. This surface is classified in the Cassie's states. On the other hands, the surface of rose petal is classified into Cassie impregnating wetting state. The difference between these two states is the penetration of water into grooves of the micro structures. In the case of our superhydrophobic surface, the penetration of water into the grooves between crystals would make the Cassie impregnating wetting state because the crystal sizes are about a few μm. Therefore, when the surface is turned upside down, water captured in microcrystals hangs on the surface.

4.3.3 Photomicropatterning by the Crystal Growth

If the crystal growth is controlled by photochromic reaction, the crystal growth can be

caused selectively in the desired space upon photoirradiation. In order to clarify the effect of photochromic reaction for the crystal growth, only the left side of the crystallization film was irradiated with 365-nm light for 100 s, and then the film was heated for 60 min at 180 °C. Figure 4-6 shows the photograph of the surface under normal view along with the measured contact angles with water in the UV-irradiated and non-irradiated areas. The non-irradiated area looks like much crystallization, whereas the UV-irradiated area has smaller crystals, indicating a difference in the degree of crystallization. In the UV-irradiated area, diarylethene **2a** in the PMMA film reacted to the closed-ring isomer **1b** in about 8.8% conversion, whereas no such reaction took place in the non-irradiated area. The melting point of the needle-like γ-crystal in the UV-irradiated area is lower than that in the non-irradiated area because of the impurity effect of the closed-ring isomer in the film. Thus, a few percent of the closed-ring isomers promoted the melting of the crystal. The contact angles with water on the UV-irradiated and non-irradiated areas were also determined to be 138° and 155°, respectively. This difference is due to a difference in the surface roughness brought about by melting of the crystal. In UV-irradiated area, the contact angle decreases because an interval between concavity and convexity on the surface becomes broad by lowering of the degree of crystal growth (*i.e.* the surface is less rough).

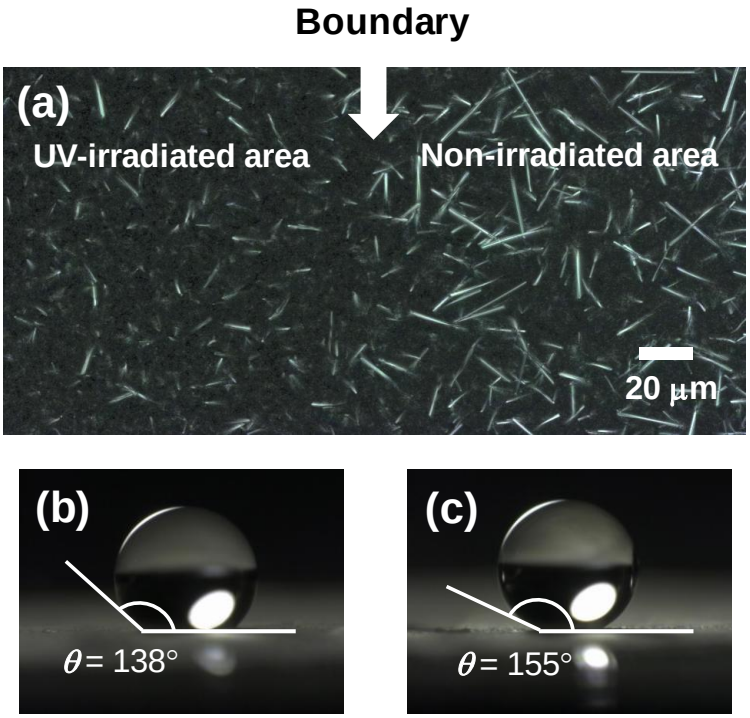

Figure 4-6. The photographs of the surface under normal view (a) and the contact angles in the UV irradiated area (b) and non-irradiated area (c), respectively.

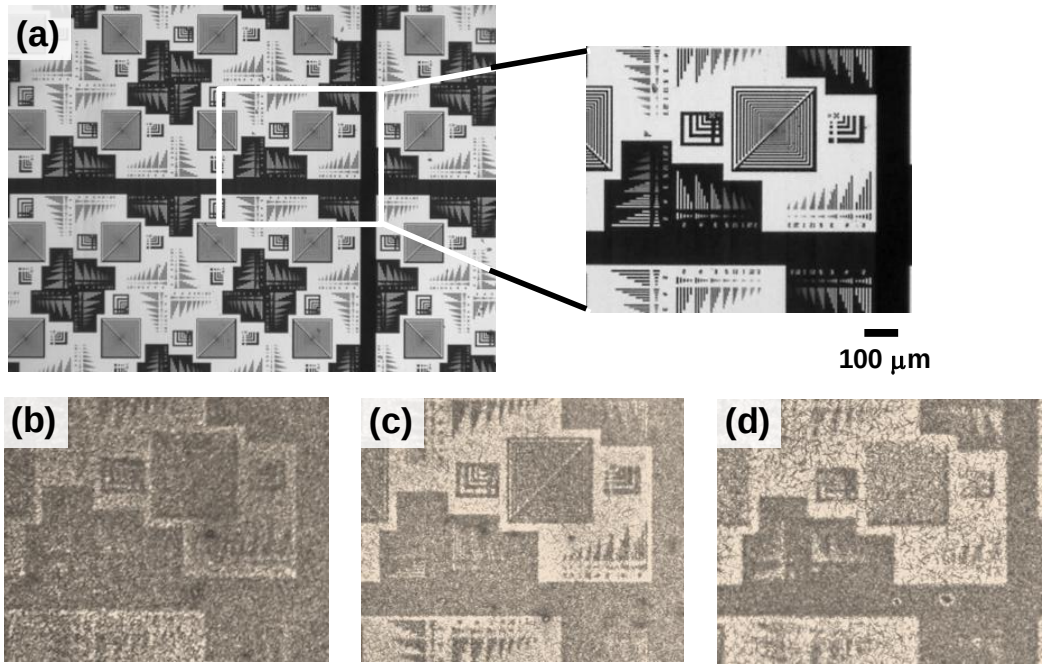

Figure 4-7. The photographs of the photopatterning observed under normal view, produced by various UV irradiation time. (a) shows a photomask used in this experiment. The sample was prepared by heating for 60 min at 130 °C, irradiation with 365 nm light for 80 (b), 100 (c), and 120 s (d) under the photomask, and heating for 60 min at 180 °C.

High-resolution micro-photopatterning is an important technique for a variety of industrial applications. The micropatterning by the crystal growth of the γ-crystal using a photomask was investigated. The photopatterning resolution was then checked by optical microscopy under normal view. The UV irradiation time was optimized to improve the photopatterning resolution. Figure 4-7 shows photographs of the photopatterning observed under normal view. The best photopatterning was observed by heating for 60 min at 180 °C after irradiation with 365-nm light for 120 s, which gave a resolution of about 10 μm.

4.4 Summary

The new fabrication method of superhydrophobic surface with high-water adhesive property has been investigated. The crystal growth of the polymorphic diarylethene enables us to make the superhydrophobic surface with high-water adhesive property. The ease of the penetration of water into the rough surface is very important. Furthermore, the author demonstrated photomicropatterning of the rapid polymorphic crystal growth of the diarylethene in a PMMA film. The crystal growth by Ostwald ripening could be controlled by the presence of a few percent of the photoisomer of the diarylethene. The high density area of microcrystals had a larger contact angle with water than that of low density area. Such a photopatterning process offers a useful tool for controlling surface wettability in applications.

4.5 References

1. L. Feng, S. Li, Y. Li, H. Li, L. Zhang, J. Zhai, Y. Song, B. Liu, L. Jiang, D. Zhu, *Adv. Mater.* **2002**, *14*, 1857.
2. T. Wagner, C. Neinhuis, W. Barthlott, *Acta Zool.* **1996**, *77*, 213.
3. Z. Gu, H. Uetsuka, K. Takahashi, R. Nakajima, H. Onishi, A. Fujishima, O. Sato, *Angew. Chem. Int. Ed.* **2004**, *42*, 894.
4. X. Gao, L. Jiang, *Nature* **2004**, *432*, 36.
5. L. Jin, X. Feng, L. Feng, T. Sun, J. Zhai, T. Lin, L. Jiang, *Adv. Mater.* **2005**, *17*, 1977.
6. Y. Zheng, X. Gao, L. Jiang, *Soft Matter* **2007**, *3*, 178.
7. L. Feng, Y. Zhang, J. Xi, Y. Zhu, N. Wang, F. Xia, L. Jiang, *Langmuir* **2008**, *24*, 4114.
8. S. Kobatake, M. Yamada, T. Yamada, M. Irie, *J. Am. Chem. Soc.* **1999**, *121*, 8450.
9. D. Öner, T. J. McCarthy, *Langmuir* **2000**, *16*, 7777.
10. L. Gao and T. J. McCarthy, *Langmuir* **2006**, *22*, 2966.
11. S. Wang, L. Jiang, *Adv. Mater.* **2007**, *19*, 3423.

Part III
Photoinduced Shape Changes of Diarylethene Crystals

Chapter 5

Crystal Thickness Dependence of Photoinduced Crystal Bending

5.1 Introduction

In the past decade, the studies on molecular materials which change shape or size in response to external stimuli such as light have been developed. They can be used for photomechanical actuators without any direct contact and electronic wires. In order to obtain such a wonderful property, a lot of chemists have directed their power towards the research on photoresponsive materials.[1-3] For photomechanical actuators, it is required for compounds to change their molecular structure or arrangement upon photoirradiation.[3-15]

As mentioned in General Introduction, diarylethene derivatives can undergo photochromic reaction even in the crystalline phase as well as in the solution.[16-19] As the first example of photomechanical effect using a diarylethene crystal, a photoreversible step-and-valley formation on a diarylethene crystal surface has been reported.[20] This is ascribed to a slight change in molecular volume that occurs between the open- and closed-ring isomers during photochromic reactions. Single microcrystals of diarylethenes have been found to exhibit rapid and reversible crystal shape deformation upon alternating UV and visible light irradiation.[6]

Recently, the research on the photoinduced bending for practical applications has been reported. Morimoto and Irie reported that the two-component co-crystals composed of 1,2-bis(2-methyl-5-(1-naphthyl)-3-thienyl)perfluorocyclopentene and perfluoronaphthalene with 1-5 mm size in length are reversibly bent upon alternating irradiation with UV and visible light.[8] The co-crystal can lift the metal ball with the 200-600 times heavier weight than that weight of the crystal. The millimeter-size crystals exhibit outstanding performance as light-driven actuators in the real macroscopic world. They also reported that the mixed crystals composed of two diarylethene derivatives, 1-(5-methyl-2-phenyl-4-thiazolyl)-2-(5-methyl-2-*p*-tolyl-4-thiazolyl)perfluorocyclopentene and 1,2-(5-methyl-2-*p*-tolyl-4-thiazol-yl)perfluorocyclopentene, also exhibit reversibly bending upon alternating irradiation with UV and visible light.[9] The mixed crystals can be reversibly bent over 1000 cycles and exhibit bending in wide temperature range from 4.6 to 370 K. However, there are few reports on the photoinduced bending speed on the faces irradiated with UV light and the crystal thickness dependence of the bending speed. [21,22]

This chapter provides the photoinduced crystal bending of a diarylethene, 1,2-bis(2-methyl-5-(4-(1-naphthoyloxymethyl)phenyl)-3-thienyl)perfluorocyclopentene (**3a**). The microcrystals of diarylethene **3a** can be reversibly bent upon alternating irradiation with UV and visible light over 80 cycles. The dependence of the photoinduced bending speed on

the faces irradiated with UV light and on the thickness of the crystal has been investigated. The photoinduced crystal bending speed depending on the crystal thickness can be well explained by Timoshenko's bimetal model.

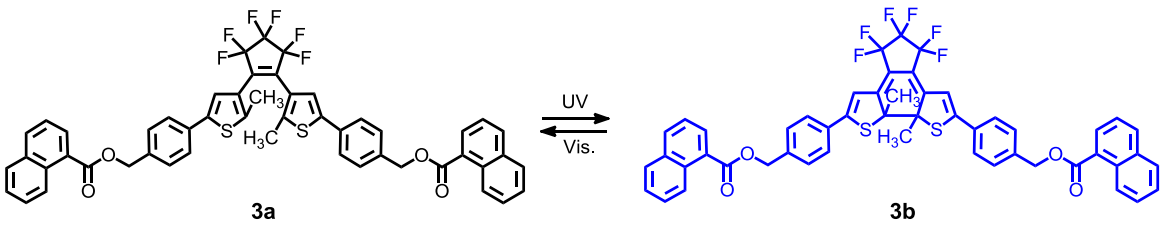

3a **3b**

5.2 Experimental Section

5.2.1 General

^{1}H NMR spectroscopy (Bruker AV-300N) was measured at 300 MHz. Deuterated chloroform ($CDCl_3$) and tetramethylsilane (TMS) were used as the solvent and the internal standard, respectively. Mass spectra were obtained using a JEOL JMS-700/700S mass spectrometer. High-performance liquid chromatography (HPLC) was carried out using a Hitachi L-7150/L-2400 HPLC system equipped with a Kanto Chemical Mightysil Si 60 Column. Photoinduced crystal bending was observed using a Keyence VHX-500 digital microscope. The polarized absorption spectra were measured using a Nikon ECLIPSE E600POL polarizing optical microscope attached a Hamamatsu PMA-11 photonic multi-channel analyzer as the photodetector. UV light irradiation was carried out using a Keyence UV-LED UV-400/UV-50H (365-nm light) and a super high pressure mercury lamp (100 W; UV-1A filter (365-nm light)) attached with the polarizing optical microscope. Visible light irradiation was carried out using a halogen lamp (100 W).

5.2.2 Materials

Synthesis of 3a. A solution of 1,2-bis-(2-methyl-5-(4-hydroxymethylphenyl) -3-thienyl)perfluorocyclopentene[23] (300 mg; 0.52 mmol), 1-naphthoic acid (344 mg; 2.0 mmol), dicyclohexylcarbodiimide (454 mg; 2.2 mmol), and 4-dimethyl aminopyridine (142 mg; 1.2 mmol) in anhydrous tetrahydrofuran (THF) (12 mL) was stirred under argon for 4 h at room temperature. To the reaction mixture was added an aqueous sodium hydrogen carbonate solution, and the mixture was extracted with ether. The organic layer was dried over $MgSO_4$. After removal of the solvent, the residue was purified by column chromatography on silica-gel using *n*-hexane/ethyl acetate (7:3) as the eluent. Pure **3a** was obtained by a further purification with HPLC. Yield: 400 mg (86.5%). **3a**: ^{1}H NMR (300 MHz, $CDCl_3$): δ = 1.97 (s, 6H, CH_3), 5.46 (s, 4H, CH_2), 7.30 (s, 2H, Thienyl H), 7.4-7.7 (m, 14H, Ar), 7.89 (d, *J* = 8.0 Hz, 2H, Ar), 8.03 (d, *J* = 8.2 Hz, 2H, Ar), 8.24 (dd, *J* = 1.2, 7.3 Hz, 2H, Ar), 8.95 (d, *J* = 8.5

Hz, 2H, Ar). HR-MS (FAB) *m/z* = 888.1803; Calcd. for $C_{51}H_{34}F_6O_2S_2$ *m/z* = 888.1815 (M^+).

5.2.3 X-ray Crystallography

The data collection was performed on a Rigaku RAXIS RAPID imaging plate diffractometer with $Mo_{K\alpha}$ radiation (λ = 0.71073 Å) monochromated by graphite. The crystal structures were solved by a direct method using SIR92 and refined by the full-matrix least-squares method on F^2 with anisotropic displacement parameters for non-hydrogen atoms using SHELXL-97.[24] The positions of all hydrogen atoms were calculated geometrically and refined by the riding model. The data in CIF format have been deposited at the Cambridge Crystallographic Data Centre with deposition number CCDC 942519 for **3a**.

5.2.4 Calculation of the Initial Speed of the Curvature Change

The value of the curvature against UV irradiation time (*t*) was fitted by polynomial function, the polynomial degree of 6. The initial speed of the curvature change was calculated by derivation of the function at *t* = 0.

5.3 Results and Discussion

5.3.1 Crystal Shape and Molecular Packing

Rod-like single microcrystals of **3a** were prepared by recrystallization from *n*-hexane/acetone solution. Single crystal X-ray crystallography for a crystal of **3a** showed a triclinic crystal system and a space group of $P\bar{1}$ (Table 5-1). Figure 5-1 shows the shape and the molecular packing determined by X-ray crystallographic analysis of crystal **3a**. The face indices of the rod-like crystal were determined as shown in the figure. The (0 1 0) and (0 $\bar{1}$ 0) faces are always well-developed in comparison with the (0 0 1) and (0 0 $\bar{1}$) faces. The long edge of the crystal is parallel to the *a*-axis. The melting point of **3a** is ca. 154 °C. In the crystalline phase, all **3a** molecules exist in an antiparallel conformation. The distance between the reactive carbons was determined to be 3.54 Å, which is short enough to undergo photocyclization in the crystalline phase.[25] The color of crystal **3a** changes from colorless to blue upon UV light irradiation, and the blue color disappears upon visible light irradiation. Figure 5-2 shows the polar plots of absorbance of the blue color at 600 nm viewed from (0 0 $\bar{1}$) and (0 1 0) faces. Absorbance on the (0 1 0) face increased with UV light irradiation time in comparison with that on (0 0 $\bar{1}$) face at a rate of more than four times. The difference of the absorption intensity on their faces is ascribed to the molecular orientation viewed from their faces. The direction of the absorption anisotropy viewed on (0 1 0) and (0 0 $\bar{1}$) faces is different. The faces of the crystal can be distinguished by measuring the absorption anisotropy.

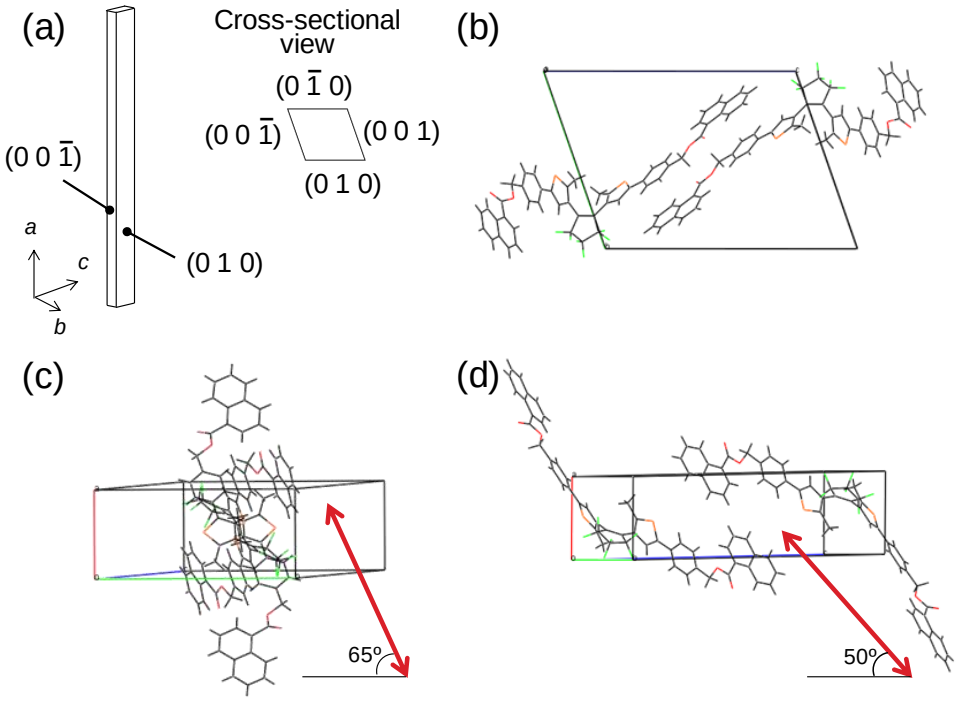

Figure 5-1. Crystal shape of **3a** (a) and molecular packing diagrams viewed from cross-section (b), (0 0 $\bar{1}$) face (c), and (0 1 0) face (d). The red arrows exhibit absorption anisotropy shown in Figure 5-2.

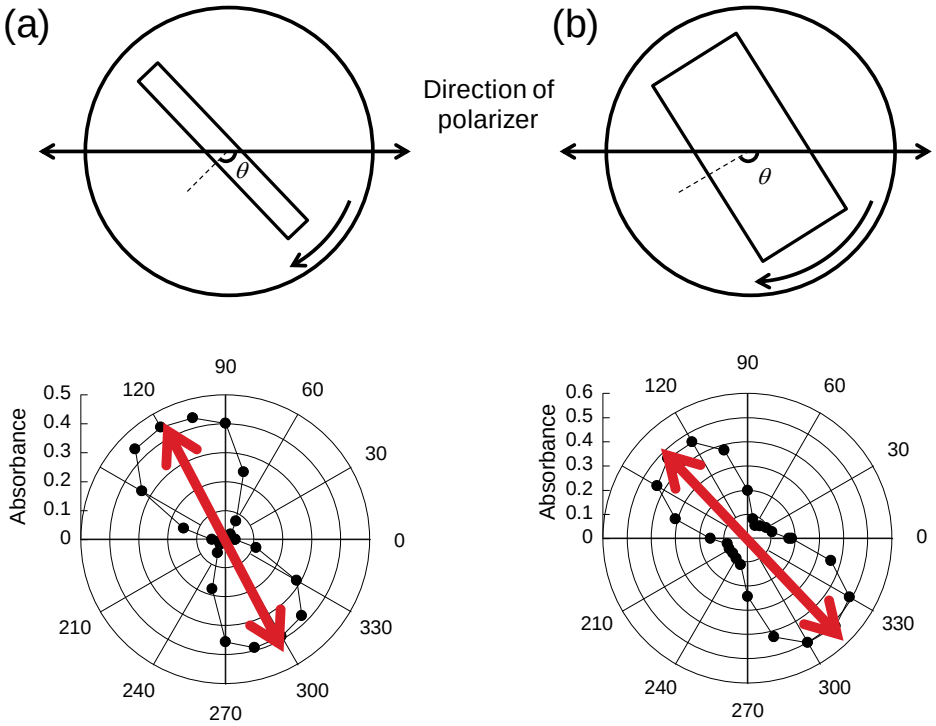

Figure 5-2. Polar plots of absorbance at 600 nm on (0 0 $\bar{1}$) face (a) and (0 1 0) face (b).

Table 5-1. X-ray crystallographic data for 1,2-bis(2-methyl-5-(4-(1-naphthoyloxymethyl)phenyl)-3-thienyl)perfluorocyclopentene.

Empirical formula	$C_{51}H_{34}F_6O_4S_2$
Formula weight	888.92
Temperature	138(2) K
Crystal system	Triclinic
Space group	$P\bar{1}$
Unit cell dimensions	a = 6.838(2) Å b = 15.416(6) Å c = 20.719(8) Å α = 70.74(3)° β = 88.28(3)° γ = 89.84(3)°
Volume	2060.9(13) $Å^3$
Z	2
Density	1.432 g cm^{-3}
Crystal size	0.60 × 0.20 × 0.10 mm^3
Goodness-of-fit on F^2	1.046
Final R [$I > 2\sigma(I)$]	$R1$ = 0.0442, $wR2$ = 0.0868
R (all data)	$R1$ = 0.0864, $wR2$ = 0.0912

5.3.2 Photoinduced Bending and Repeatability

Figure 5-3 shows repeating cycles of the photoinduced bending of the rod-like crystal (crystal size 15 × 24 × 650 μm) of **3a** upon alternating irradiation with UV and visible light to (0 1 0) face. Upon irradiation with UV light (λ = 365 nm) from the left side of the crystal, the crystal turned blue and was bent in the direction away from the incident light. The tip of the crystal reversibly moved as much as 60 μm upon photoirradiation, and the photoreversible bending could be repeated more than 80 times without crystal decomposition.

The photoinduced crystal bending results in the changes of the cell dimensions before and after UV light irradiation. The changes in the cell dimension may be determined by *in situ* X-ray crystallographic analysis before and after the photoirradiation. Here, the changes in the cell dimensions are estimated by using the changes in the crystal shape upon UV light irradiation. Figure 5-4 shows the crystal shape of **3a** before and after UV irradiation to (0 1 0) face. The crystal size is 0.62 × 9.3 × 113 μm before photoirradiation. The thickness of the

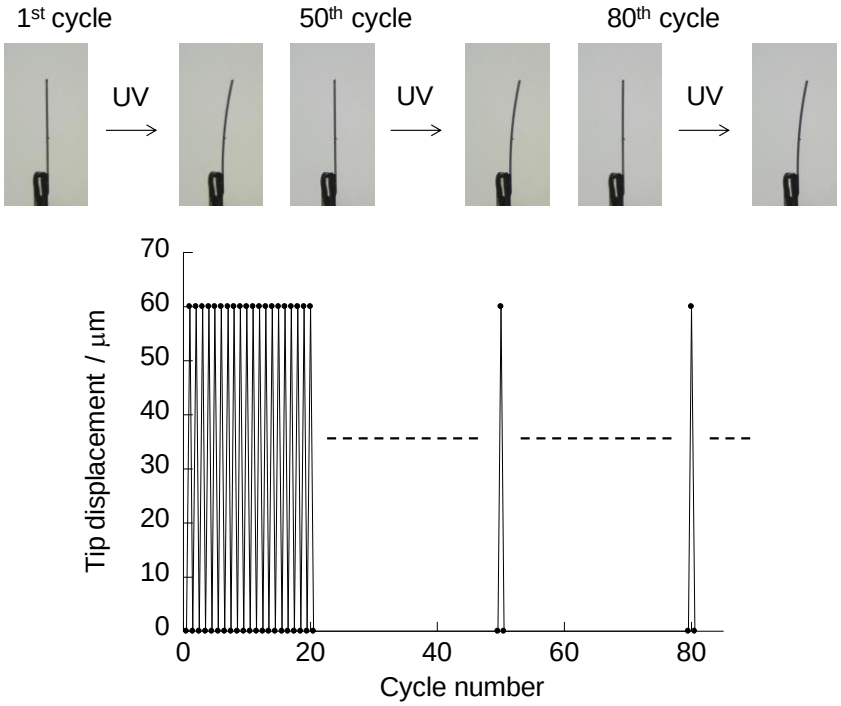

Figure 5-3. Reversible photoinduced bending of a rod-like crystal of **3a** upon alternating irradiation with ultraviolet (365 nm) light for 5 s and visible (> 500 nm) light for 2.5 min.

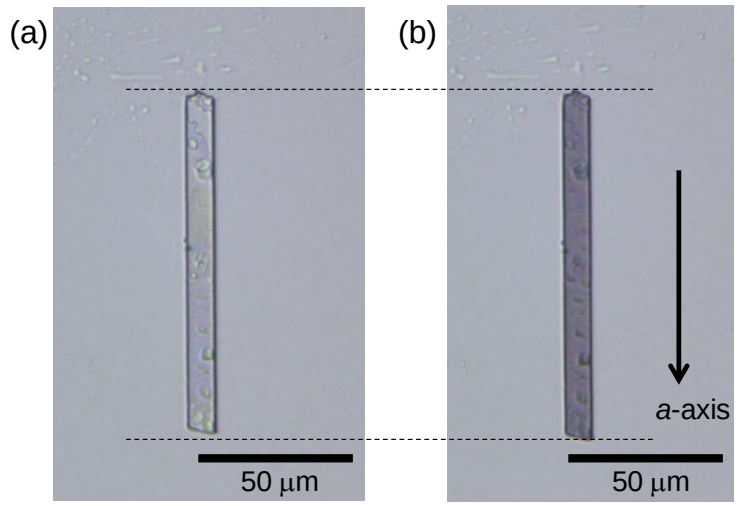

Figure 5-4. Optical microscopic photographs of a thin crystal of **3a** (crystal size: 0.62 × 9.3 × 113 μm) before (a) and after UV irradiation for a few minutes (b).

crystal is so thin that the photoisomerization takes place over the whole crystal. In such a case, the crystal was not bent. However, the crystal was expanded to the *a*-axis as much as 1.97 μm after photoirradiation, which corresponds to the expansion of the *a*-axis as much as 1.74%. It corresponds that the cell parameter of the *a*-axis changed from 6.836 to 6.955 Å.

5.3.3 Dependence of the Photoinduced Bending Speed on the Faces Irradiated with UV Light

The crystal has a rhombic cross-section. Figure 5-5 shows the motion of the crystal tip during the crystal bending observed from top of the crystal. The rod-like crystal was irradiated from (0 0 1) face (right side) and (0 1 0) face (lower side) with UV light, and the bending behavior was monitored. The rate of tip-head movement depends on the light intensity. The experiment was performed under the same light intensity. When the crystal was irradiated from (0 0 1) face with UV light, the movement of the crystal was small and slow. In contrast, when the crystal was irradiated from (0 1 0) face, it was bent largely and rapidly.

Figure 5-6 shows photographs in the photoinduced bending viewed from side position upon UV light irradiation to (0 0 1) and (0 1 0) faces from left side. Figure 5-7 shows the curvature change against UV irradiation time to (0 0 1) and (0 1 0) faces. The fitting of the time-dependence of the curvature change cannot be established because the condition of UV light irradiation during bending changes by the difference in curvature. Therefore, the initial velocity (V_{init}) by fitting in a polynomial function and derivation of the function at t = 0 was estimated. The initial speeds of the curvature change in the case of UV light irradiation to (0 0 1) face and (0 1 0) face are 0.111 and 0.165 $mm^{-1} s^{-1}$, respectively. This apparent difference in the crystal bending behavior is ascribed to the molecular orientation viewed from the faces. When viewed from (0 0 1) face, the long axis of the diarylethene molecule is quite perpendicular to the face, as can be seen from Figure 5-1. In this case, the diarylethene molecules have a low absorption coefficient.[17] In contrast, when viewed from (0 1 0) face, the

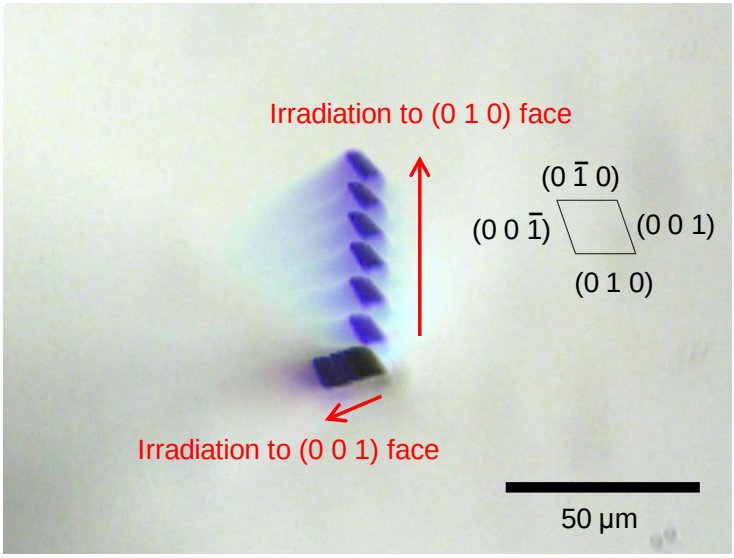

Figure 5-5. Optical microscopic photograph of the crystal bending observed from cross-section upon UV light irradiation. The photograph was superimposed for 7 frames of each 1/7 s upon photoirradiation to (0 0 1) face and (0 1 0) face.

long axis of the diarylethene molecules is parallel to the face. The diarylethene molecules have a larger absorption coefficient. In fact, the depth of photoreaction was investigated. It was very difficult to observe it when UV irradiation was carried out to (0 1 0) face because the photoreaction took place only crystal surface at ca. 1 μm or less. On the other hands, it was ca. 50 μm when UV irradiation was carried out to (0 0 1) face, as shown in Figure 5-8. As a result, UV light irradiation from (0 0 1) face leads to relatively homogeneous photo-coloration over the whole crystal. However, photoirradiation from (0 1 0) face results in heterogeneous photocoloration in depth in the crystal. The heterogeneous photocoloration affects the speed of the bending.

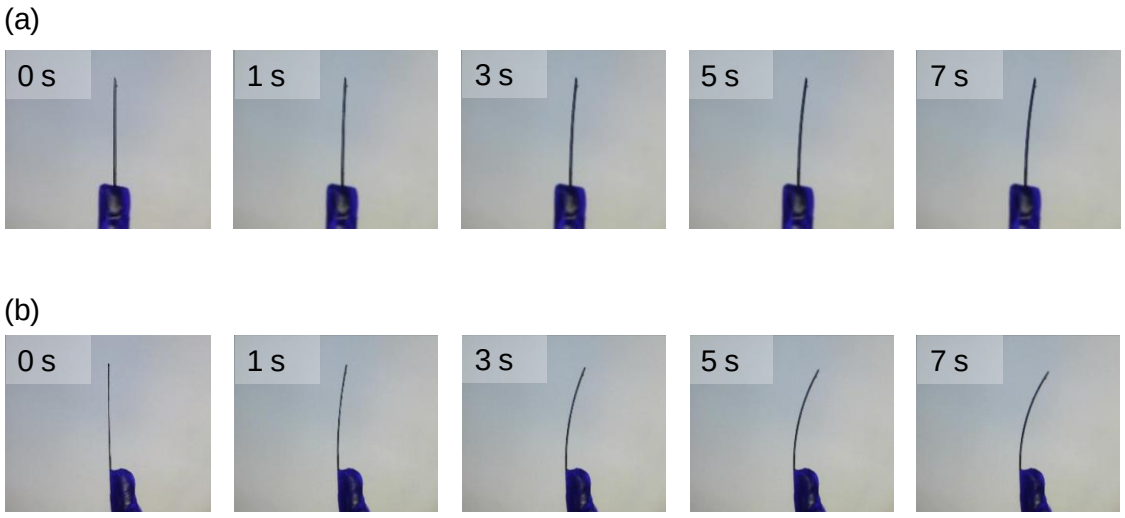

Figure 5-6. Photoinduced crystal bending upon irradiation with UV light to (0 0 1) face (a) and (0 1 0) face (b).

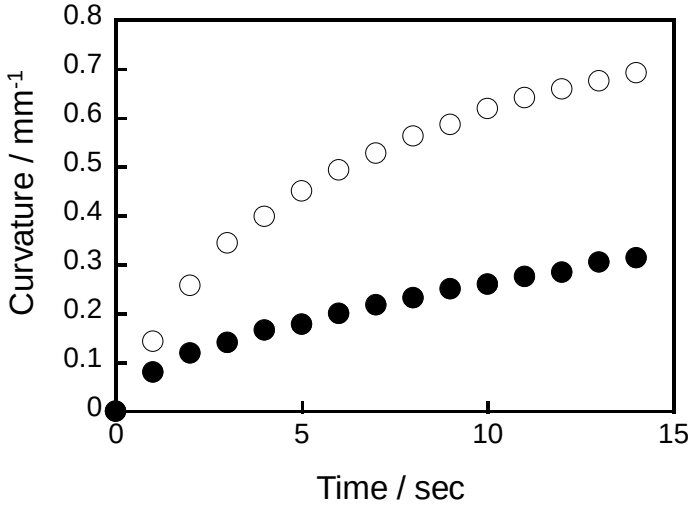

Figure 5-7. Change of the curvature to irradiation time with UV light to (0 0 1) face (●) and to (0 1 0) face (○).

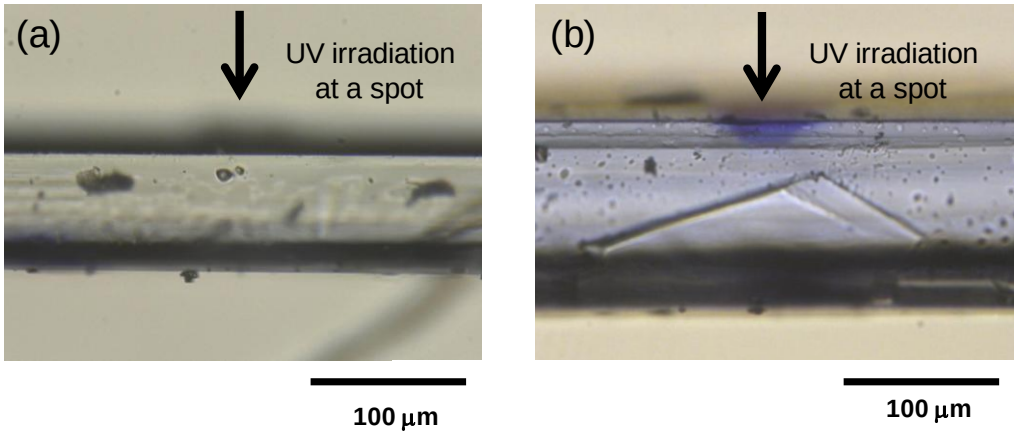

Figure 5-8. Optical microscopic photographs of the side view of the photoirradiated crystal upon irradiation with UV light to (0 1 0) face (a) and (0 0 1) face (b).

5.3.4 Dependence on the Crystal Thickness in the Photoinduced Bending and Timoshenko's Bimetal Model

The dependence property on the crystal thickness in the photoinduced bending was investigated. Figure 5-9 shows the photoinduced crystal bending of different thickness samples before (0 s) and after UV light irradiation (3, 5, and 7 s) to (0 1 0) face from left sides. Figure 5-10 shows the curvature change of different thickness samples by UV irradiation time.

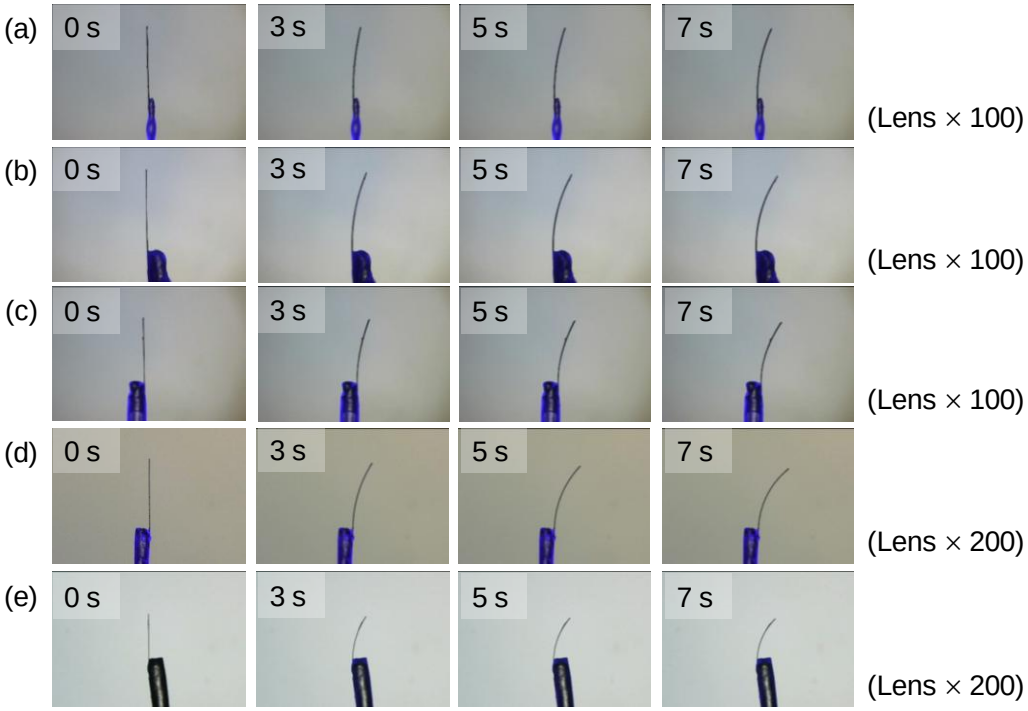

Figure 5-9. Photoinduced crystal bending upon irradiation with UV light to (0 1 0) face in different thickness samples: (a) 16.70, (b) 12.58, (c) 9.97, (d) 5.34, and (e) 3.82 μm.

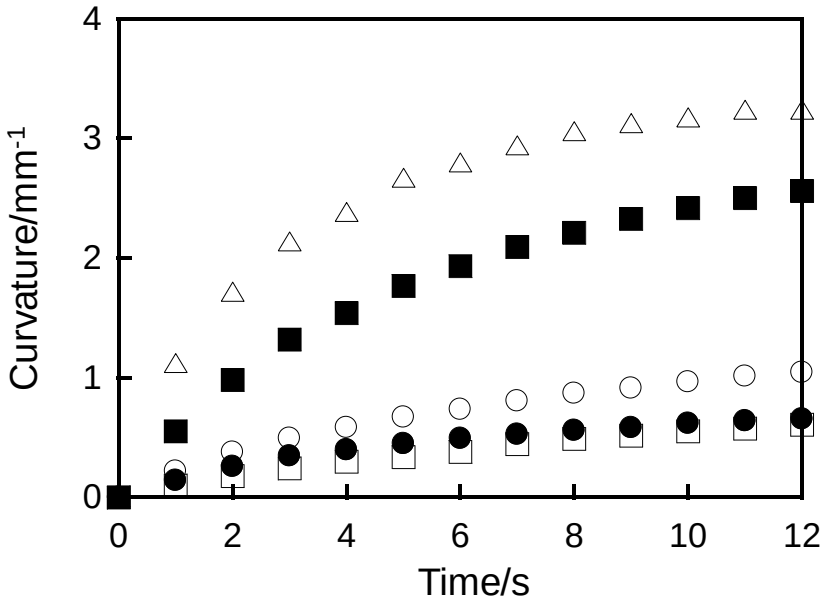

Figure 5-10. Changes of curvature to irradiation time with UV light to (0 1 0) face in different thickness samples: (△) 3.82, (■) 5.34, (○) 9.97, (●) 12.58, and (□) 16.70 μm.

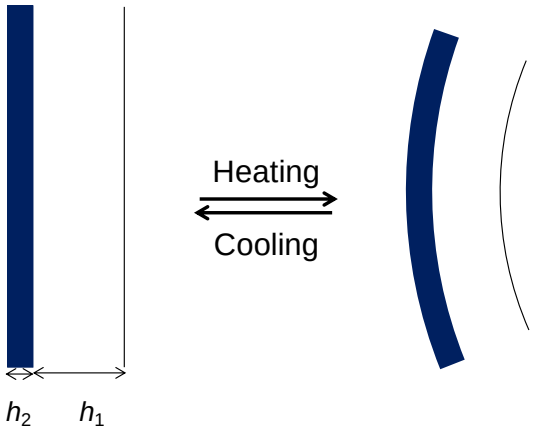

Figure 5-11. Illustration of Timoshenko's bimetal model.

The V_{init} values of the curvature change of the crystal having the thickness of 3.82, 5.34, 9.97, 12.58, and 16.70 μm were determined to be 1.489, 0.635, 0.256, 0.164, and 0.122 mm^{-1} s^{-1}, respectively. The speed of the bending depends on the thickness of the crystal. When the thickness is thin, the crystal is bent largely and rapidly. However, when the crystal thickness is 0.62 μm, the crystal cannot be bent and can be expanded.

As mentioned above, the mechanism of the photoinduced bending of diarylethene crystals is explained by heterogeneous photoisomerization of the molecules in depth because of high absorption of the crystal in the UV region. The expansion of the irradiated part of the crystal causes bending in the direction away from the incident light. This is based on the simplified bimetal model. In order to discuss the relationship between the initial speed of the

curvature change and the thickness of the crystal, the Timoshenko's equation which is widely known as the simplified bimetal model was introduced, as shown in equation (1) and Figure 5-11.[26]

$$\text{Curvature} = \frac{1}{R} = \frac{\alpha_2 - \alpha_1}{h_2} \frac{6mn(1+m)}{1+4mn+6m^2n+4m^3n+m^4n^2} \qquad (1)$$

where R is the curvature radius, α_i (i = 1, 2) are the actuation strains, h_i (i = 1, 2) are the layer thicknesses, $m = h_1/h_2$, $n = E_1/E_2$, and E_i (i = 1, 2) are the Young's moduli. Actuation strain α means that the actuator wants to expand/contract in the plane of the film in the absence of the other layer. In other word, $\alpha_2 - \alpha_1$ means the difference of the coefficient of expansion. The strain caused by the photoreaction in the crystal changes as a gradient. The bimetal model proposed by Timoshenko is not so simple for the strain in materials. Although it is consisting of two component materials, the strain changes as gradient in the direction of thickness. The bimetal model is well similar to the photoinduced crystal bending behavior. The difference of the photoreacted area between the actual experiment and the bimetal model is illustrated in Figure 5-12. The gradient in the reacted area in the experiment is different from that in the model. However, the strain in the crystal should be similar to that in the model. Therefore, the bimetal model was adapted to examine the relationship between the speed of the bending and the thickness of the crystal.

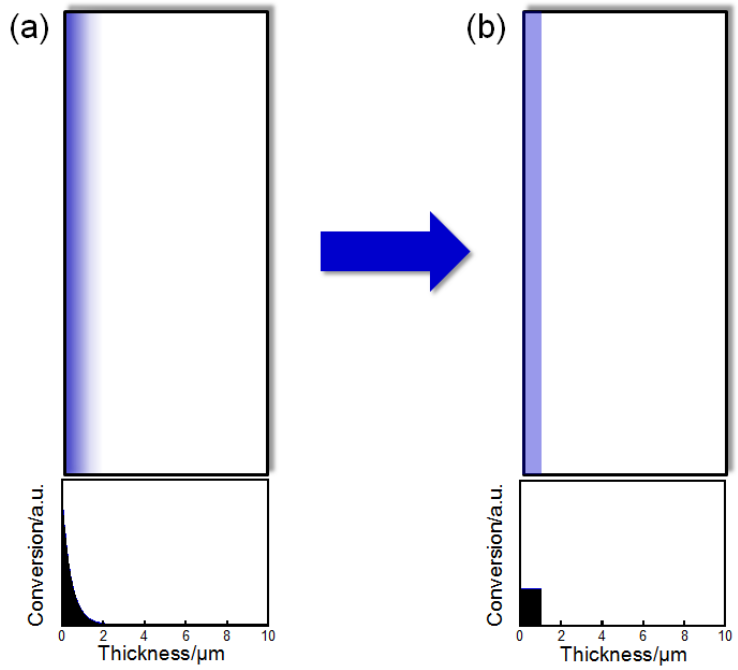

Figure 5-12. Illustration of the photoreacted area in a crystal in actual experiment (a) and the bimetal model (b). The incident light is irradiated from left side.

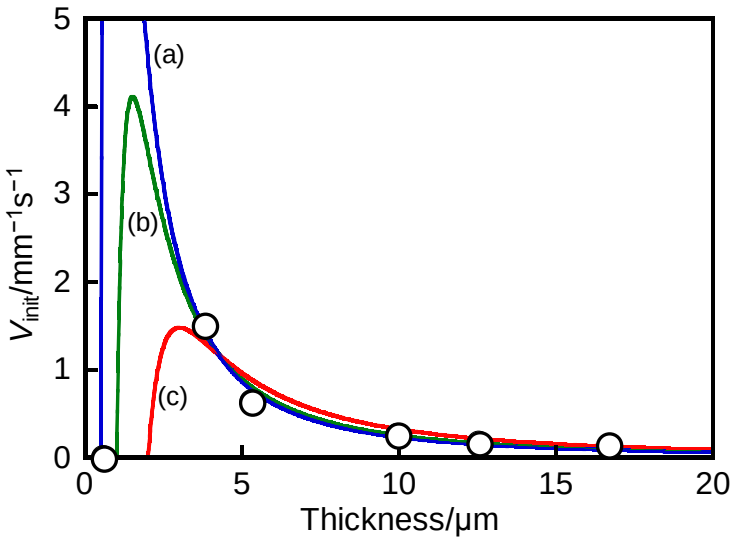

Figure 5-13. The initial speed (V_{init}) of the curvature change to the crystal thickness. The fitting curves were calculated by Timoshenko' equation: h_2 = 0.5 (blue line), 1.0 (green line), 2.0 μm (red line).

Figure 5-13 also shows the initial speed of the curvature change against the thickness of the crystal. The data were analyzed based on the assumption that Young's modulus E_1 is the same as E_2 because only a few % of diarylethene molecules in the crystal are converted from the open-ring isomer to the closed-ring isomer in the discussed condition.[8] Fitting was performed for three patterns, h_2 = 0.5 (blue line), 1.0 (green line), 2.0 μm (red line). In the case of h_2 = 0.5 μm (blue line), the fitting curve cannot explain the fact that the crystal only expands when the crystal thickness is 0.62 μm. Using h_2 = 2.0 μm (red line), the fitting curve do not so match the experimental data. The best fitted curve is shown as a green line in the figure when h_2 = 1.0 μm. The value of $\alpha_2 - \alpha_1$ used for the best fitting was 0.0046. This value is enough to induce the large bending.[9]

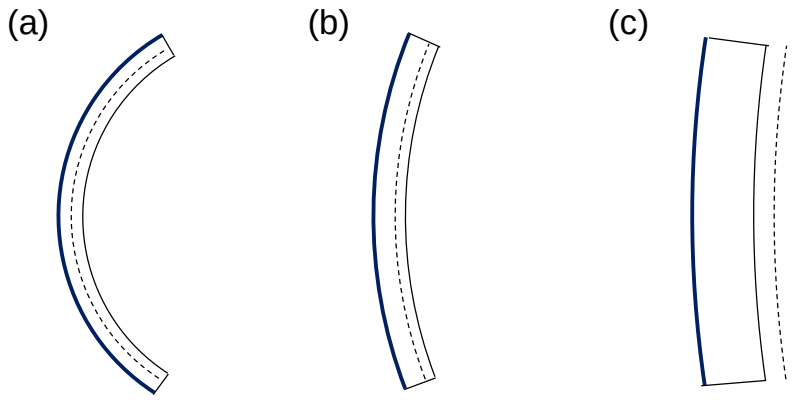

Figure 5-14. Shape of bending crystal and the line of zero strain (- - - -) by a difference of crystal thickness: (a) 3.82, (b) 5.34, (c) 9.97 μm.

Moreover, the line of zero bending strain was also calculated.[27] Figure 5-14 shows the shape of bending crystal and the line of zero strain in the case of crystals having different thickness. The line of the zero strain means that the line length does not change before and after bending. In other words, the crystal length in the left and right side of the line of zero strain changes longer and shorter after bending, respectively. When the crystal is bent largely (crystal thickness = 3.82 μm), the line of zero strain is almost center in the crystal. By the expansion of the photoreacted layer, the expansion and contraction of the non-reacted layer in left and right side of the line of zero strain were respectively caused. As the degree of bending decreases, the contraction of nonreacted layer became small (crystal thickness = 5.34 μm). When the crystal thickness is 9.97 μm, the line of zero strain is out of the crystal. The non-reacted layer expands. Bimetal model is the complete two-component model. In fact, the reaction in the crystal has occurred as a gradient. The model cannot completely explain the bending mechanism. However, the experimental results can be well explained by the simple bimetal model using Timoshenko's equation.

5.4 Summary

It has been demonstrated that 1,2-bis(2-methyl-5-(4-(1-naphthoyloxymethyl)phenyl)-3-thienyl)perfluorocyclopentene (**3a**) undergoes photochromism in the single crystalline phase and shows reversible photoinduced crystal bending upon alternating UV and visible light irradiation. The photoinduced bending can be repeated over 80 cycles. It is revealed that the photoinduced bending is caused by the expansion of the direction to *a*-axis and a gradient in the extent of photoisomerization. Moreover, it is found that the photoinduced bending behavior depends on the face irradiated with UV light. This is ascribed to the difference of the molecular packing. Furthermore, the dependence property on the crystal thickness in the photoinduced bending has been investigated. The correlation between the crystal thickness and initial speed of curvature change was well explained by Timoshenko's bimetal model. These findings bring good perspectives for design of photomechanical actuators.

5.5 References

1. Y. Nabetani, H, Takamura, Y. Hayasaka, T. Shimada, S. Takagi, H. Tachibana, D. Masui, Z. Tong, H. Inoue, *J. Am. Chem. Soc.* **2011**, *133*, 17130.
2. M. Kobayashi, J. Abe, *J. Am. Chem. Soc.* **2012**, *134*, 20593.
3. Y. Yu, M. Nakano, T. Ikeda, *Nature* **2003**, *425*, 145.
4. M. Yamada, M. Kondo, J. Mamiya, Y. Yu, M. Kinoshita, C. J. Barrett, T. Ikeda, *Angew. Chem. Int. Ed.* **2008**, *47*, 4986.
5. N. Hosono, T. Kajitani, T, Fukushima, K. Ito, S. Sasaki, M. Takata, T. Aida, *Science* **2010**, *330*, 808.

6. S. Kobatake, S. Takami, H. Muto, T. Ishikawa, M. Irie, *Nature* **2007**, *446*, 778.
7. K. Uchida, S. Sukata, Y. Matsuzawa, M. Akazawa, J. J. D. de Jong, N. Katsonis, Y. Kojima, S. Nakamura, J. Areephong, A. Meetsma, B. L. Feringa, *Chem. Commun.* **2008**, 326.
8. M. Morimoto, M. Irie, *J. Am. Chem. Soc.* **2010**, *132*, 14172.
9. F. Terao, M. Morimoto, M. Irie, *Angew. Chem. Int. Ed.* **2012**, *51*, 901.
10. S. Kobatake, H. Hasegawa, K. Miyamura, *Cryst. Growth Des.* **2011**, *11*, 1223.
11. R. O. Al-Kaysi, C. J. Bardeen, *Adv. Mater.* **2007**, *19*, 1276.
12. L. Zhu, R. O. Al-Kaysi, R. J. Dillon, F. S. Tham, C. J. Bardeen, *Cryst. Growth Des.* **2011**, *11*, 4975.
13. L. Zhu, R. O. Al-Kaysi, C. J. Bardeen, *J. Am. Chem. Soc.* **2011**, *133*,12569.
14. H. Koshima, N. Ojima, H. Uchimoto, *J. Am. Chem. Soc.* **2009**, *131*, 6890.
15. H. Koshima, H. Nakaya, H. Uchimoto, N. Ojima, *Chem. Lett.* **2012**, *41*, 107.
16. S. Kobatake, T. Yamada, K. Uchida, N. Kato, M. Irie, *J. Am. Chem. Soc.* **1999**, *121*, 2380.
17. M. Irie, T. Lifka, S. Kobatake, N. Kato, *J. Am. Chem. Soc.* **2000**, *122*, 4871.
18. S. Kobatake, M. Irie, *Bull. Chem. Soc. Jpn.* **2004**, *77*, 195.
19. M. Morimoto, M. Irie, *Chem. Commun.* **2005**, *41*, 3895.
20. M. Irie, S. Kobatake, M. Horichi, *Science* **2001**, *291*, 1769.
21. C. W. Lange, M. Földeàki, V. I. Nevodchikov, V. K. Cherkasov, G. A. Abakumov, C. G. Pierpont, *J. Am. Chem. Soc.* **1992**, *114*, 4220.
22. E. V. Boldyreva, *Russ. J. Coord. Chem.* **2001**, *27*, 297.
23. M. Pärs, C. C. Hofmann, K. Willinger, P. Bauer, M. Thelakkat, J. Koehler, *Angew. Chem. Int. Ed.* **2011**, *50*, 11405.
24. G. M. Sheldrick, *SHELXL-97*, *Program for Crystal Structure Refinement*, University of Göttingen, Germany, **1997**.
25. S. Kobatake, K. Uchida, E. Tsuchida, M. Irie, *Chem. Commun.* **2002**, 2804.
26. S. Timoshenko, *J. Opt. Soc. Am.* **1925**, *11*, 233.
27. M. Christophersen, B. Shapiro, E. Smela, *Sens. Act. B* **2006**, *115*, 596.

Chapter 6

Photoinduced Twisting of a Photochromic Diarylethene Crystal

6.1. Introduction

The photomechanical crystal has attracted the attention of many chemists. There are various types of the photoinduced crystal shape change such as contraction, expansion, bending, separation, curling and so on, as shown in General Introduction.[1-21] Recently, 9-anthracenecarboxylic acid (9AC) crystal has been shown to twist upon UV light irradiation.[16] 9AC can undergo a reversible [4 + 4] photocyclodimerization in the crystalline phase. Bardeen and co-workers have suggested that the crystal twisting is induced by generating interfacial strain within the microcrystal between unreacted monomer and photoreacted dimer regions. The crystal relaxes back to the original shape over the course of minutes accompanying thermal dissociation of the dimer back into its monomeric form. On the other hand, diarylethene crystals show reversible photomechanical works by only photoirradiation. The crystal shape can maintain in the dark. It is an advantage for applications to control of photomechanical behavior in the desired time.

In this chapter, a photoinduced twisting of a photochromic diarylethene crystal is discussed. The colorless needle-like crystal of the diarylethene rapidly can twist accompanying the color change to blue upon irradiation with UV light. The twisting of the crystal relaxed back to the original shape in a few seconds with visible light irradiation. Such a photoinduced crystal twisting provides a new type of photomechanical actuators.

6.2 Experimental Section

6.2.1 General

^{1}H NMR spectroscopy (Bruker AV-300N) was measured at 300 MHz. Deuterated chloroform ($CDCl_3$) was used as the solvent and tetramethylsilane (TMS) as an internal standard, respectively. Mass spectra were obtained using a JEOL JMS-700/700S mass spectrometer. High-performance liquid chromatography (HPLC) was carried out using a Hitachi L-7150/L-2400 HPLC system equipped with a Kanto Chemical Mightysil Si 60 Column. The photoinduced crystal twisting was observed using a Keyence VHX-500 digital microscope. X-ray single-crystal structure analysis was carried out using Rigaku AFC/Mercury CCD diffractometer with graphite monochromated $Mo_{K\alpha}$ radiation. The structure was solved by direct methods and refined by the full-matrix least-squares method on F^2. The polarized absorption spectra were measured using a Nikon ECLIPSE E600POL polarizing optical microscope attached a Hamamatsu PMA-11 photonic multi-channel analyzer as the photodetector. UV irradiation was carried out using a Keyence UV-LED

UV-400/UV-50H (365-nm light), and a super high pressure mercury lamp (100 W; UV-1A filter (365 nm light excitation)) attached with the polarizing optical microscope. Visible light irradiation was carried out using a halogen lamp (100 W).

6.2.2 Materials

1-[2-Methyl-5-(4-(1-naphthoyloxy)methylphenyl)-3-thienyl]-2-(2-methyl-5-phenyl-3-thienyl)perfluorocyclopentene (**4a**). A solution of 1-[2-methyl-5-(4-hydroxymethylphenyl)-3-thienyl]-2-(2-methyl-5-phenyl-3-thienyl)perfluorocyclopentene[22] (500 mg; 0.91 mmol), 1-naphthoic acid (313 mg; 1.82 mmol), dicyclohexylcarbodiimide (410 mg; 2.0 mmol), and 4-dimethylaminopyridine (120 mg; 1.0 mmol) in anhydrous tetrahydrofuran (THF) (12 mL) was stirred under argon for 4 h at room temperature. To the reaction mixture was added an aqueous sodium hydrogen carbonate solution, and the mixture was extracted with ether. The organic layer was dried over $MgSO_4$. After removal of the solvent, the residue was purified by column chromatography on silica-gel using *n*-hexane/ethyl acetate (7:3) as the eluent. Pure **4a** was obtained by a further purification with HPLC. Yield: 578 mg (90.1%). **4a**: ^{1}H NMR (300 MHz, $CDCl_3$): δ = 1.96 (s, 3H, CH_3), 1.97 (s, 3H, CH_3), 5.46 (s, 2H, CH_2), 7.2-7.7 (m, 14H, Ar), 7.90 (d, *J* = 8.0 Hz, 1H, Ar), 8.04 (d, *J* = 8.2 Hz, 1H, Ar), 8.24 (dd, *J* = 1.3, 7.3 Hz, 1H, Ar), 8.95 (d, *J* = 8.6 Hz, 1H, Ar). HR-MS (FAB) *m/z* = 704.1277; Calcd. for $C_{39}H_{26}F_6O_2S_2$ *m/z* = 704.1278 (M^+).

6.3 Results and Discussion

6.3.1 Photoinduced Crystal Twisting

Figure 6-1 illustrates the photoreversible single crystal twisting of 1-[2-methyl-5-(4-(1-naphthoyloxymethyl)phenyl)-3-thienyl]-2-(2-methyl-5-phenyl-3-thienyl)perfluorocyclopentene (**4a**) upon alternating irradiation with UV (λ = 365 nm) and visible light (λ > 500 nm). The single crystal was prepared by recrystallization from *n*-hexane/ether solution. The thickness, width, and length of the crystal are ca. 1.5 μm, 11 μm, and 320 μm, respectively. Upon UV light irradiation to the whole crystal, the molecules in the crystal underwent the photocyclization reaction from the open-ring isomer to the closed-ring isomer, and the crystal of **4a** rapidly twisted accompanying the color change of the crystal from colorless to blue. The twisting and color of the crystal was maintained in the dark. By irradiation with visible light, the blue color disappeared by the back reaction to the initial open-ring isomer and the twisting of the crystal relaxed back to the original shape in a few seconds. Such reversible twisting upon alternating irradiation with UV and visible light could be repeated over 30 cycles, as shown in Figure 6-2. These results have revealed that the crystal twisting is induced by photochromic reaction of diarylethene molecules in the crystal.

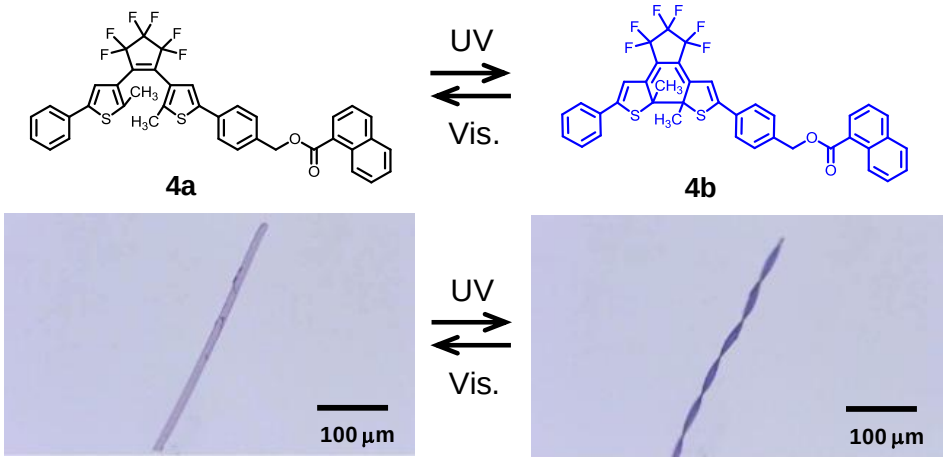

Figure 6-1. Molecular structure change and photoreversible crystal twisting of diarylethene **4a** upon irradiation with UV (λ = 365 nm) and visible light (λ > 500 nm).

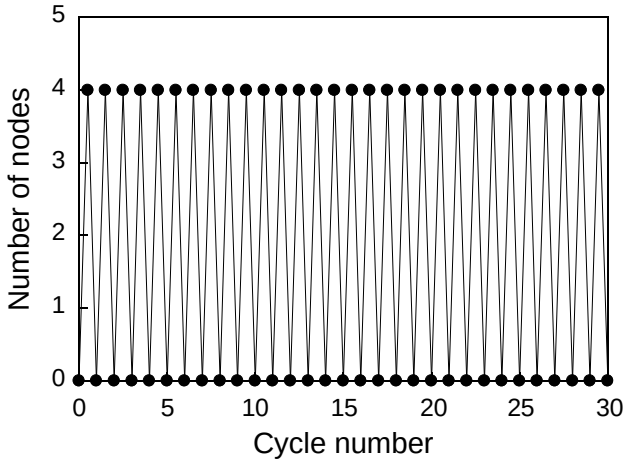

Figure 6-2. Reversibility of the crystal twisting. The number of nodes in the twisted crystal is examined: UV light irradiation for 8 s and visible light irradiation for 30 s. The photoreversible twisting can be repeated over 30 cycles.

6.3.2 Direction of the Twisting

There are two types in the direction of the twisting, left-handed helix and right-handed helix. The helix which twists counterclockwise to the direction of the movement is called left-handed helix. The reverse one is called right-handed helix, as shown in Figure 6-3. In order to know whether both helix types exist, the crystals on the petri dish were concurrently irradiated with UV light and the number of the left- and right-handed helical crystals was counted. Both helix types were confirmed at the almost same ratio, as shown in Figures 6-4 and 6-5. It was noticed that the direction of the twisting depends on the face irradiated with UV light. However, a half of all the crystals were not twisted. It is ascribed that the twisting depends on the crystal thickness.

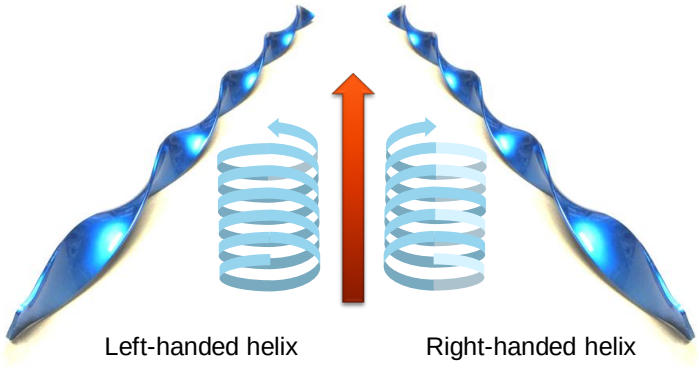

Figure 6-3. Type of twisting; left-handed helix and right-handed helix.

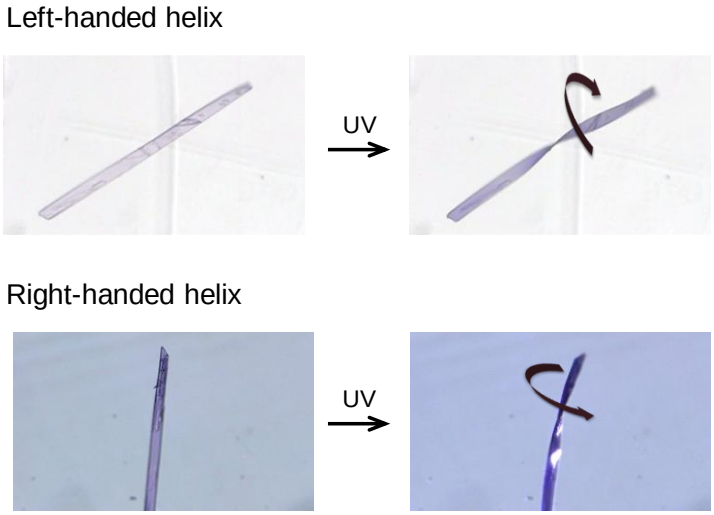

Figure 6-4. Photoinduced crystal twisting in left-handed helix and right-handed helix.

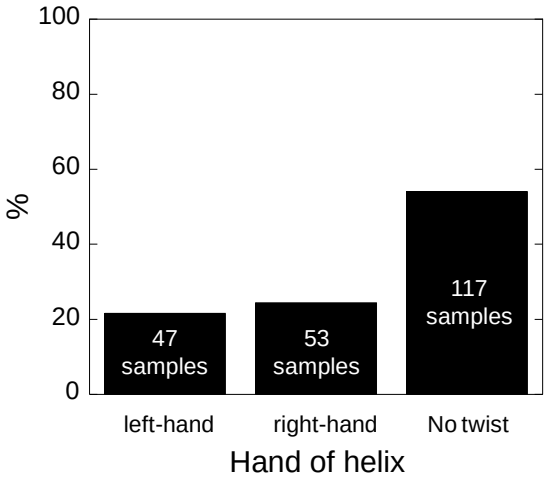

Figure 6-5. Histogram of photoinduced twist: the content of left-handed helix, right-handed helix, and no twist. "No twist" includes contraction. The number of total samples is 217.

6.3.3 Crystal Shape and Molecular Packing

Single crystal X-ray crystallography for a crystal of **4a** showed a monoclinic crystal system and a space group of $P2_1$ (Table 6-1).[23] The crystal is a chiral, but the origin is due to a disorder of perfluorocyclopentene. Therefore, if the disorder is absent, the space group should be $P2_1/c$. Figure 6-6 shows the shape and the molecular packing of crystal **4a** before UV irradiation, viewed from the $(0\ \bar{1}\ 0)$ face. The packing diagrams viewed from other surfaces are shown in Figure 6-7. The diarylethene molecules are regularly oriented to the direction of *a* axis with a tilt angle of ca. 50°, and aligned perpendicularly to the $(0\ \bar{1}\ 0)$ face. All of the diarylethene molecules are fixed in a photoreactive antiparallel conformation, and the distance of the reactive carbon atoms in the thiophene rings are 3.50 Å. It is short enough for the diarylethene to undergo photocyclization in the crystalline phase.[24]

Table 6-1. X-ray crystallographic data for 1-(2-methyl-5-(4-(1-naphthoyloxymethyl)phenyl)-3-thienyl)-2-(2-methyl-5-phenyl-3-thienyl)perfluorocyclopentene.

Empirical formula	$C_{39}H_{26}F_6O_2S_2$
Formula weight	704.74
Temperature	93(2) K
Crystal system	Monoclinic
Space group	$P2_1$
Unit cell dimensions	a = 6.1012(7) Å b = 45.471(6) Å c = 11.3555(14) Å β = 93.380(7)°
Volume	3144.8(7)
Z	4
Density	1.488 g cm^{-3}
Crystal size	0.15 × 0.03 × 0.03 mm^3
Goodness-of-fit on F^2	1.027
Final R [$I > 2\sigma(I)$]	$R1$ = 0.0797, $wR2$ = 0.1858
R (all data)	$R1$ = 0.1200, $wR2$ = 0.2175
Flack parameter	0.28(12)

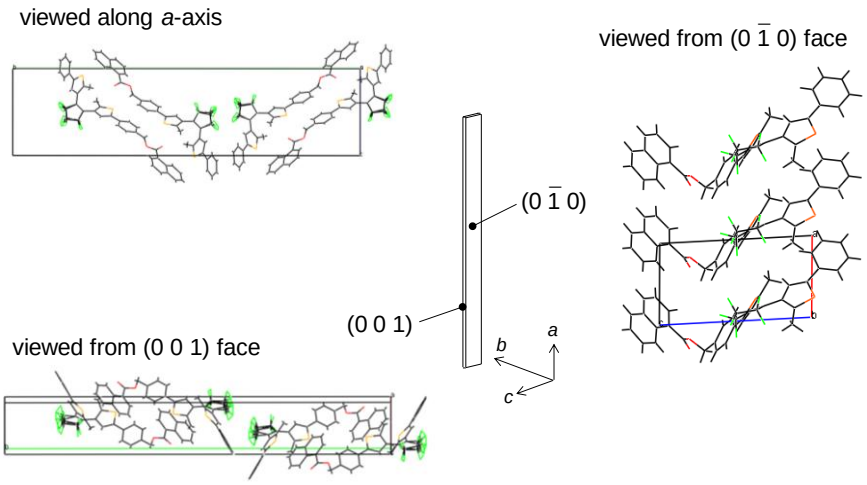

Figure 6-6. Crystal shape and molecular packing.

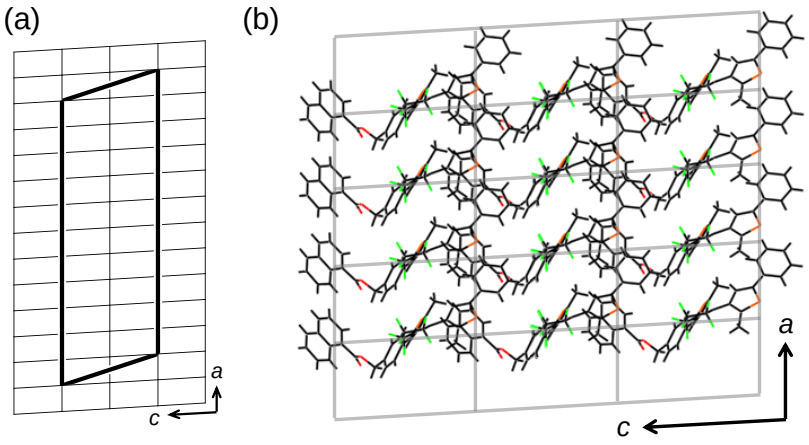

Figure 6-7. Molecular packing of crystal **4a**. The crystal shape (a) and molecular packing (b) of **4a** in the crystal viewed from the (0 $\bar{1}$ 0) face are depicted. The crystal shape in (a) is shown by bold line.

6.3.4 Mechanism of the Twisting

The difference of the crystal surface on (0 1 0) and (0 $\bar{1}$ 0) is distinguished according to the shape of the crystal surface and the absorption anisotropy of the closed-ring isomer, as shown in Figure 6-8. When the (0 $\bar{1}$ 0) face was irradiated with UV light, the crystal twisted in right-handed helix. On the other hand, the crystal twisted in left- handed helix when the (0 1 0) face was irradiated with UV light, as shown in Figure 6-9. When UV light irradiation was performed from both sides on (0 $\bar{1}$ 0) and (0 1 0) faces in the whole crystal, the crystal was contracted, as shown in Figure 6-10. This result indicates that the crystal twisting was caused

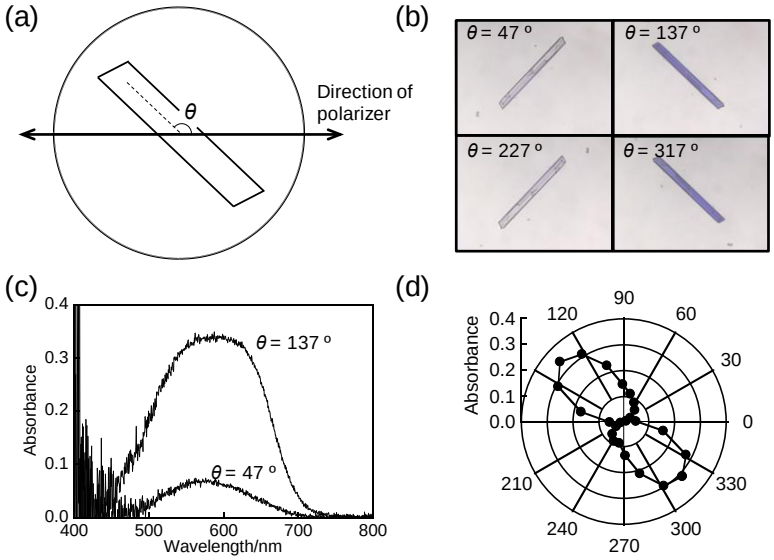

Figure 6-8. Polarized absorption spectra of the closed-ring isomer in the crystal on the (0 1 0) face: (a) crystal shape and direction, (b) photographs of the photoirradiated colored crystal observed under polarized light, (c) polarized absorption spectrum, (d) polar plots of absorbance at 590 nm.

(a) UV irradiation to the (0 $\bar{1}$ 0) face (in right-handed helix)

(b) UV irradiation to the (0 1 0) face (in left-handed helix)

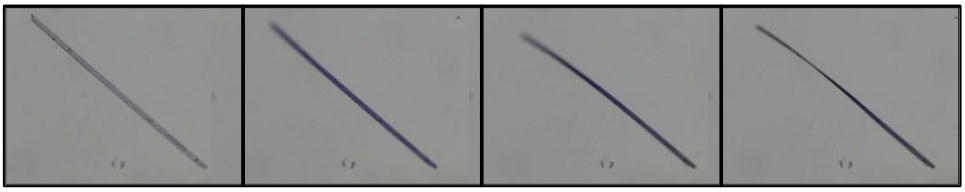

Figure 6-9. Dependence of twisting direction on the face irradiated with UV light. The same crystal was used in (a) and (b).

by the heterogeneity of the photochromic reaction in the thickness direction of the crystal because of high absorbance of the crystal. Some of diarylethene crystals have been so far reported to cause the photoinduced reversible bending.[1-5] In the present case, the contraction is considered to occur in the diagonal direction. When irradiated with UV light, the photoisomerization of the diarylethene molecules from the open-ring isomer **4a** to the

closed-ring isomer **4b** occurs in the crystalline phase. The twisted thiophene rings become coplanar and thickness of each molecule is reduced. The closed-ring isomers in the photoirradiated crystal can stack each other accompanying the change in the cell dimensions. This change in the cell dimensions causes the contraction or the twisting of the crystal.

The change in the cell dimensions upon UV light irradiation is generally confirmed by X-ray crystallographic analysis. Here, the changes in the cell dimensions were determined from the shape change of the contracted crystal after UV light irradiation (Figure 6-10). The crystal was irradiated with UV light from all of direction because of homogeneous photoisomerization. The coordinates on four corners of the crystal before and after UV light irradiation was plotted in rectangular coordinate system. When transforming from rectangular coordinate system to oblique coordinate system, the cell dimensions changed so that coordinates might become the same in two different oblique coordinate systems. The cell parameters correspond to change from a = 6.10 Å, c = 11.36 Å, and β = 93.4° to a' = 5.98 Å, c' = 10.08 Å, and β' = 96.5°, respectively. The a- and c-axes contracted as much as 2.0 and 11%, respectively, and β angle enlarged as much as 3.3%. The shape of the unit cell viewed from (0 $\bar{1}$ 0) face before and after UV light irradiation is shown in Figure 6-11. The contraction of the unit cell takes place in the direction of top-left to bottom-right when the unit cell was viewed from (0 $\bar{1}$ 0) face. On the other hand, the contraction of the unit cell takes place in the direction of top-right to bottom-left when the unit cell was viewed from (010) face. The photochromic reaction undergoes in a gradient to the thickness direction

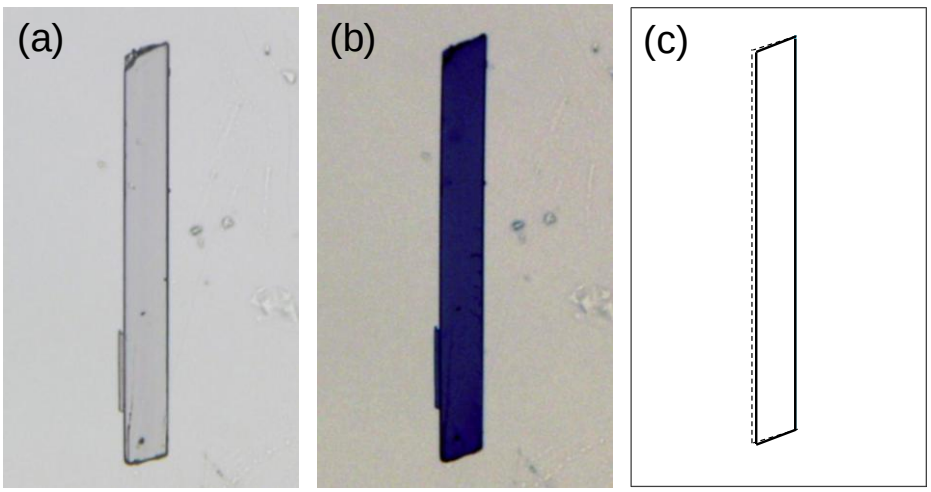

Figure 6-10. Shape of the contracted crystal. The colorless crystal (a) was irradiated with UV light to form the colored crystal (b). The colored crystal was produced with UV light irradiation from both sides on the crystal surfaces for a few minutes. The photoisomerization took place homogeneously in the crystal. (c) shows the crystal shapes before (dashed line) and after (solid line) UV light irradiation. The right edges of the colorless and colored crystals are superimposed.

because of high absorption in the crystal. Therefore, the crystal can twist in right-handed helix or left-handed helix depending on the contraction direction, as shown in Figure 6-12. There is an induction period of ca. 2 s until the crystal begins to twist (Figure 6-13). A strain required to perform twist arises in this period. The photoirradiation time to the reversed side during the twisting is shorter than the period. The direction of the twisting can be determined by the starting irradiation face.

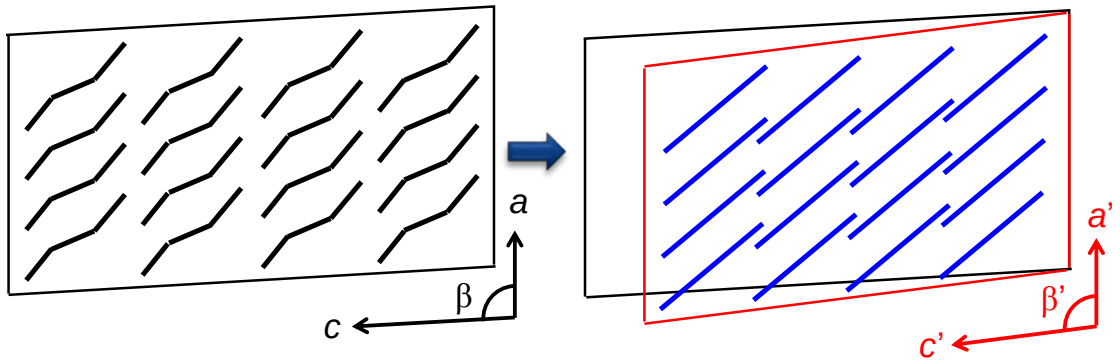

Figure 6-11. Shape of the unit cell viewed from (0 $\bar{1}$ 0) face before and after UV light irradiation. The diarylethene molecules were shown by line. The expected molecular packing of the closed-ring isomer after UV light irradiation was depicted as blue lines.

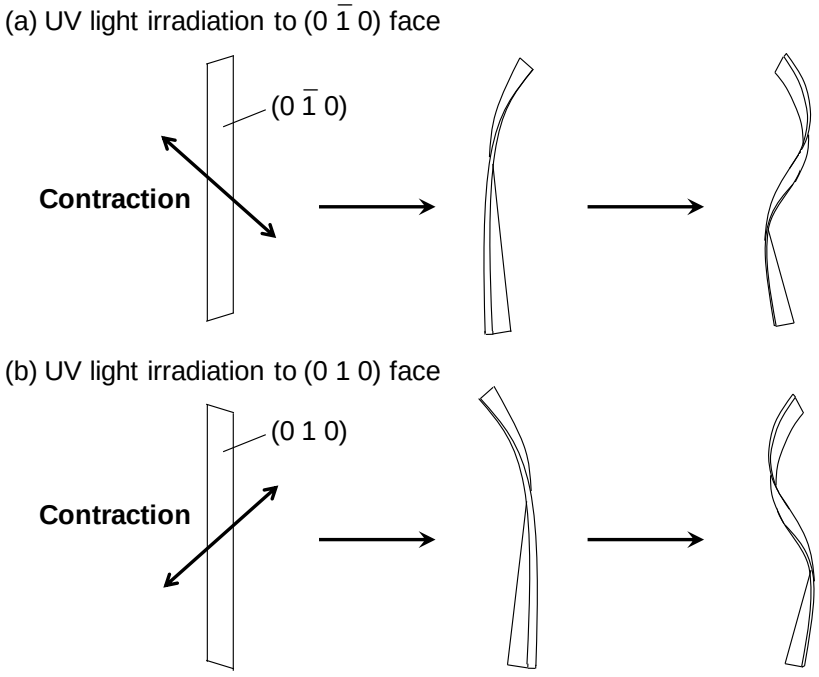

Figure 6-12. Relationship between the direction of the twisting and the face irradiated with UV light. The crystal twists in right-handed helix (a) and in left-handed helix (b). The arrows show the direction of contraction of the crystal surface.

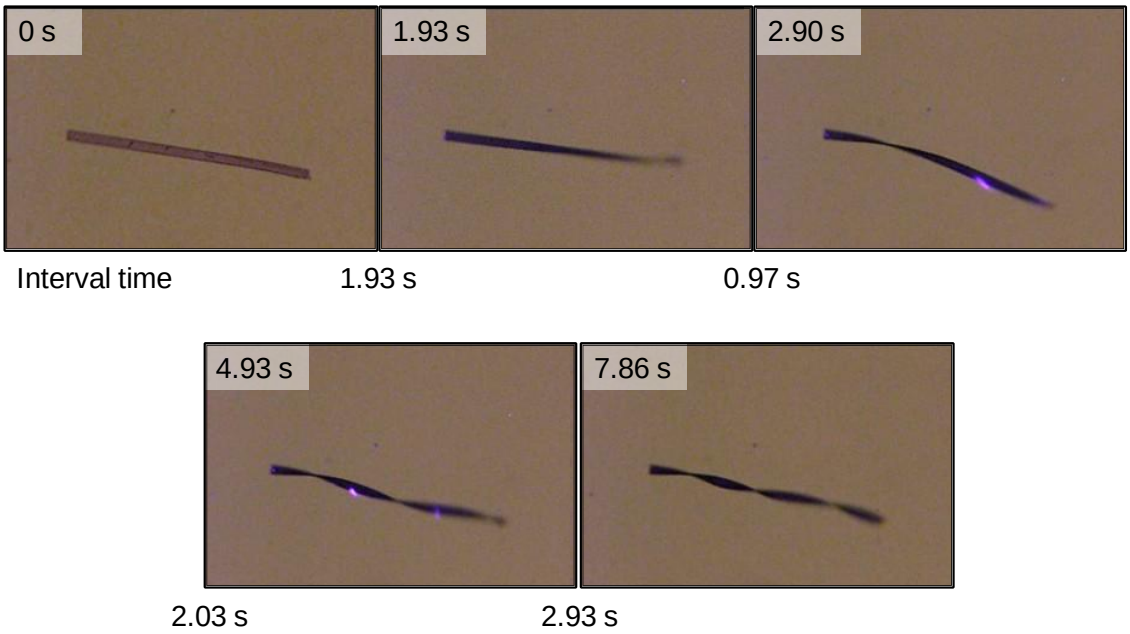

Figure 6-13. Induction period until the crystal begins to twist. Upper-left time in each picture shows UV irradiation time. Lower time between pictures shows interval time.

6.4 Summary

Photoinduced crystal twisting of diarylethene crystal was newly found. The photoreversible twisting of the diarylethene crystal could be repeated over 30 cycles by alternating irradiation with UV and visible light. The crystal twisting takes place in both left-handed helix and right-handed helix. The direction of the twisting depends on the face irradiated with UV light. Furthermore, the direction of contraction in the unit cell was determined using the contracted crystal which underwent the photocyclization reaction in the whole crystal by irradiation from both sides on the crystal surfaces. From these results, the twisting of the crystal requires both the gradient of the photocyclization conversion in the thickness direction and the contraction of the crystal in the diagonal direction.

6.5 References

1. S. Kobatake, S. Takami, H. Muto, T. Ishikawa, M. Irie, *Nature* **2007**, *446*, 778.
2. K. Uchida, S. Sukata, Y. Matsuzawa, M. Akazawa, J. J. D. de Jong, N. Katsonis, Y. Kojima, S. Nakamura, J. Areephong, A. Meetsma, B. L. Feringa, *Chem. Commun.* **2008**, 326.
3. L. Kuroki, S. Takami, K. Yoza, M. Morimoto, M. Irie, *Photochem. Photobiol. Sci.* **2010**, *9*, 221.
4. M. Mrimoto, M. Irie, *J. Am. Chem. Soc.* **2010**, *132*, 14172.
5. F. Terao, M. Morimoto, M. Irie, *Angew. Chem. Int. Ed.* **2012**, *51*, 901.

6. H. Koshima, H. Nakaya, H. Uchimoto, N. Ojima, *Chem. Lett.* **2012**, *41*, 107.
7. H. Koshima, N. Ojima, H. Uchimoto, *J. Am. Chem. Soc.* **2009**, *131*, 6890.
8. H. Koshima, N. Ojima, *Dyes Pigm.* **2012**, *92*, 798.
9. O. S. Bushuyev, T. A. Singleton, C. J. Barrett, *Adv. Mater.* **2013**, *25*, 1796.
10. O. S. Bushuyev, A. Tomberg, T. Friščić, C. J. Barrett, *J. Am. Chem. Soc.* **2013**, *135*, 12556.
11. H. Koshima, K. Takechi, H. Uchimoto, M. Shiro, D. Hashizume, *Chem. Commun.* **2011**, *47*, 11423.
12. H. Koshima, R. Matsuo, M. Matsudomi, Y. Uemura, M. Shiro, *Cryst. Growth Des.* **2013**, *13*, 4330.
13. R. O. Al-Kaysi, A. M. Müller, C. J. Bardeen, *J. Am. Chem. Soc.* **2006**, *128*, 15938.
14. R. O. Al-Kaysi, C. J. Bardeen, *Adv. Mater.* **2007**, *19*, 1276.
15. L. Zhu, R. O. Al-Kaysi, R. J. Dillon, F. S. Tham, C. J. Bardeen, *Cryst. Growth Des.* **2011**, *11*, 4975.
16. L. Zhu, R. O. Al-Kaysi, C. J. Bardeen, *J. Am. Chem. Soc.* **2011**, *133*, 12569.
17. L. Zhu, A. Agarwal, J. Lai, R. O. Al-Kaysi, F. S. Tham, T. Ghaddar, L. Muellera, C. J. Bardeen, *J. Mater. Chem.* **2011**, *21*, 6258.
18. T. Kim, M. K. Al-Muhanna, S. D. Al-Suwaidan, R. O. Al-Kaysi, C. J. Bardeen, *Angew. Chem. Int. Ed*. **2013**, *52*, 6889.
19. T. Kim, L. Zhu, L. J. Mueller, C. J. Bardeen, *CrystEngComm* **2012**, *14*, 7792.
20. J.-K. Sun, W. Li, C. Chen, C.-X. Ren, D.-M. Pan, J. Zhang, *Angew. Chem. Int. Ed.* **2013**, *52*, 6653.
21. P. Naumov, J. Kowalik, K. M. Solntsev, A. Baldridge, J.-S. Moon, C. Kranz, L. M. Tolbert, *J. Am. Chem. Soc.* **2010**, *132*, 5845.
22. S. Kobatake, H. Kuratani, *Chem. Lett.* **2006**, *35*, 628.
23. CCDC 941833 (**4a**) contains the supplementary crystallographic data for this paper. These data can be obtained free of charge from The Cambridge Crystallographic Data Centre via www. ccdc.cam.ac.uk/data_request/cif.
24. S. Kobatake, K. Uchida, E. Tsuchida, M. Irie, *Chem. Commun.* **2002**, 2804.

Conclusions

In this thesis, the photochromic reaction behavior and solid state property changes of diarylethene crystals, especially polymorphic phase transition, surface wettability change, and photoinduced crystal shape change, are described.

In Chapter 1, the polymorphism and the thermodynamic phase transition through crystal-to-crystal process of diarylethene **1a** have been described. It is clarified that the phase transition occurs like the domino taking advantage of the molecule which moved first by considering from the motion of diarylethene molecules in the phase transition.

In Chapter 2, the thermodynamic phase transition from a plate-like crystal to a needle-like crystal via crystal-to-melt-to-crystal process has been described. The crystal shape and molecular packing are quite different between polymorphic crystals to result in the phase transition accompanying the melting of crystal. It is also clarified that the phase transition temperature can be controlled by the photochromic reaction from the open-ring isomer to the closed-ring isomer upon UV light irradiation. The photomicropatterning can be established with the resolution of ca. 20 μm scale.

In Chapter 3, the crystallization of diarylethene **2a** in a polymer by heating and the control of the crystallization by UV irradiation have been described. It is clarified that the presence of the closed-ring isomer in **2a**/PMMA can suppress the crystallization. The contact angles of water droplet is determined to be 81.6° and 116.5° at the UV-irradiated and non-irradiated areas, respectively. The photomicropatterning of the crystallization can be established with the resolution of ca. 4 μm scale.

In Chapter 4, the new fabrication method of superhydrophobic surface with high-water adhesive property has been described. The crystal growth of the polymorphic diarylethene **2a** enables to make the superhydrophobic surface with high-water adhesive property. The ease of the penetration of water into the rough surface is very important. The photomicropatterning of the rapid polymorphic crystal growth of the diarylethene has also been demonstrated in a PMMA film. The crystal growth by Ostwald ripening can be controlled by the presence of a few percent of the photoisomer of the diarylethene. The high density area of microcrystals had a larger contact angle with water than that of low density area. Such a photopatterning process offers a useful tool for controlling surface wettability in applications.

In Chapter 5, the relationship between the crystal thickness and the photoinduced bending speed of the crystal of diarylethene **3a** has been described. The bending speed of different thickness crystals can be evaluated by the initial speed of the curvature change. The relationship between the initial speed of the curvature change and the crystal thickness has been well explained by simplified Timoshenko's bimetal model. This result must bring good perspectives for design of photomechanical actuators.

In Chapter 6, the photoinduced crystal twisting of diarylethene **4a** has been described. The crystal of **4a** photoreversibly twists upon alternating irradiation with UV and visible light. It can be repeated over 30 cycles. The crystal twisting takes place in both left-handed helix and right-handed helix in the same ratio. The direction of the twisting depends on the face irradiated with UV light and the photoinduced crystal twisting is caused by contracting in the diagonal direction of the crystal. Such a photoinduced crystal twisting provides a new type of photomechanical actuators.

Diarylethene crystals used in this thesis show photochromism in the crystalline phase and unique solid state property changes such as polymorphic phase transition, surface wettability change, and photoinduced crystal shape change. Their solid state property changes can be controlled by photochromic reaction of diarylethene molecules in the crystalline phase upon photoirradiation without any direct contact and electronic wires. It is concluded that investigation and consideration of the solid state property changes of diarylethene crystals lead to new functional photoresponsive materials.

List of Publications

1. Thermodynamic Phase Transition Through Crystal-to-Crystal Process of Photochromic 1,2-Bis(5-phenyl-2-propyl-3-thienyl)perfluorocyclopentene
D. Kitagawa, S. Kobatake, *Chem.−Asian. J.* **2014**, *9*, 289–293.
---------- Chapter 1

2. Control of Surface Wettability and Photomicropatterning with a Polymorphic Diarylethene Crystal upon Photoirradiation
D. Kitagawa, I. Yamashita, S. Kobatake, *Chem.−Eur. J.* **2011**, *17*, 9825–9831.
---------- Chapter 2

3. Photoinduced Micropatterning by Polymorphic Crystallization of a Photochromic Diarylethene in a Polymer Film
D. Kitagawa, I. Yamashita, S. Kobatake, *Chem. Commun.* **2010**, *46*, 3723–3725.
---------- Chapter 3

4. Morphology, Wettability, and Photomicropatterning of Superhydrophobic Surface with High Adhesive Force by Crystal Growth of a Photochromic Diarylethene
D. Kitagawa, S. Kobatake, *Chem. Sci.* **2012**, *3*, 1445–1449.
---------- Chapter 4

5. Crystal Thickness Dependence of Photoinduced Crystal Bending of 1,2-Bis(2-methyl-5-(4-(1-naphthoyloxymethyl)phenyl)-3-thienyl)perfluorocyclopentene
D. Kitagawa, S. Kobatake, *J. Phys. Chem. C.* **2013**, *117*, 20887–20892.
---------- Chapter 5

6. Photoinduced Twisting of a Photochromic Diarylethene Crystal
D. Kitagawa, H. Nishi, S. Kobatake, *Angew. Chem. Int. Ed.* **2013**, *52*, 9320–9322.
---------- Chapter 6

Acknowledgments

This thesis work was carried out during the academic years from 2010 to 2013 at Department of Applied Chemistry and Bioengineering, Graduate School of Engineering, Osaka City University. The author is sincerely grateful to Prof. Dr. Seiya Kobatake for his kind direction, helpful suggestion, and cordial consistent encouragement throughout this work.

The author would like to express his deep gratitude to Prof. Dr. Hiroshi Ohshima and Prof. Dr. Yasuo Hatanaka for careful review of this thesis and fruitful suggestion. The author also expresses his deep gratitude to Prof. Dr. Akikazu Matsumoto for helpful cooperation and support in analysis equipments. The author also wishes his deep gratitude to all stuffs of Department of Applied Chemistry and Bioengineering for their teaching as a useful basis of this thesis work and to all colleagues and graduates in Kobatake Laboratory of Osaka City University for their collaborations, kind help, and friendship.

The author would like to appreciate Research Fellowship for Young Scientists, Japan Society for the Promotion of Science.

Finally, the author heartily wishes to sincere appreciation to his fiancée, Chiaki Tanioku, and his parents for their understanding, care, and encouragement.

March, 2014

Daichi Kitagawa